Development of a numerical rapid assessment tool to simulate fate and environmental impact of fluidized sediment layers

Title
Development of a numerical rapid assessment tool to simulate fate and environmental impact of fluidized sediment layers

Project	Attribute	Pages
11203293-000	11203293-000-ZKS-0002	32

Keywords
Numerical tool, 1DV model, model development, fluidized sediment layers, sediment transport, environmental impact assessment

Executive Summary

Within the dredging industry, it is common practice to generate fluidized sediment layers when executing dredging projects in, for example, port areas. The fluidized sediment layer that is generated can flow by gravity to deeper sections where it can be trapped. During flow, the fluidized layer will interact with the ambient water column under local hydrodynamic forcing (i.e. tidal currents or waves). Mixing of the fluidized layer with the overlying water can lead to an increase in turbidity. Before a dredging project is executed, this turbidity plume must be evaluated carefully, so the environmental impact of the dredging activities can be estimated and mitigated. The sedimentation footprint of the fluidized layer should be evaluated as well, both from an environmental and operational point of view.

In this project, we have developed a rapid assessment numerical tool to assess the environmental impacts of fluidized sandy and / or muddy sediment layers induced by a moving turbidity source. Given a set of initial conditions for the fluidized layer, the tool can be used to:

- Compute the thickness and density of the fluidized layer as function of the distance from the source in relation to the hydrodynamics in the water column and bed slope;
- Calculate a turbidity source term (in kg/s), which can be used in far-field modelling of turbidity plumes (in analogy with the method described in Becker et al., 2014).

To facilitate rapid computations, the tool is based on the Deltares 1DV model (e.g. Winterwerp & Uittenbogaard, 1997). We have adapted the 1DV model to make it suitable for a Lagrangian 1DV modelling approach. The Lagrangian 1DV approach entails that we follow the development of the fluidized layer flow along a user-defined trajectory using a moving frame of reference.

This report describes the development and verification activities of the numerical rapid assessment tool carried out in this project. These are:

1. Validation of the Lagrangian 1DV approach;
2. Specification of fluidized layer initial conditions in the 1DV model;
3. Testing sensitivity of model outcome to fluidized layer initial profiles; and
4. Implementation of mud dynamics formulations.

These 4 developments were carried out successfully. A beta research executable of the rapid assessment numerical tool has been completed. Because model setup is relatively easy and computational effort is small, this tool enables users to make rapid calculations. This makes it particularly useful in the engineering and design phases of dredging projects, where engineers must be able to act quickly upon receiving information about the project site and changes in project execution. Furthermore, this approach enables users to test the sensitivity of model

Deltares

Title
Development of a numerical rapid assessment tool to simulate fate and environmental impact of fluidized sediment layers

Project	**Attribute**	**Pages**
11203293-000	11203293-000-ZKS-0002	32

outcomes to different parameter settings. However simple to use, it is important to note that the assumptions underlying the model must be carefully considered to correctly apply the model.

References
TKI reference #: DEL 087;
Deltares project #: 11203293

Version	Date	Author	Initials	Review	Initials	Approval	Initials
1.0	nov. 2019	Erik Hendriks Luca Sittoni		Thijs van Kessel Han Winterwerp	TvK	Frank Hoozemans	

Status
final

Contents

Appendices

1 Introduction

This report summarizes the activities and findings of Phase I of the project “Development of a numerical rapid assessment tool to simulate fate and environmental impact of fluidized sediment layers”. This project is a collaborative Topconsortium Kennis en Innovatie (TKI) Deltatechnologie project between Deltares and Boskalis. The project is divided in two main phases:

- Phase I: development and verification of the numerical tool; and
- Phase II: validation and application of this tool on specific dredging operations

This report only presents the results of Phase I. The results of Phase II are produced by Boskalis and are not published as they may contain data and information confidential to Boskalis. In the remainder of this report, the word “project” refers to “Phase I”.

1.1 Project scope

Within the dredging industry, it is common practice to generate fluidized sediment layers when executing dredging projects in, for example, port areas. The fluidized sediment layer that is generated can flow by gravity to deeper sections where it can be trapped. During flow, the fluidized layer will interact with the ambient water column under local hydrodynamic forcing (i.e. tidal currents or waves). Interaction of the fluidized layer with the water column can lead to an increase in turbidity of the water. Before a project is executed, this turbidity plume must be evaluated carefully, so the environmental impact of the dredging activities can be estimated and mitigated.

In this project, we develop a rapid assessment numerical tool to assess the environmental impacts of fluidized sandy and / or muddy sediment layers induced by a moving turbidity source. To facilitate rapid computations, the tool is based on the Deltares 1DV model (e.g. Winterwerp & Uittenbogaard, 1997), which is described in detail in this report. The tool should be able to model the following two aspects of the fluidized sediment layer flow and its interaction with the ambient water:

1. The transport path and stability (i.e. fate) of the fluidized sediment layer (location, extent, thickness and density of the layer); and complementary
2. The entrainment of sediment from the fluidized layer into the water column (which can be used as turbidity source for environmental evaluation).

The fate of the fluidized layer, and therefore the effectivity and impact of these dredging operations, depends on several factors. The most important factors are: bed slope, ambient flow conditions, initial density, and thickness and momentum of the generated fluidized layer. The model should be able to handle these factors adequately.

1.2 Goals and deliverables

The main goal of this project is to develop and verify the numerical rapid assessment tool. This tool should have the following capabilities:

- Compute the thickness and density of the fluidized layer as function of the distance from the source in relation to the hydrodynamics in the water column and bed slope;
- Be capable to calculate a turbidity source term (in kg/s), which can be used in far-field modelling of turbidity plumes (in analogy with the method described in Becker et al (2014)); and
- Be (offline) coupled with a near-field production model (provided by Boskalis). This model provides initial conditions for the 1DV model computations. The near-field production model is not developed further in this project.

The project deliverables are:
- This report, describing model verification and model development;
- A beta research executable of the numerical tool; and
- A user guide on how to use the numerical tool (Appendix D of this report).

This report is publicly available through the TKI Deltatechnologie webpage. Deltares will deliver the tool to a third party upon request. The beta research executable version is subject to the Pre-Release Software Licensing Agreement for testing of Pre-Release Software, both for Boskalis and for any third party.

1.3 Project organisation

As mentioned before, this project is a collaborative Topconsortium Kennis en Innovatie (TKI) Deltatechnologie project between Deltares and Boskalis. From the Deltares side, the project was managed by Luca Sittoni, MSc with support of Erik Hendriks. The principal technical investigator was dr. Thijs van Kessel. Model development and model validation was mainly carried out by Erik Hendriks. Code development was supervised by dr. Rob Uittenbogaard, Adri Mourits and Jan van Kester. Prof. Han Winterwerp has reviewed project progress and has been consulted for the implementation of mud dynamics in the model.

From the Boskalis side, the project was managed by Thomas Vijverberg. Arno Nobel, Irena Doets, Luis Alfaro and Roeland Lievens tested the model and have applied the model to specific dredging cases (i.e. Phase II).

1.4 Report organisation

This report consists of a brief main report, which includes the main findings and results of this project, accompanied by four appendices. These appendices contain model development and verification details, mathematical derivations and a user guide. Below, the different chapters are briefly discussed.

Chapter 2 discusses the background and the assumptions underlying the design of the numerical tool. It also introduces the Deltares 1DV model, which is used as the basis for the numerical tool. Chapter 3 presents the findings from the model verification studies and the most important developments to the 1DV model carried out in this project.

Chapter 4 discusses how to use the model. Chapter 5 presents the most important conclusions and outlook for following studies and discusses whether the project goals have been met.

The contents of the Appendices included with this report are described in more detail in Appendix A.

2 Theoretical framework

The numerical tool that is developed in this project needs to meet two main criteria: it needs to be a 1) rapid assessment tool, and at the same time it needs to be 2) reliable. These two criteria require the correct balance between simple schematization and accurate physical processes. In this chapter, we present the model setup in line with these two criteria, and with characteristics described in Section 1.2.

2.1 Model setup – Lagrangian 1DV

In our approach, we model the fluidized layer flow by using a Lagrangian 1-Dimensional Vertical (1DV) model. In the following subsections, we will explain why we have chosen for this modelling approach.

2.1.1 Fluidized layer flow as a 2DV process

The starting point of our approach is that we assume the fluidized layer flow can be schematized as a 2DV process. This assumption is only valid when lateral spreading is limited, for instance when the fluidized layer is flowing through a confined channel. This means that both lateral gradients and processes are neglected.

The conceptual sketch of a fluidized sediment layer moving through space is drawn in Figure 2.1. The fluidized sediment layer is generated on the left side at time t_0 (upper panel Figure 2.1). At this time, the fluidized layer has a certain initial velocity and initial density, where the density of the fluidized layer is determined by the water density and the amount of suspended sediment present in the layer. The initial velocity and initial density of the fluidized layer determine its initial momentum. This initial momentum contributes to the initial movement of the fluidized layer: assuming the fluidized layer has a positive velocity (defined positive in x-direction), it will start moving to the right (upper panel Figure 2.1), where the head of the fluidized layer is located at $x = x_0$ at time $t = t_0$.

However, the main force driving the fluidized layer is the density difference between the fluidized layer and its environment. The density gradient leads to a pressure gradient that drives the flow. Basically, this means that the fluidized layer flow is a density current. After a certain time t_1, it has moved by a distance x_1 (middle panel Figure 2.1). During this same time, the fluidized layer may have lost sediment due to deposition, or due to mixing of sediment into the overlying water. Due to the decrease of sediment present in the layer, the density difference between the fluidized layer and its environment decreases. Hence, the density gradient decreases and thus, the pressure gradient decreases. This leads to a decrease in fluidized layer velocity. This process continues until all sediment has either been deposited on the bed or has mixed into the water column. This is the maximum distance travelled by the fluidized layer, denoted by x_e (with corresponding time t_e) in the lower panel of Figure 2.1.

An important aspect of the conceptual sketch in Figure 2.1 is that this has an Eulerian frame of reference. The coordinates of the frame of reference are fixed, with the fluidized layer moving through the domain.

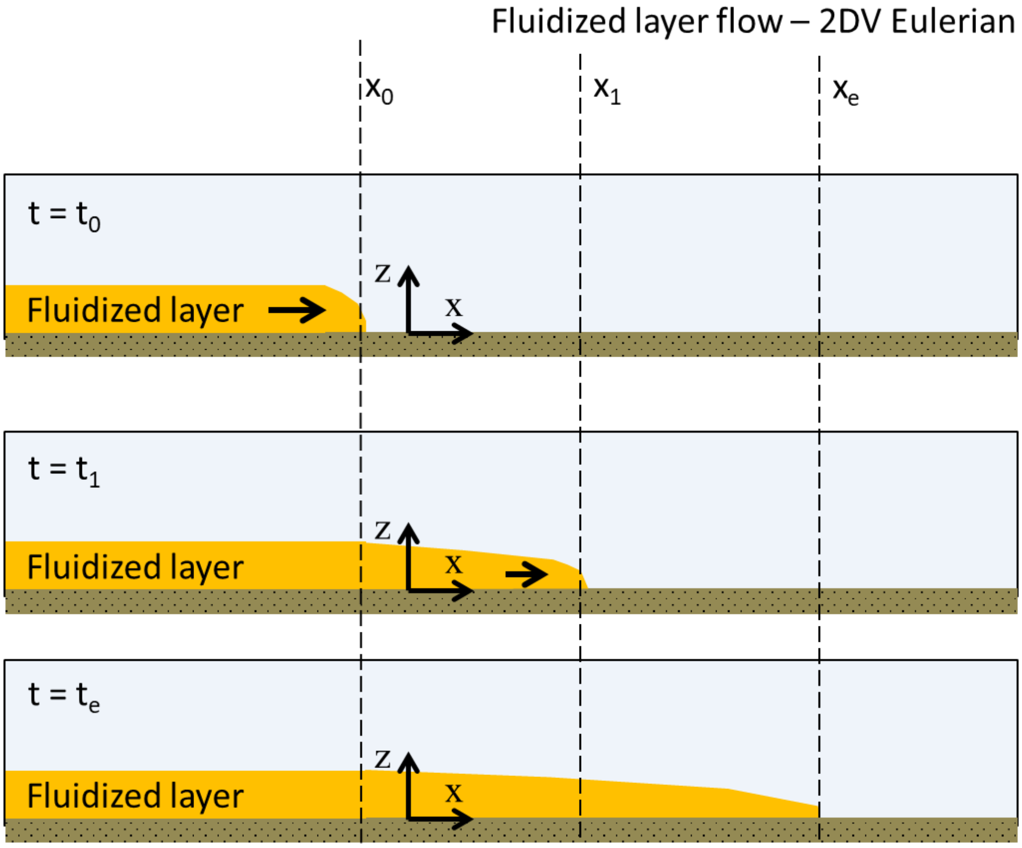

Figure 2.1 Conceptual sketch of a fluidized sediment layer, moving over a flat bed. Fluidized sediment is generated at the left hand side of this figure. The fluidized layer is mainly driven by the density difference between the layer and its environment.

2.1.2 Fluidized layer flow down a slope

In reality, the bed will generally not be flat but has a certain slope. This bed slope may be beneficial for the dredging activity, as it may increase the travel distance of the fluidized layer. To understand this, we must realize that the pressure gradient driving the flow consists of two contributions. The pressure gradient consists of a barotropic and a baroclinic term. The barotropic term only depends on a water level gradient The baroclinic term was implicitly described in the previous section: this term depends on the density gradient, i.e. the available suspended sediment mass. However, the bed slope enhances the baroclinic term. When a density current is flowing down a slope, the baroclinic term increases due to gravity.

As sketched in Figure 2.2, the fluidized layer will move down the slope, again starting on the left side. Due to gravity, the fluidized layer will flow over a longer distance, as the baroclinic pressure gradient enhances the total pressure gradient. For an equal initial momentum of the fluidized layer, the fluidized layer will travel further along a downward slope than along a flat bed (x_e in Figure 2.2 is further away from x_0 than was the case in Figure 2.1).

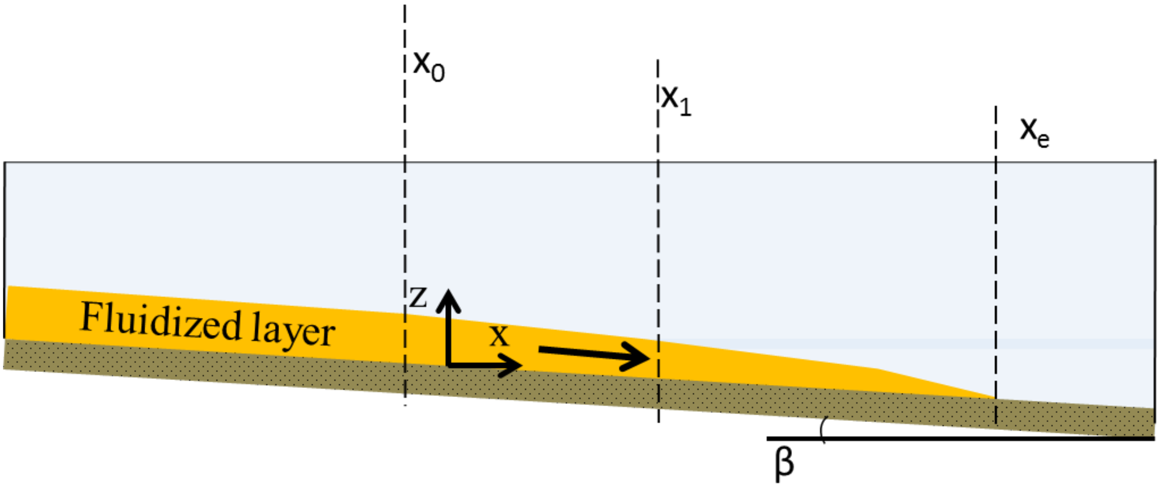

Figure 2.2 Conceptual sketch of a fluidized sediment layer, moving down a slope. Fluidized sediment is generated at the left hand side of this figure. The fluidized layer is mainly driven by the baroclinic contribution to the pressure gradient, due to the density difference with its environment and the bed slope.

2.1.3 From 2DV to a Lagrangian 1DV approach

As we have discussed in the previous two subsections, we schematize the fluidized layer flow as a 2DV process. In order to further decrease computational effort, we opt for one more schematization. Here, we must keep in mind that vertical processes are very important for the model we are developing. These vertical exchange processes happen both at the top of the fluidized layer and at the bottom of the fluidized layer. At the top of the layer, sediment is exchanged with the overlying water column due to turbulent mixing. At the bottom of the layer, sediment is exchanged with the bed due to erosion and deposition. Both processes need to be represented correctly in the model, so it has the capabilities described in Section 1.2.

Therefore, we further schematize the process as a 1DV process, following the fluidized layer as it moves away from the source. Consequently, we need to transform the 1DV momentum equation from a Eulerian framework to a Lagrangian framework. Whereas flow is uniform in the Eulerian framework, it is stationary in the Lagrangian framework. The main assumption for this transformation is that observed changes when moving with the flow (i.e. the Lagrangian reference frame) are only space-dependent. The full transformation is given In Appendix B.1.

In this Lagrangian reference frame (Figure 2.3) the time coordinate is denoted by τ, and we move along the slope with the same speed as the fluidized layer, effectively following it. The initial conditions are applied at $\tau = \tau_0$. The vertical coordinate is z, with $z = -d$ at the bed to $z = \zeta$ at the free surface. The propagation speed of the fluidized layer (u_c) is defined as:

$$u_c = \frac{\int_{-d}^{\zeta} uc\, dz}{\int_{-d}^{\zeta} c\, dz} \tag{2.1}$$

In Equation (2.1), u denotes local velocity and c denotes sediment concentration in the Eulerian framework. Hence, u_c is a concentration-weighted velocity. The distance travelled by the fluidized layer (L_x) is then computed by integrating the propagation speed over τ:

$$L_x = \int_0^\tau u_c \, d\tau \qquad (2.2)$$

There must be a small return flow in the water column to make sure there is continuity (also drawn in Figure 2.3). This continuity requirement arises since we are moving a single water column through space, without water being added or lost from this water column.

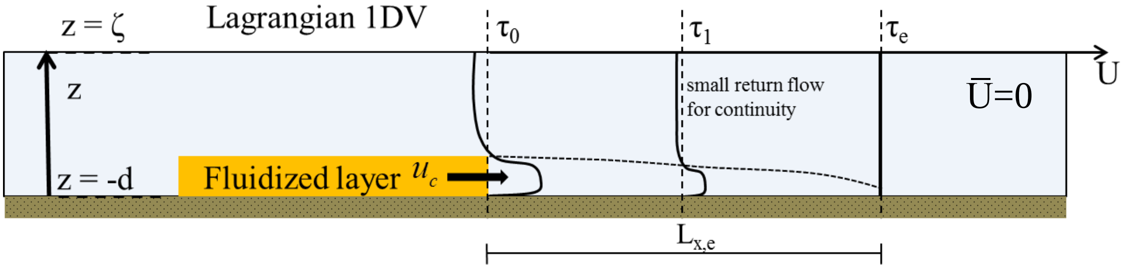

Figure 2.3 Conceptual sketch of Lagrangian 1DV frame of reference for modelling fluidized layer flow. Initial conditions are applied at $\tau = \tau_0$.

A more detailed description of the Lagrangian 1DV approach is given in Appendix B.1. This is accompanied by the derivation of the applicable set of equations, which is given in Appendix B.2.

Table 2.1 Characteristics and assumptions of hydrodynamic modelling approaches.

Approach	**Characteristics & assumptions**	**Computational effort**
3D	non-uniform in longitudinal direction non-uniform in lateral direction non-stationary	large
2DV	non-uniform in longitudinal direction uniform in lateral direction non-stationary	moderate
Eulerian 1DV	uniform in longitudinal direction uniform in lateral direction non-stationary	small
Lagrangian 1DV	non-uniform in longitudinal direction uniform in lateral direction stationary	small

The characteristics and assumptions of different modelling approaches are listed in Table 2.1 . We distinguish two crucial assumptions in the Lagrangian 1DV approach. First, the fluidized layer flow is uniform in lateral direction and, second, the flow is stationary in the Lagrangian frame of reference.

2.1.4 User-related features of Lagrangian 1DV approach

The advantages of modelling fluidized layer flow using a Lagrangian 1DV approach are the following:

- Model setup is easy
- Small computational effort
- High vertical resolution possible

Because model setup is relatively easy and computational effort is small, this approach enables the user to make rapid calculations. This approach is particularly useful in the engineering and design phases of dredging projects, where engineers must be able to act quickly upon receiving information about the project site and changes in project execution. In these projects, data is often limited, and a range of input settings need to be tested. This is also possible using the Lagrangian 1DV model. Since the Lagrangian 1DV approach allows for a high vertical model resolution, it can accurately compute vertical processes. This high resolution is desirable, as vertical gradients are large and exchange of sediment between the fluidized layer and overlying water column is complex.

The distance travelled along a slope by the fluidized layer is computed by applying Equations (2.1) and (2.2). However, when concentrations in the fluidized layer are of the same order of magnitude as in the ambient water, this approach may no longer be valid. In that case, u_c is mainly influenced by the ambient water velocity, and not by the velocity in the fluidized layer. Hence, the Lagrangian 1DV model results should be assessed carefully to see if the assumptions underlying the approach are not violated.

2.2 Description of the 1DV model and developments

In this section, we elaborate on the current status of the modelling tool that has been developed further in this project: the 1DV model of Deltares. Over the past two decades, this model has been used in a variety of projects and environments and has proven to be an elegant and powerful modelling tool. We start by discussing the current status of the 1DV model and the developments to date. Next, we discuss the required adaptations to the model to make it suitable for a Lagrangian 1DV application.

2.2.1 Conceptual description of 1DV point model

As a basis for the Lagrangian 1DV model, we use the 1DV point model. The 1DV point model is based upon the Delft3D-FLOW model, by stripping all the horizontal gradients, except for the horizontal pressure gradient. This model was originally developed to study the implementation of the k-ε turbulence model by Uittenbogaard et al. (1992) and van Kester (1994) (Winterwerp, 1999). More detailed information on this model can be found in Appendix B.1.1.

The computational domain of the 1DV point model is bordered by the water surface and a reference plane (bed). The model basically redistributes velocity and sediment over the vertical computational domain (”the water column”). Sediment may be added or lost by erosion from and deposition to a sediment stock below the reference plane. Because the 1DV model is essentially a single water and bed column of Delft3D, all processes implemented and tested in 1DV are also included or can eventually be included in Delft3D.

The 1DV point model is forced with a depth-mean flow velocity U(t), which may vary over time, a time varying water level h(t), constant wave forcing (Hs and Tp), and an initial vertical sediment concentration distribution $c_0(z)$.

The Deltares 1DV point model exists within various beta-versions. The beta version that is used as a starting point for this project includes the following relevant processes:

1. Turbulent mixing and vertical exchange of horizontal momentum using the k-ε turbulence model, also including buoyancy effects on the vertical velocity and concentration profile;
2. Multiple sediment fractions;
3. Hindered settling (Richardson-Zaki);
4. Erosion specified by the Zyserman & Fredsoe (1994) reference concentration; and
5. Ambient velocity.

Functionalities 3 and 4 of the model, hindered settling and erosion, have only been applied to sandy sediment mixtures in previous studies.

The 1DV model consists of a collection of FORTRAN routines. The discretization and solving methods are exactly the same as those used in Delft3D-FLOW. Input and output of the model are organized through ASCII files, and MatLab routines, but no Graphical User Interface (GUI).

2.2.2 From 1DV point model to a Lagrangian 1DV model

To successfully model fluidized layer flow using a Lagrangian 1DV approach, we need to make several adaptations to the 1DV point model. These are briefly discussed here and are elaborated upon in more detail in Appendix B.1 and B.2.

The main adaptation is to transform the frame of reference for the model from a Eulerian frame of reference (i.e. fixed in space) to a Lagrangian frame of reference (i.e. moving with the fluidized layer). Therefore, we assume that the fluidized layer flow is stationary, i.e. changes along the slope are only space-dependent and not time-dependent. If we apply this assumption, we can use the approximation of the alongslope distance as it is given in Equation (2.2) and schematically shown in Figure 2.3.

Another essential adaptation is to include a baroclinic contribution to the pressure gradient (as explained in Section 2.1.2). In the 1DV point model, the pressure gradient is the main driver of the flow, but it only consists of a barotropic contribution. This barotropic pressure gradient only depends on a water level gradient and does not represent a pressure gradient due to density differences. When modelling fluidized layer flow, it is crucial to include the baroclinic (i.e. density-dependent) contribution to the pressure gradient. This is crucial because the fluidized layer flow is a gravity-driven flow, the speed at which it propagates depends on the density of the fluidized layer and how steep the slope is that it is flowing over.

As a part of this project, these adaptations were implemented in the 1DV code by Rob Uittenbogaard. In the main report, validation of the Lagrangian 1DV approach is discussed in Section 3.2.

3 Main activities and results

3.1 Task overview

This project consists of four main tasks, related to the development and validation of the 1DV model. These are discussed in the various sections of this chapter.

The main tasks are:

1 Validation of the Lagrangian 1DV approach;
2 Specification of fluidized layer initial conditions in the 1DV model;
3 Testing sensitivity of model outcome to fluidized layer initial profiles; and
4 Implementation of mud dynamics formulations.

3.2 Validation of the Lagrangian 1DV approach

In this section, we present the results of the Lagrangian 1DV model validation. This validation consists of three different steps. First, we compare Lagrangian 1DV computations with laboratory experiments on turbidity currents, which is a specific type of fluidized layer flow down a slope. To find appropriate laboratory experiments, we performed a brief literature survey. Second, we compare the 1DV model with field data. The third step is to validate if the 1DV model can be used for both downsloping and upsloping beds. Here, we only present the most important results from these three steps. The validation is more extensively described in Appendix C.1.

We opt for comparing the Lagrangian 1DV model to turbidity current data, as turbidity currents are comparable to fluidized sediment layers induced by a moving turbidity source. These are both particle-laden gravity currents, driven by a density difference between the fluidized layer and the ambient water. Layer density and sediment characteristics are also comparable. Hence, if the Lagrangian model can be used to adequately model turbidity currents, we expect it can also be applied to fluidized sediment layers induced by a moving turbidity source.

3.2.1 Lagrangian 1DV model compared to lab experiments

In the past decades, turbidity currents have been extensively studied by means of laboratory experiments and numerical model studies. For our validation, we focus on two experimental studies, carried out by Parker et al (1987) and Sequeiros et al (2009), respectively. In these studies, the dynamics of self-accelerating turbidity currents were investigated, using non-cohesive sediment.

Parker et al. (1987) conducted 24 experimental runs to investigate the behaviour of turbidity currents laden with non-cohesive silt (silica flour). In these experiments the turbidity currents moved down a slope, where the bed was covered with similar silt. The motion of the head was not studied; measurements were concentrated on the continuous part of the current that was essentially constant in time but developing in space. Only internal supercritical currents were studied. The currents were free to erode sediment from, and deposit sediment on the bed. Vertical profiles of velocity and sediment concentration were measured downstream of the sediment inlet. These measurements allow for the development of approximate similarity relations, and comparison with numerical models.

Parker et al. (1987) measured profiles of concentration and velocity along the slope of their flume. Profiles were measured at three locations, at 1.5, 4.5 and 8.5 meters downstream of the flume inlet. For these three locations, we compare the velocity and concentration profiles computed by the 1DV model with data of one representative experimental run. Results are shown in Figure 3.1 and Figure 3.2. The 1DV settings are compared with experimental settings in Table 3.1. Values for z_0 (bed roughness) and $\bar{U}$ (depth-averaged velocity) were not given by Parker et al. (1987) but have been calculated, see Appendix C.1.2.1 for details. Other settings were chosen such that they agree with the experimental settings.

Table 3.1 Experimental settings of experiment 13 as presented by Parker et al (1987), compared with Lagrangian 1DV settings.

Parameter	Parker et al. (1987)	Lagrangian 1DV setting
Slope	0.05	0.05
Average fluidized layer velocity (U_0)	0.27 m/s	0.27 m/s
Inlet height (h_0)	0.08 m	0.08 m
Water discharge through inlet (Q_{w0})	15 l/s	not specified
Sediment discharge through inlet (Q_{s0})	164.6 g/s	not specified
Volumetric sediment concentration at inlet (C_0)	$4.1*10^{-3}$	not specified
Sediment density	2650 kg/m^3	2650 kg/m^3
Average fluidized layer sediment concentration (Q_{s0}/Q_{w0})	10.9 g/l	10.9 g/l
d_{50} of sediment	30 µm	30 µm
d_{90} of sediment (estimated from PSD curve)	50 µm	50 µm
z_0 (calculated)	not specified	$5*10^{-6}$ m
$\bar{U}$ (calculated)	not specified	0.025 m/s
initial velocity profile	not specified	double logarithmic profile
initial concentration profile	not specified	step function (i.e. constant)

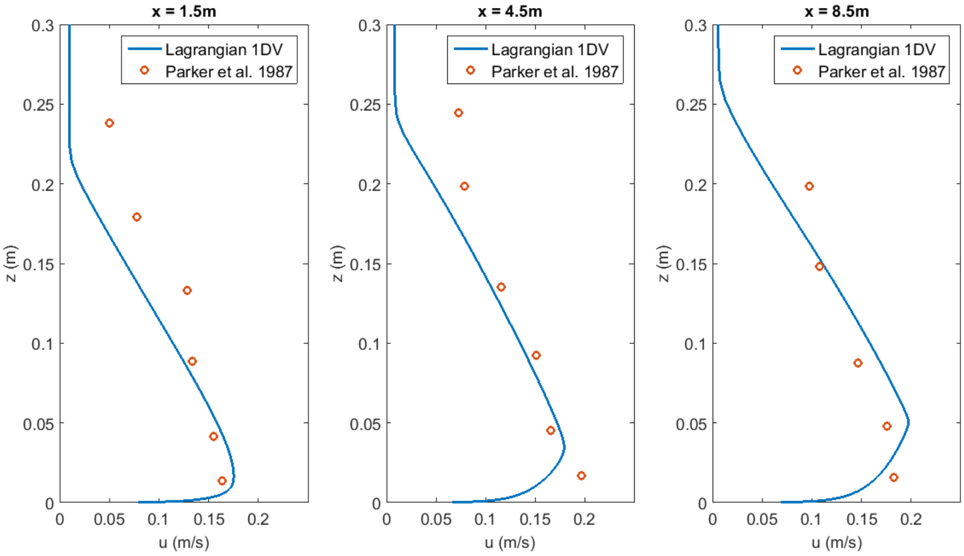

Figure 3.1 Velocity profiles computed using the Lagrangian 1DV model compared to the measurements of Parker et al. (1987).

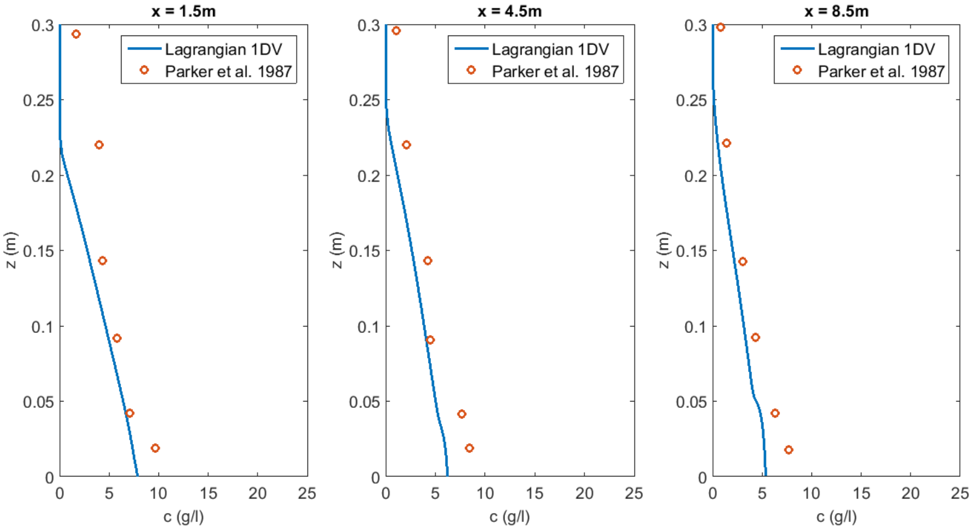

Figure 3.2 Concentration profiles computed using the Lagrangian 1DV model compared to the measurements of Parker et al. (1987).

The Lagrangian 1DV model shows a good agreement with the data of Parker et al (1987). Within the turbidity current, from 0 to 0.2m above the bed, the velocity is computed accurately. Above the turbidity current, the velocity is slightly underestimated by the model. The computed concentration profiles show a similar trend to the measured concentrations.

For the boundary at the bed, we have chosen the Zyserman and Fredsoe (1994) reference concentration. This reference concentration is imposed on the lowest grid cell, based on the value of the Shields parameter. At locations x = 4.5 m and x = 8.5 m, we observe that this reference concentration influences the concentrations above, as there is a small inflection at 0.025 m and 0.05m above the bed, respectively. While this boundary condition may be valid for modelling turbidity currents, is should not be used for calculating the sedimentation footprint of a fluidized layer, as a sediment concentration is imposed instantaneously on the lowest grid cell.

Other options would be to specify that no sediment is eroded from the bed or to use a pickup function. If the fluidized layer flow is mainly depositional, which is the case for fluidized layers generated by dredging, a ‘no-erosion’ formulation will suffice. We advise to use this boundary condition when modelling fluidized layer flow using the Lagrangian 1DV model.

Sequeiros et al. (2009) investigated self-acceleration of the head of a turbidity current. A self-accelerating turbidity current was generated in the laboratory for certain combinations of velocity, concentration, and characteristics of the sediment. These characteristics include grain size distribution, sediment cohesiveness or lack thereof, and density. All the above parameters play an important role in the development of the turbidity current; only under appropriate conditions will the entrainment of sediment from the bottom overcome deposition, so creating a necessary condition for self-acceleration. We have chosen a representative experimental run to compare with the Lagrangian 1DV model. The details of this representative run can be found in Appendix C (Table C.3).

Sequeiros et al (2009) measured concentrations in the head of the generated turbidity current along the slope of their flume. As we can see from Figure 3.3, the 1DV model only partially agrees with the data of Sequeiros et al. (2009). For the first two measurement stations (at x = 4.8 and 8.0 m) we observe a large difference between experimental data and the model. Further away from the inlet, model results approached the experimental results. This is probably due to the non-stationary character of the head of the turbidity current. This violates the primary assumption of the Lagrangian 1DV model. This non-stationarity probably diminishes along the slope, bringing it in closer agreement with results of the 1DV model.

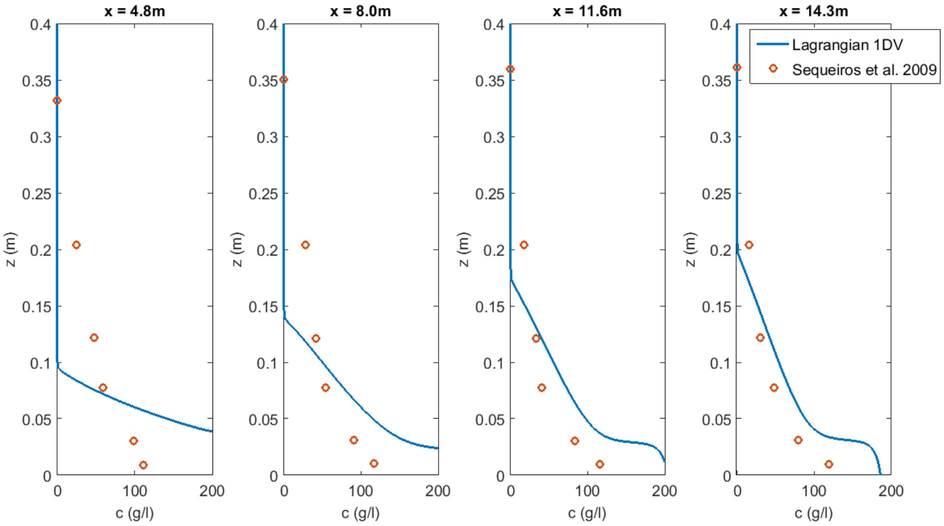

Figure 3.3 Concentration profiles computed using the Lagrangian 1DV model compared to the measurements of Sequeiros et al. (2009)

Both Parker et al. (1987) and Sequeiros et al. (2009) reported sediment sorting along the pathway of the turbidity current, i.e. downstream fining of the deposited sediment. Even though several multiple sediment fractions can be imposed in the 1DV model, it is not feasible to include a full particle size distribution. Hence, a representative grain size should be chosen by the modeller.

3.2.2 Model compared to field observations at Scripps Canyon

After validating the 1DV model against laboratory data, we also performed a brief validation using data from Scripps Canyon, USA. This is one of the few well-documented sites where non-cohesive turbidity currents occur. Turbidity currents in this canyon were reported by, for instance, Inman et al. (1976) and by Marshall (1978). Mastbergen and van den Berg (2003) argue that turbidity currents in Scripps canyon are caused by breaching of fine sand deposits at the head of the canyon tributaries. The large amounts of fine sand that are temporarily stored at the head of these canyons may then flow through the canyon as a turbidity current.
Mastbergen and van den Berg (2003) compared measurements in Scripps canyon with a 1-Dimensional Horizontal (1DH) model, i.e. a two-layer depth-averaged model. Below, we compare the 1DV model with their results and some of the available field data.

Mastbergen and van den Berg (2003) defined different scenarios, where the starting point of the turbidity current retrogrades. This is due to the ongoing breaching of the sand deposit at the head of the submarine canyon. We compare the 1DV model with two of these scenarios, the “24” and the “37” scenarios. These numbers denote the number of hours after the breaching has commenced. As an initial condition for the 1DV model, we use the maximum sediment transport rate as given by Mastbergen and van den Berg. This maximum sediment transport rate occurs when the breach reaches the canyon bedrock, and no more sand is incorporated into the turbidity current. From this point onwards, the sediment transport rate computed by Mastbergen and van den Berg remains constant.

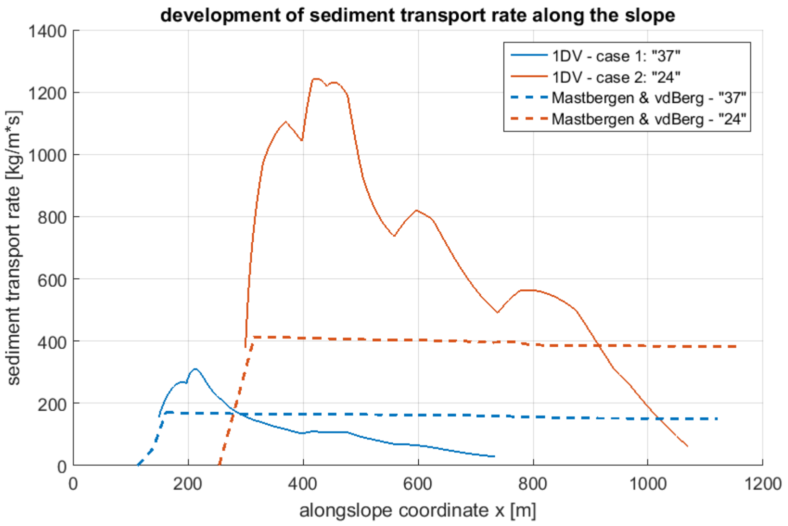

Figure 3.4 Comparison of sediment transport rates computed using the Lagrangian 1DV model with results of Mastbergen and van den Berg (2003).

In Figure 3.4, we have plotted the alongslope development of the sediment transport rate computed by the 1DV model (solid line). The model results of Mastbergen and van den Berg (2003) are indicated with dashed lines. The sediment transport rates computed with the 1DV model initially exceed the constant sediment transport rates of Mastbergen and van den Berg (2003). This is caused by a strong acceleration of the turbidity current due to the baroclinic contribution to the pressure gradient. As a result, the horizontal velocity increases where most sediment is located (i.e. in the turbidity current). This leads to an increase in the sediment transport rate. However, as there is no source of sediment in the model (erosion is switched off), this increase is not realistic. Probably, the Lagrangian 1DV approach does not correctly compute the sediment transport rate using this specific set of initial conditions. After several hundreds of meters, we also see that the turbidity currents decelerate faster than in the cases computed by Mastbergen and van den Berg (2003). This is due to the ongoing deposition in the 1DV model: eventually, most sediment has deposited whereas Mastbergen and van den Berg argue that sedimentation is only expected to occur when gentle slopes are encountered. As there is hardly any field data available for these turbidity currents, it remains unclear which model predicts the sediment transport rate most accurately.

In Figure 3.5, we plotted the velocity at 2m above the bed as a function of alongslope distance. The red cross marks the location in Scripps canyon where velocities of 2 m/s were measured (Inman et al, 1976), before the velocity meter was eventually lost due to the large force of the turbidity current. The 1DV model computes velocities that have the correct order of magnitude. Model computations suggest that velocities within the turbidity current may even be higher; where the velocity magnitude mainly depends on the steepness of the slope and the amount of available sediment in the turbidity current. This is illustrated by the two different cases, as the main difference between these cases is the available amount of sediment and the location on the slope where the turbidity current started.

The Lagrangian 1DV approach is most accurate when the initial conditions lie close to stationary conditions, i.e. the driving force due to gravity is almost in equilibrium with the friction term. Additionally, if the gravity current does not decelerate nor accelerate suddenly along its trajectory, the streamlines of the gravity current run parallel to the slope. This is the case for mild slopes (1:100 or less) and when initial conditions do not deviate strongly from stationary conditions. The approach may still work for steeper slopes, when initial conditions are in close agreement with stationary conditions.

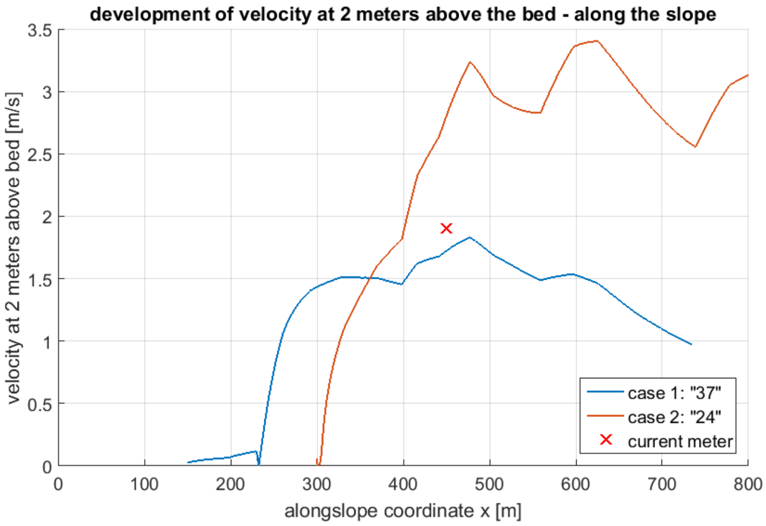

Figure 3.5 Velocities computed using the Lagrangian 1DV model, compared to the flow velocity measurement at 2 meters above the bed, reported by Inman et al (1976).

3.2.3 Bed slope: downsloping vs. upsloping

As was mentioned in Chapter 2, the baroclinic contribution to the pressure gradient depends on two main factors: the available sediment mass and the bed slope. In this part of the validation, we test if the model handles up- and downsloping beds correctly. We have created three bathymetries to test this: an upsloping, downsloping and flat bed. The alongslope bed levels are drawn in Figure 3.6. Please note that the definition for water depth is similar to Delft3D-FLOW: water depth is directed positive downwards as shown in Figure 3.6. For the first 30 meters, all three bathymetries are flat. After 30 meters, a slope of 1/20 is imposed for the downsloping bathymetry and upsloping bathymetry.

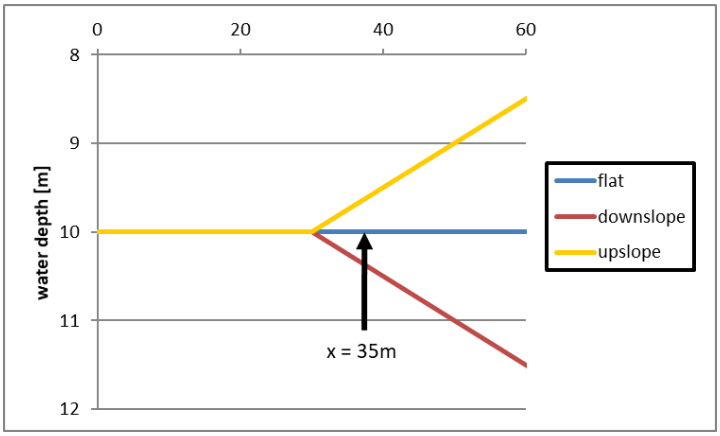

Figure 3.6 Bathymetries for validation of slope effect in baroclinic pressure gradient. At x=35m, we plot vertical profiles of horizontal velocity, horizontal pressure gradient and sediment concentration.

The initial conditions are identical for all three model runs and are listed in Table C.7 in Appendix C.1.6. To compare the effect of bed slope, we examine vertical profiles total pressure gradient, horizontal velocity and sediment concentration at x = 35 m, 5 meters after the incline change. With total pressure gradient we mean the sum of the baroclinic and barotropic contributions to the pressure gradient.

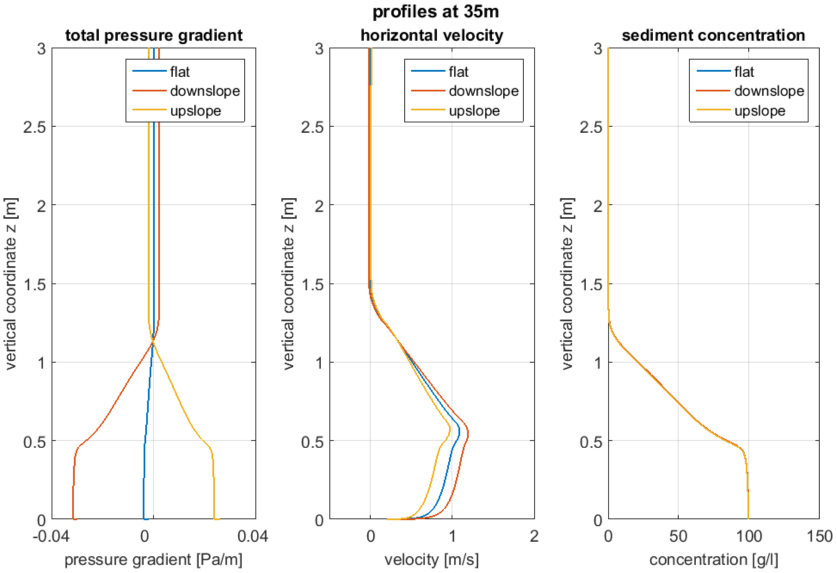

Figure 3.7 Profiles of total pressure gradient, horizontal velocity and sediment concentration at x=35m for the three considered cases: flat, downsloping and upsloping bed. Colours in the plot correspond with the bathymetries drawn in Figure 3.6.

From Figure 3.7, we see that for the flat bed, the pressure gradient has a small negative value for the part of the vertical profile with a high sediment concentration. This is due to the influence of settling on the horizontal sediment concentration gradient. In other words: the sediment concentration decreases along the slope due to settling, leading to a negative pressure gradient.

However, we also see from Figure 3.7, that when a bed slope is present, this will dominate the magnitude and sign of the horizontal pressure gradient. When there is a downward slope, the total pressure gradient becomes more negative, and the flow will experience a larger acceleration. When there is an upward slope, the pressure gradient becomes positive, decelerating the density current. Both these effects can be seen from the middle panel in Figure 3.7. Of course, since this is only 5 m after the slope started, the influence on the sediment concentration profile is still very limited (Figure 3.7, right panel). However, we plotted the profiles for this location since the incline is rather steep, and at x = 50 m flow reversal occurred for the upsloping bathymetry.

Summarizing, we conclude that the model correctly handles the three different bathymetries. However, when modelling an upsloping bathymetry, one should be wary for the possibility of encountering negative velocities. This may lead to a negative displacement of the Lagrangian framework, rendering the Lagrangian 1DV results invalid.

3.2.4 Conclusions of Lagrangian 1DV validation

From the different validation exercises, the following main conclusions can be drawn:

- The Lagrangian 1DV model shows a good qualitative agreement with the experimental data of Parker et al (1987).
- Output of the Lagrangian 1DV model agrees only partially with experimental data of Sequeiros et al (2009). This is probably because Sequeiros et al (2009) measured a non-

stationary part of a turbidity current, which violates one of the main assumptions of the Lagrangian 1DV model.

- The Lagrangian 1DV model computes velocities that are in the same order of magnitude as observed in Scripps Canyon, as reported by Inman et al (1976). Sediment transport rates deviated from model results by Mastbergen and van den Berg (2003) and are likely not valid.
- Lagrangian 1DV approach is most accurate when a gravity current does not decelerate nor accelerate suddenly along its trajectory. This is the case for mild slopes (1:100 or less) and when initial conditions do not deviate strongly from stationary conditions.
- The Lagrangian 1DV model correctly handles upsloping and downsloping bathymetries, through an adjustment of the pressure gradient driving the fluidized layer flow.

Summarizing, we can say that the Lagrangian 1DV model performs as expected. However, users should carefully consider whether the model is applicable to a certain case when interpreting the results.

3.3 Specification of fluidized layer initial conditions in 1DV model

After validating the model with turbidity current data, we make the transition to modelling fluidized sediment layers induced by a moving turbidity source. To model these correctly, we need to carefully specify the initial conditions for the fluidized layer. The initial conditions for the fluidized layer flow can be characterised by three main parameters:

- Fluidized layer height (h_{fl})
- Average fluidized layer velocity (u_{fl})
- Average fluidized layer concentration (c_{fl})

These parameters can be specified through the model input. Using these parameters, initial profiles for the fluidized layer can be constructed. However, before constructing these profiles, we need to specify which properties of the fluidized layer need to agree with the input. For this, we consider four properties of the fluidized layer:

- Velocity
- Sediment mass
- Momentum
- Sediment mass flux

As these properties are interrelated, they cannot agree with the input simultaneously, as is also discussed in Appendix C.2. In our approach, we choose to make two properties agree with the input, i.e., the sediment mass and the sediment mass flux. These two properties need to agree with the input since the dominant driving force, the baroclinic pressure gradient, mainly depends on the amount of available sediment. Hence, if we want to calculate how far the fluidized layer travels, we need to make sure the sediment mass and sediment mass flux agree with the values specified in the model input. When we assume all sediment is contained in the fluidized layer with height h_{fl}, these two properties are given by:

$$
\begin{aligned}
h_{fl} c_{fl} &= \int_0^{h_{fl}} c \, \mathrm{dz} \\
u_{fl} c_{fl} h_{fl} &= \int_0^{h_{fl}} u(\mathrm{z}) \, c(\mathrm{z}) \, \mathrm{dz}
\end{aligned}
\tag{3.1}
$$

To obtain the specified sediment mass flux, we use u(z) as the controlling variable. We can also calculate how much the fluidized layer-averaged velocity $\overline{u}$ will differ from the specified u_{fl}, by using the following formula:

$$
\overline{u} = \frac{u_{fl} c_{fl} + \overline{\Delta u \Delta c}}{c_{fl}} \tag{3.2}
$$

In Equation (3.2), Δu and Δc denote deviations around the average for u(z) and c(z). If the product of Δu and Δc over the layer is not zero, $\overline{u}$ deviates from u_{fl}.

Furthermore, a user-specified depth-averaged velocity $\overline{U}$ is specified in the 1DV model. A new velocity profile is assigned to the part of the water column that is lower than h_{fl}. If the height of the fluidized layer h_{fl} cannot be neglected compared to the total water depth h, this may lead to a velocity surplus for the entire vertical compared to the user-specified velocity $\overline{U}$. To correct for this, the velocity profile is adjusted based on the user-specified settings for the fluidized layer velocity and fluidized height, so the initial depth-averaged velocity (for the entire water column) is equal to the user-specified velocity $\overline{U}$. More details on the definition of initial conditions are given in Appendix C.2.

3.4 Testing sensitivity of model outcome to fluidized layer initial profiles

We use the outcomes of the previous section as a starting point for constructing the initial profiles. In this section we investigate how sensitive the model output is to the shape of the initial profile. An extensive description of the sensitivity study is given in Appendix C.3.

3.4.1 Velocity profile

The sensitivity of model outcome to the shape of the initial velocity profile is tested first. To properly test this sensitivity, the fluidized layer-averaged velocity $\overline{u}$ is kept constant between the different model runs. From Equation (3.2) it follows that if Δc is equal to zero, $\overline{u}=u_{fl}$. Since, u_{fl} is specified through the user input, we can then control $\overline{u}$. Hence, we choose a constant concentration profile for the fluidized layer. We have defined three possible initial velocity profile shapes: logarithmic, double-logarithmic and a hybrid (logarithmic-mixing layer) profile. These three options are shown in Figure 3.8.

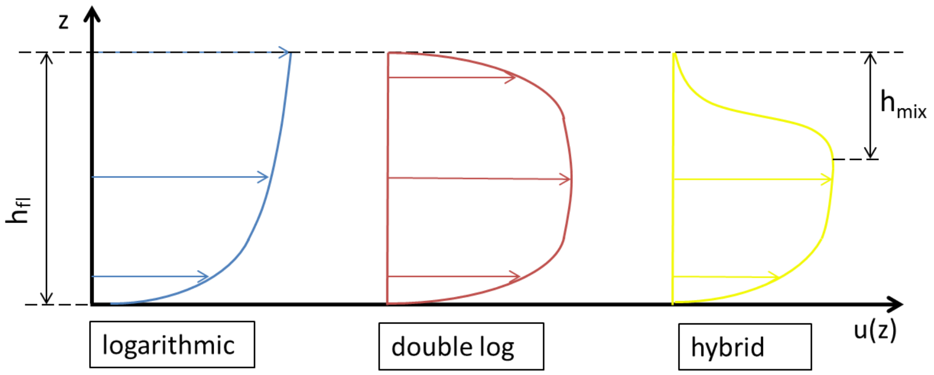

Figure 3.8 Definition sketch of the three available velocity profiles.

The logarithmic velocity profile is a standard velocity profile for turbulent boundary layer flow and occurs when the flow has a free surface on its upper boundary. The double logarithmic profile is found in turbulent pipe flow and occurs when the fluidized layer flow is confined between an upper and lower boundary. The hybrid profile is similar to velocity profiles suggested by Parker et al (1987) and Mastbergen and van den Berg (2003) for turbidity currents. It consists of a logarithmic velocity profile for the lower part and a mixing layer for the upper part. The mixing layer is described by a hyperbolic tangent function, and its height is indicated by h_{mix} in

Figure 3.8. These three velocity profiles can be used to describe most turbulent flow patterns.

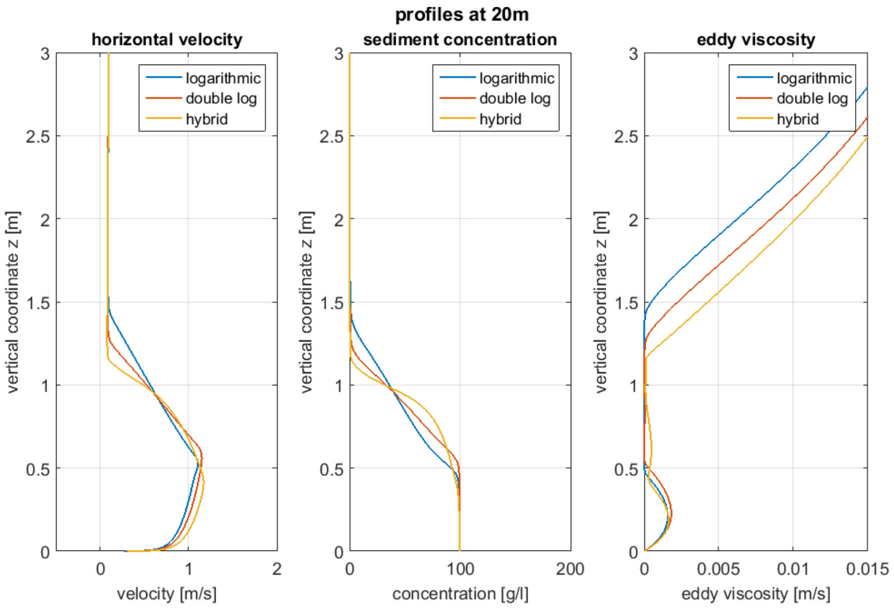

Figure 3.9 Vertical profiles of horizontal velocity, sediment concentration and eddy viscosity at x=20m for the three different initial velocity profiles.

We assessed the results from model runs where the shape of the initial velocity profile was varied between one of three options described above. Differences between the three different velocity profiles were not very large at 20 m, as can be seen from Figure 3.9. Here we see vertical profiles of horizontal velocity, sediment concentration and eddy viscosity that were taken at an alongslope distance of x = 20 m (profiles at other alongslope distances can be seen in Appendix C.3). The logarithmic velocity profile in the fluidized layer mixed some of the sediment higher up in the water column, because of the large shear between the fluidized layer and the ambient water. The double log profile also experiences some shear, whereas the hybrid profile shows the smoothest transition, and thus the least sediment mixing. We see that the sediment concentration also has a direct influence on the eddy viscosity profile. Because sediment is mixed over a higher section of the vertical, we see that turbulent mixing (expressed by the eddy viscosity) is suppressed over a larger part of the water column. The sedimentation footprint of the fluidized layer is hardly affected by the choice of velocity profile.

3.4.2 Concentration profile

After testing the sensitivity of model outcome on the initial velocity profile, we continue with testing the model sensitivity to the initial concentration profile. We do this in two steps: first, we only impose sediment mass and sediment mass flux conservation to our initial profile. Second, we introduce an additional condition: a constant ‘centre of gravity’ for the fluidized layer.

For our first step, we create a series of initial concentration profiles based on a hyperbolic tangent. The resulting initial concentration profiles are shown in Figure 3.10. The sediment mass is 100 kg/m^2 for all profiles, but their vertical distribution is clearly different. The sediment mass flux is 100 kg/m*s for all runs. This sediment mass flux is the product of the sediment mass (kg/m^2) and the velocity (m/s).

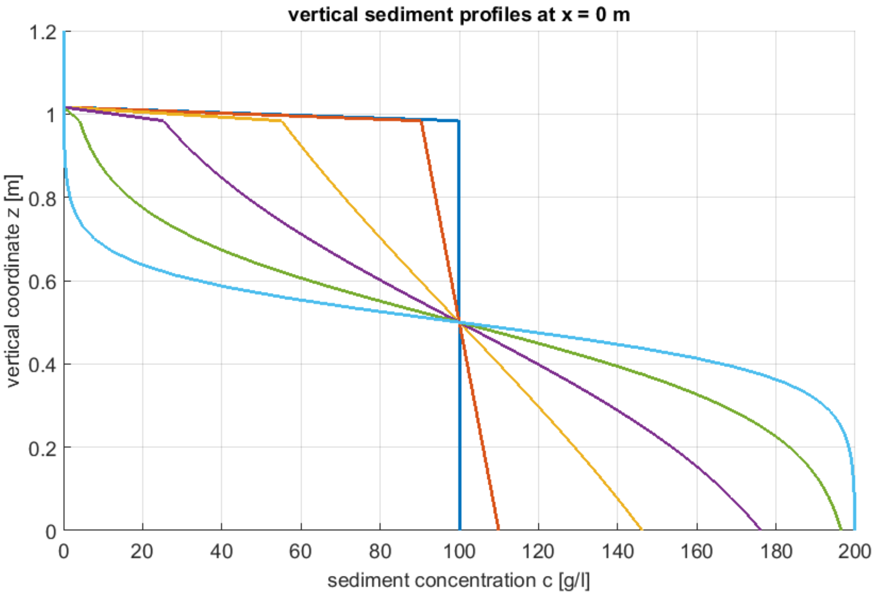

Figure 3.10 Initial concentration profiles described by hyperbolic tangent functions. All profiles have a total sediment mass of 100 kg/m^2.

When we run the model using these different concentration profiles, we see that the sediment mass flux along the trajectory of the fluidized layer is clearly different for the different concentration profiles (see Figure 3.11). The colours used in Figure 3.10 and Figure 3.11 correspond to one another. For instance, the sediment mass flux for the cyan profile decreases much faster than the other profiles as we progress along the slope.

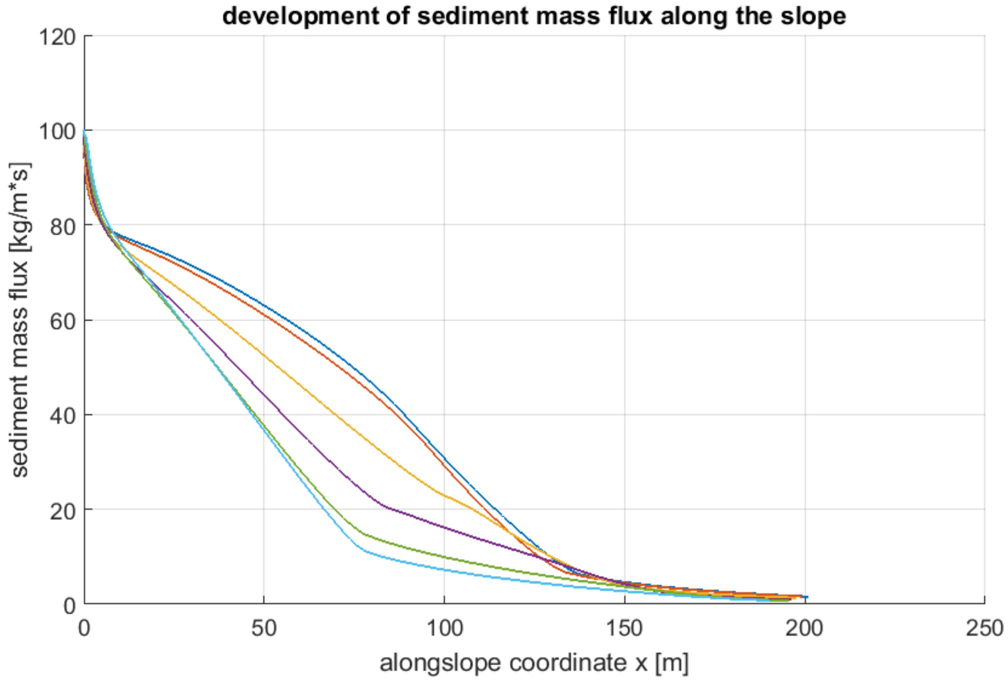

Figure 3.11 Development of sediment mass flux along the slope for the set of hyperbolic tangent concentration profiles.

The main difference between these profiles is that their centre of gravity is clearly different: it ranges from 0.5 m above the bed (dark blue profile) to approximately 0.25 m above the bed (cyan profile). Therefore, we will now test the sensitivity of model outcome when we keep this centre of gravity constant for different initial profiles. We compare three different conceptual profiles, which are schematically shown in Figure 3.12. Again, sediment mass and mass flux are constant for the three different runs. In this figure, we have indicated the height of the fluidized layer (h_{fl}) and the height of the centre of gravity ($h_{gravity}$). When comparing these three profiles, we should interpret h_{fl} as the height of the velocity profile. Furthermore, all sediment is found between the bed and a distance h_{fl} above the bed.

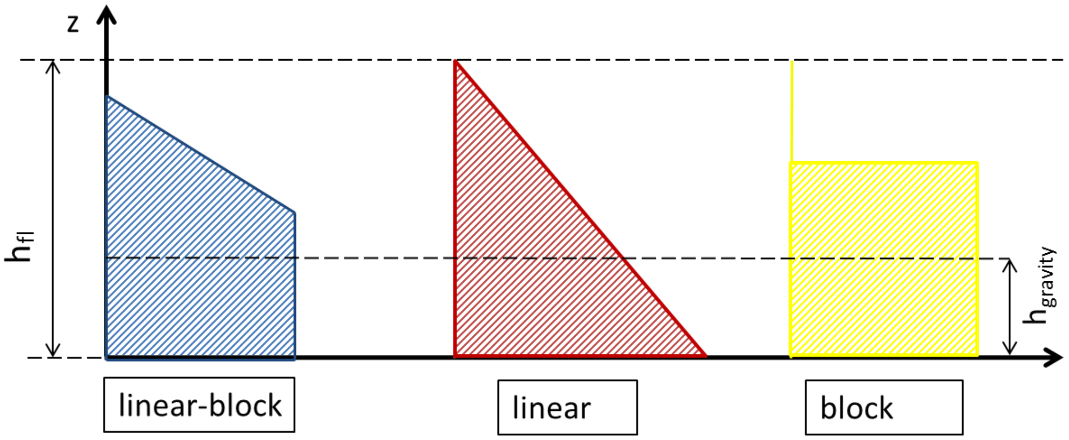

Figure 3.12 Definition sketch of the three concentration profiles used for the sensitivity study of the 'centre of gravity'.

The sediment mass for the three different profiles is 100 kg/m^2 and the initial sediment mass flux is 100 kg/m*s. When we now plot the development of the sediment mass flux along the slope, we obtain the following result (Figure 3.13). We see that when the centre of gravity of the fluidized layer remains constant, the development of the sediment mass flux is almost independent of the concentration profile.

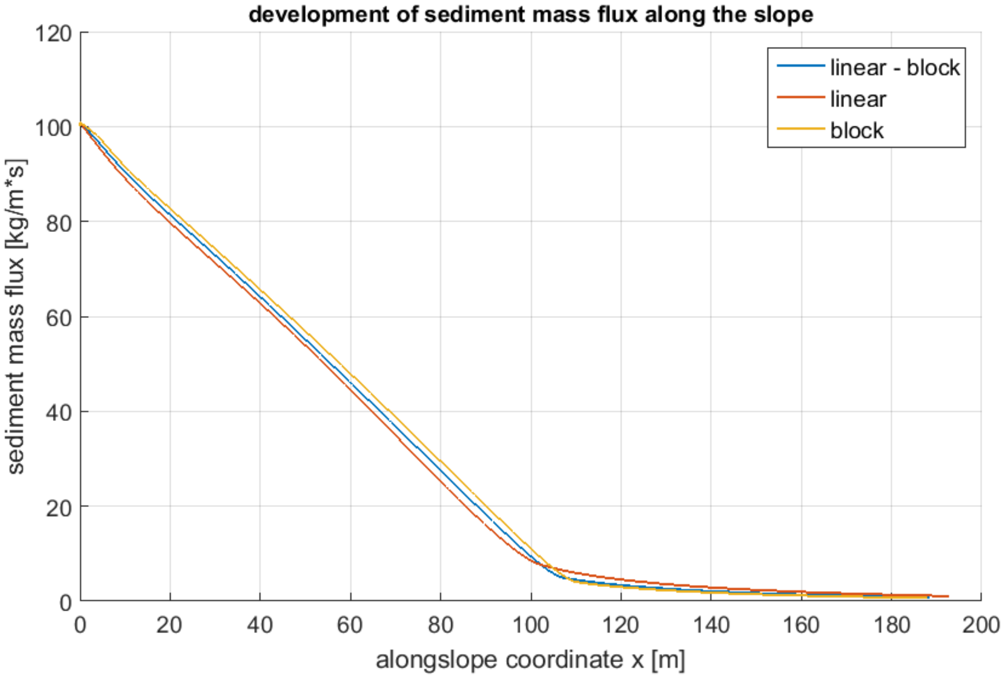

Figure 3.13 Development of sediment mass flux along the slope for the set of initial concentration profiles with constant centre of gravity.

3.4.3 Conclusions of sensitivity study

The sensitivity of Lagrangian 1DV model outcome was tested for different initial fluidized layer conditions. The main conclusions are:

- When setting up the Lagrangian 1DV model, it is advised to give most attention to the setup of the initial concentration profile, since its potential influence is (much) larger than the influence of the velocity profile.
- Model outcome is very sensitive to the initial concentration profile, when only conservation of sediment and sediment mass flux apply. The main sensitivity of model outcome lies in 'centre of gravity' of the fluidized layer. If this remains constant for different initial profiles, the shape of the initial concentration profile does not have a large effect.

The logarithmic velocity profile in the fluidized layer leads to larger mixing as the amount of shear on the interface between fluidized layer and ambient water is largest. For a smoother transition, the hybrid velocity profile (shown in

- Figure 3.8) is more suitable.

3.5 Implementation of mud dynamics formulations

To allow using the Lagrangian 1DV model also for fluidized layer flows that consist of mud (i.e. cohesive sediment), two types of processes need to be included in the model. These processes are:

- Hindered settling
- Erosion and deposition of mud

Implementations to the Lagrangian 1DV model are performed in such a way that they are consistent with the existing formulations in Delft3D. More details on the implementation and validation of these processes are given in Appendix C.4.

3.5.1 Hindered settling

Different formulations for hindered settling exist. In the Lagrangian 1DV model, we opt for the Richardson-Zaki formulation, since this is applicable to both sandy and muddy sediment suspensions. The Richardson-Zaki formulation, in its generalized form, is given below:

$$w_s = w_{s,0}(1-\phi_s)^n \tag{3.3}$$

Where:

- $w_{s,0}$ is the single particle settling velocity,
- ϕ_s is the volume concentration of the suspended particles, defined as: $\phi_s = \frac{c}{\rho_{gel}}$,
- n is an exponent that depends on the particle Reynolds number, for sand n=5, for mud n=4.

The Richardson-Zaki hindered settling formulation was implemented in 1DV. Its parameters can be set through the model input. The volume concentration is determined by using an upwind scheme, similar to the implementation in Delft3D-Slurry (van Es, 2017, Talmon et al., 2019). This means that the sediment concentration in a grid cell influences the settling velocity on the interface above this grid cell.

After implementation, the hindered settling formulation was verified, giving the expected results. Both the single particle settling velocity ($w_{s,0}$) and the structural dry density (ρ_{gel}) have a clear influence on the model results. The effect of the single particle settling velocity mainly becomes apparent over longer distances, since the smaller settling velocity directly influences the deposition flux (as we can see from section 3.5.2). Hence, more sediment will remain in the system, allowing the fluidized layer to travel further. Due to the strongly nonlinear exponent in the Richardson-Zaki formulation for the volume concentration, the values for the structural dry density influence model results for the entire computational domain.

3.5.2 Erosion and deposition of mud

For erosion and deposition of muddy beds, we have implemented the classical Partheniades-Krone formulation. This formulation is given by:

$$
\begin{aligned}
E &= M\,S\,(\tau_b, \tau_{cr,e}) \\
D &= w_s\,c_b\,S\,(\tau_b, \tau_{cr,d})
\end{aligned}
\tag{3.4}
$$

The erosion flux is given by the product of the erosion parameter (M) and a step function (S) that depends on the bed shear stress (τ_b) and the critical bed shear stress for erosion ($\tau_{cr,e}$). The deposition flux is given by the product of the near-bed settling velocity (w_s), near-bed sediment concentration (c_b) and a step function that depends on the bed shear stress (τ_b) and the critical bed shear stress for deposition ($\tau_{cr,d}$).

After implementing these formulations in the code, we have tested and verified them using different test cases. For results, see Appendix C.4. The results of these test cases showed that deposition is clearly dominant over erosion for fluidized sediment layers, because of the typically high sediment concentrations.

4 Using the Lagrangian 1DV model

In this chapter, we give some basic guidelines for using the Lagrangian 1DV model. We briefly discuss some of the basics of 1DV modelling, describe elements of the user guide and present typical outputs of the 1DV model.

4.1 1DV modelling basics

In this section, we present several 1DV modelling principles for proper use of the Lagrangian 1DV model. In Phase II of this project, a more detailed approach is developed for applying the Lagrangian 1DV model to answer practical engineering questions.

4.1.1 Schematization of study site

When setting up a Lagrangian 1DV model computation, several steps need to be taken before running the model. First, a proper schematization of the study site needs to be made. This includes the following three steps:

1. What are the governing hydrodynamics and sediment characteristics at the site, and how does this translate to a characteristic depth-averaged velocity?
2. What is the foreseen trajectory (based on bathymetry) of the fluidized layer flow? In confined channels this is straightforward, but on flat topographies this is more uncertain. If lateral spreading could play a role, quantify this effect and check if 1DV approach is still valid.
3. Obtain bathymetric profile of the foreseen trajectory and schematize this so it can be used in Lagrangian 1DV computation.

4.1.2 Initial conditions

For the initial conditions, specify the starting point of Lagrangian 1DV model. Make an estimate of fluidized layer velocity, fluidized layer height and fluidized layer concentration. As we have seen from Section 3.4, the sensitivity of model outcome on the concentration profile is significant (notably on its centre of gravity). Hence, it deserves recommendation to give extra attention to carefully constructing initial concentration profiles.

4.2 User guide description

A user guide for the Lagrangian 1DV model is included in Appendix D. This user guide provides a guideline for engineers on how to work with the Lagrangian 1DV model. It briefly treats the assumptions underlying the Lagrangian 1DV model and where the model may be applied. Furthermore, it lists the required input files and model settings that can be set through these input files. The outputs generated by the model and postprocessing options are also presented.

4.3 Examples of Lagrangian 1DV output

Model output can be postprocessed with MatLAB. To give an impression of this output, we have visualized the output of two test runs in this section. We only change the imposed bathymetry between these two runs. For the first run, the imposed bathymetry is flat, whereas for the second run, it has a slope of 1:20. Model settings (constant between the two runs) are listed in Table 4.1.

Table 4.1 Model parameters for producing examples of Lagrangian 1DV model output

Model parameter	**Setting**
water depth (d)	10 m
depth-averaged velocity ($\overline{U}$)	0.2 m/s
fluidized layer height (h_{fl})	1.0 m
Average fluidized layer velocity (u_{fl})	1.0 m/s
Average fluidized layer concentration (c_{fl})	100 kg/m^3
sediment type	SAND
median grain size (d_{50})	100 µm

If we run the 1DV model with these settings, we obtain the sediment concentrations along the flat bed and the slope as shown in Figure 4.1 and Figure 4.2. Here, we have only plotted the lower 2 m of the water column as most of the sediment is found there. The fluidized layer travels further along the slope than over the flat bed, as it is driven by gravity. Furthermore, we see that more sediment is mixed higher in the water column along the slope than over the flat bed. This is due to the larger shear between the fast-moving fluidized layer and the ambient water column on the slope.

If we also plot the velocity in the lower 5 m of the water column, we see comparable results (see Figure 4.3 and Figure 4.4). Along the flat bed, the fluidized layer shortly accelerates but it decelerates strongly thereafter. Along the slope, acceleration of the fluidized layer is largest in the lowest 0.5 m of the water column, where most sediment is suspended. The gradient of the horizontal velocity over depth (du/dz) is large, resulting in an increased shear. This shear leads to larger mixing over the vertical, thereby explaining the observed sediment concentrations differences between the fluidized layer flow on the slope and the flat bed. Furthermore, we observe that due to the higher velocities within the fluidized layer, a more pronounced return flow develops above the fluidized layer.

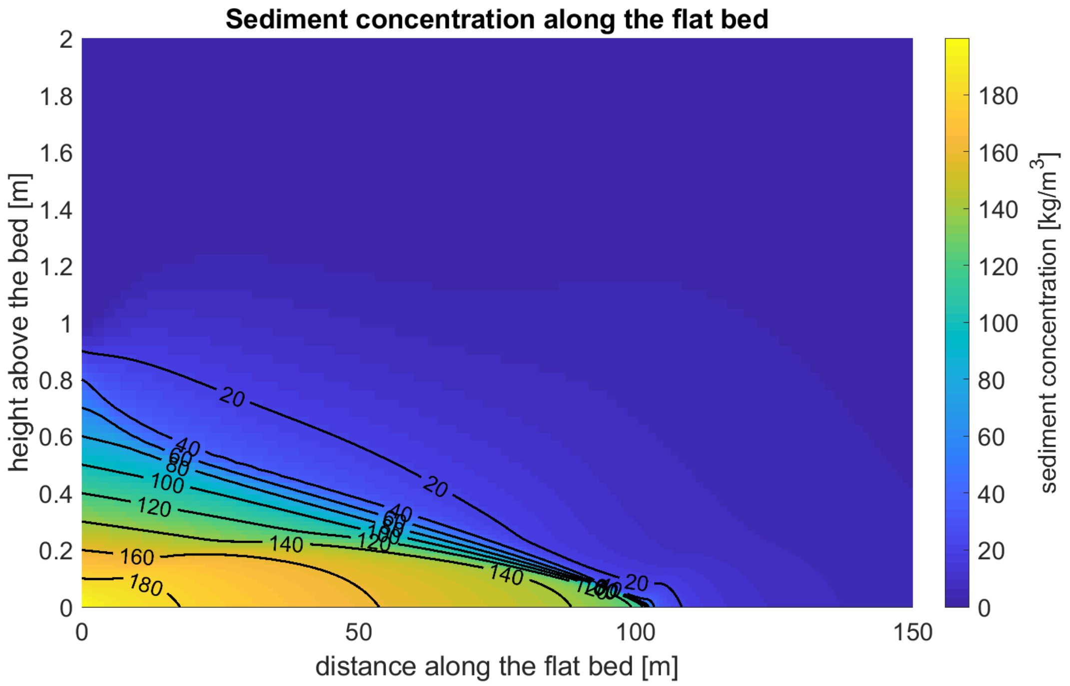

Figure 4.1 Contour plot of sediment concentration for the fluidized layer flow along the flat bed, at equilibrium.

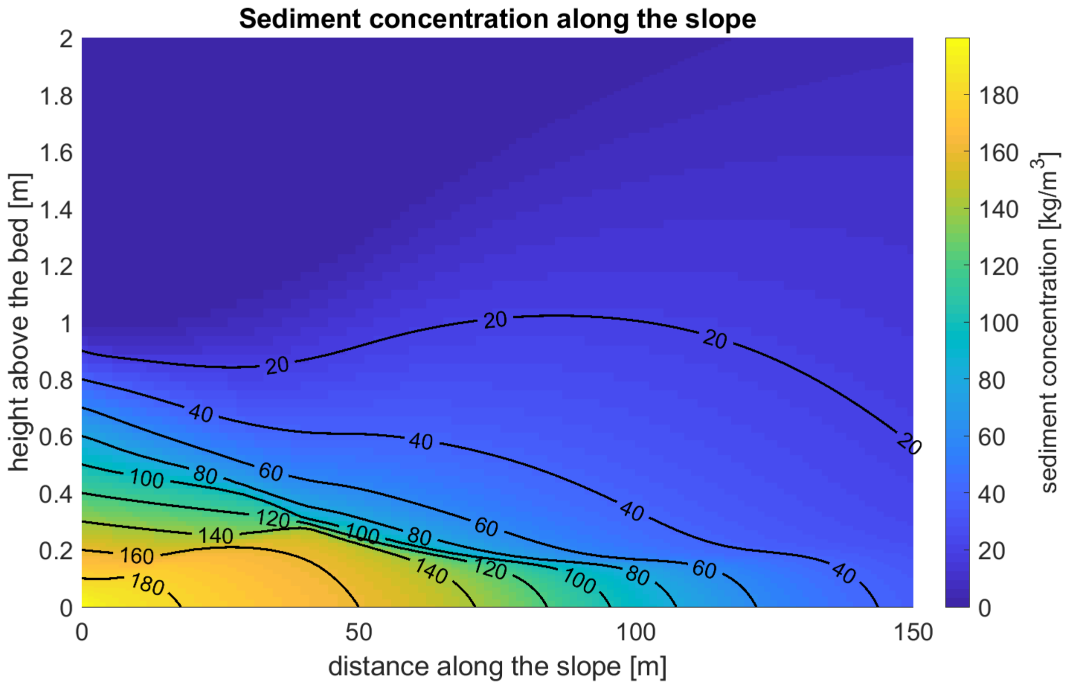

Figure 4.2 Contour plot of sediment concentration for the fluidized layer flow along the 1:20 slope, at equilibrium.

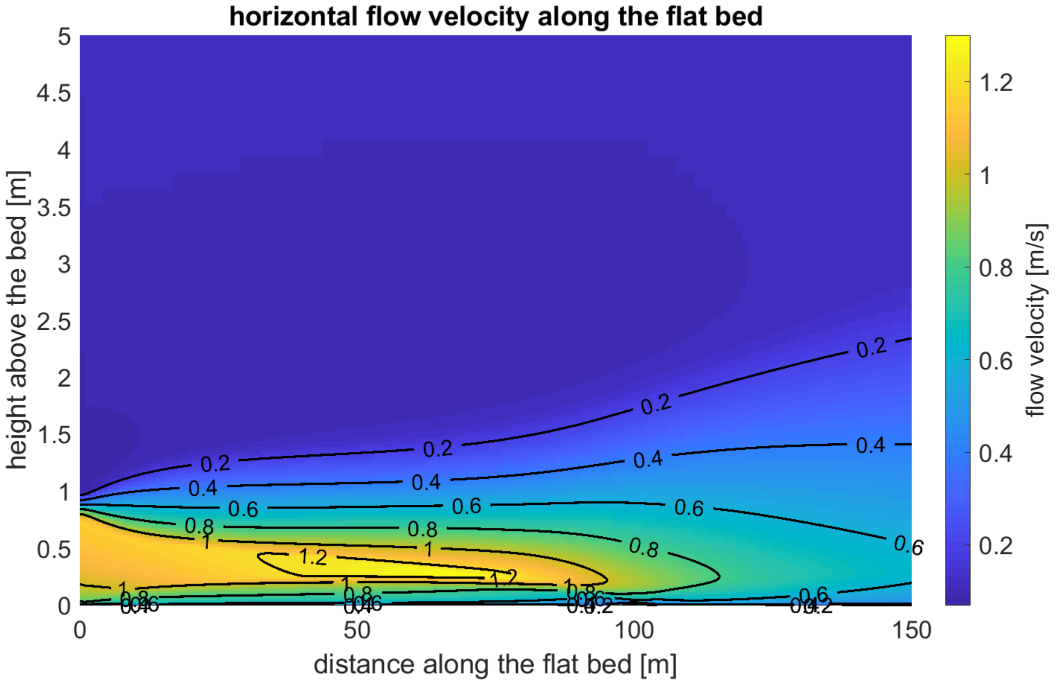

Figure 4.3 Contour plot of horizontal velocity for the fluidized layer flow along the flat bed. Note that in this plot the lower 5m of the water column are shown.

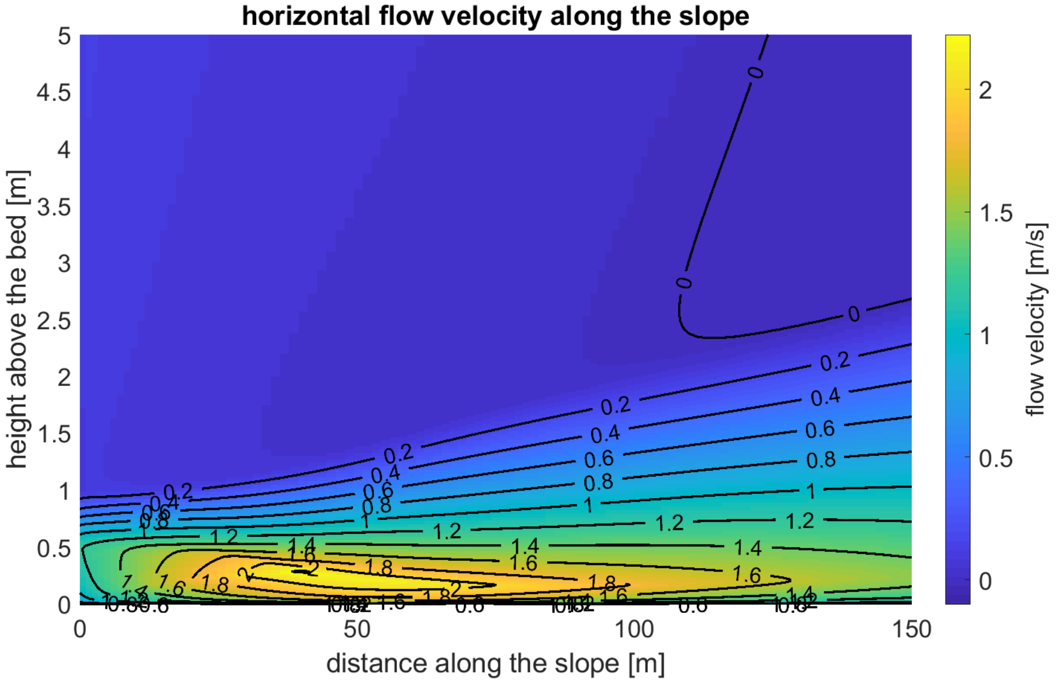

Figure 4.4 Contour plot of horizontal velocity for the fluidized layer flow along the slope. Note that in this plot the lower 5m of the water column are shown.

5 Conclusions and outlook

The goal of this project was to develop a rapid assessment tool that can be used to evaluate the environmental impact of fluidized sediment layers, generated by a moving turbidity source. At the beginning of the project, the following capabilities for the tool were formulated:

- Compute the thickness and density of the fluidized layer as function of the distance from the source in relation to the hydrodynamics in the water column and bed slope;
- Be capable to calculate a turbidity source term (in kg/s), which can be used in far-field modelling of turbidity plumes (in analogy with the method described in Becker et al (2014)); and
- Be (offline) coupled with a near-field production model (provided by Boskalis).

In this project, we have successfully developed a tool with these capabilities. This tool is based on the Deltares 1DV model. We have adapted the 1DV model to make it suitable for a Lagrangian 1DV modelling approach. The Lagrangian 1DV approach entails that we follow the development of the fluidized layer flow along a user-defined trajectory using a moving frame of reference.

The main model developments that were carried out in this project are:

1. Validation of the Lagrangian 1DV approach;
2. Specification of fluidized layer initial conditions in the 1DV model;
3. Testing sensitivity of model outcome to fluidized layer initial conditions; and
4. Implementation of mud dynamics formulations.

The main conclusions of these 4 model developments are discussed below:

1 Validation of the Lagrangian 1DV approach

The Lagrangian 1DV model shows a good qualitative agreement with selected results from literature. It also shows the expected behaviour for test cases when the fluidized layer flows over a downsloping or upsloping bed. Therefore, the Lagrangian 1DV model seems to be fit for purpose.

2 Specify initial conditions for Lagrangian 1DV model

To make sure the model can be easily set up, we specify three parameters in the model input to characterize the initial condition of the fluidized layer flow. These parameters are: the fluidized layer height (h_{fl}), average fluidized layer velocity (u_{fl}), and average fluidized layer concentration (c_{fl}). Using these parameters, vertical profiles are constructed of: velocity, concentration and turbulence. In our approach, we make sure that sediment mass and sediment mass flux, specified by the three parameters listed above, are conserved.

3 Test the sensitivity of model outcome on initial conditions

When setting up the Lagrangian 1DV model, it is advised to give most attention to the setup of the initial concentration profile, since its potential influence is (much) larger than the influence of the velocity profile. Model outcome is very sensitive to the initial concentration profile, when only conservation of sediment and sediment mass flux apply. The main sensitivity of model outcome lies in ‘centre of gravity’ of the fluidized layer. If this remains constant for different initial profiles, the shape of the initial concentration profile does not have a large effect.

4 Implement mud dynamics formulations
We have implemented formulations for hindered settling and erosion/deposition of muddy sediments implemented. After implementation, we have also verified and tested these new formulations. This makes the model suitable for modelling fluidized sediment layers that consist of sand or mud, when they are turbulent and behave as a Newtonian fluid.

With this new version of the 1DV model as a basis, possible follow-up developments include:

1. Modelling settling and consolidation of muddy sediments
   Consolidation, intended as dewatering, changes the thickness, the strength and erosion potential of the newly deposited bed. This can have applications on the thickness of the deposit or the tendency to resuspension from variable hydrodynamic conditions during or after operations. The same features and the same model can be utilized in settling estimates in soft sediment deposits, such as land reclamation or construction of natural islands where requirements are demanded on final topography. Consolidation processes are already embedded in other research versions of the 1DV model, therefore they can be easily included in this new (and official) version.

   A step further would be to include the effects of vegetation and ripening in subaerial compartments. These processes and their addition to this model are in line with Deltares' development ambitions, as they are important for various applications world-wide. However, their addition would still require a significant effort.

2. Incorporate the influence of rheological properties on fluidized layer flow
   When the sediment concentration (especially the cohesive fraction) exceeds about 100 g/l (depending on initial flow conditions and rheological properties of mud), sediment flow will likely behave as non-Newtonian and laminar. In this case, specific non-Newtonian rheology models should be applied. These models were recently developed and embedded in a specific version of the 1DV model (Hanssen, 2016) and then transferred to Delft3D (Delft3D-Slurry, Sittoni et al., 2017). Including non-Newtonian rheology to the version of the 1DV model developed in this report is therefore a logical and relatively simple step that allows improving the accuracy (in fact the correctness) of the prediction to higher sediment concentration.

Summarizing: in this project, a rapid assessment numerical tool was successfully developed. This tool can be used to assess the environmental impacts of fluidized sediment layers induced by a moving turbidity source. Because model setup is relatively easy and computational effort is small, this tool enables users to make rapid calculations. This makes it particularly useful in the engineering and design phases of dredging projects, where engineers must be able to act quickly upon receiving information about the project site and changes in project execution. Furthermore, this approach enables users to test the sensitivity of model outcome to different parameter settings. However, to correctly apply the model, the assumptions underlying the model must be carefully considered.

6 References

Becker, J., Eekelen, E. van, Van Wiechen, J., De Lange, W., Damsma, T., Smolders, T., Koningsveld, M. van (2014) Estimating source terms for far field dredge plume modelling. Journal of Environmental Management 149:282-293

Es, H.E. van (2017) “Development of a numerical model for dynamic depositioning of non-Newtonian slurries”. MSc-thesis, Delft University of Technology.

Galperin, B. , Sukoriansky, S. and Anderson, P. S. (2007), On the critical Richardson number in stably stratified turbulence. Atmosph. Sci. Lett., 8: 65-69. doi:10.1002/asl.153

Hanssen J.L.J. (2016) “Towards improving predictions of non-Newtonian settling slurries with Delft3D: theoretical development and validation in 1DV”. MSc-thesis, Delft University of Technology.

Inman, D. L., Nordstrom, E.C. and Flick, R.E. (1976). Currents in Submarine Canyons: An Air-Sea-Land Interaction. Annual Review of Fluid Mechanics. 8. 275-310. 10.1146/annurev.fl.08.010176.001423.

Kester, J.A.Th.M. van (1994). Validation of DELFT3D against mixing layer experiment; Phase 1: improved implementation of k-ε model. WL|Delft Hydraulics, report Z810

Mastbergen, D.M. and Berg, J. H. van den (2003). Breaching in fine sands and the generation of sustained turbidity currents in submarine canyons. Sedimentology. 50. 10.1046/j.1365-3091.2003.00554.x.

Parker, G., Garcia, M.H., Fukushima, Y. and W. Yu (1987), Experiments on turbidity currents over an erodible bed, Journal of Hydraulic Research, 25:1, 123-147, DOI: 10.1080/00221688709499292

Sequeiros, O. E., Naruse, H., Endo, N., Garcia, M.H., and Parker, G. (2009), Experimental study on self-accelerating turbidity currents, *J. Geophys. Res.*, 114, C05025, doi: 10.1029/2008JC005149.

Sittoni, L., Talmon, A.M., Hanssen J.L.J, Es, H.E. van, Kester, J.A.Th.M. van, Uittenbogaard, R.E., Winterwerp, J.C. and van Rhee, C., (2017) “One step further towards prediction of tailings deposition flow and sand segregation. Where we are, and what comes next.”. COSIA Innovation Summit, Calgary, Canada.

Talmon, A.M. et al. (2019) A research trajectory towards improving fines capture prediction with Delft3D-slurry. Deltares report 11201392-000-ZKS-0003
Uittenbogaard, R.E. et al. (1992). Implementation of three turbulence models in TRISULA for rectangular horizontal girds, including 2DV test cases. WL|Delft Hydraulics, report Z162

Winterwerp, J.C. and Uittenbogaard, R.E. (1997) Sediment transport and fluid mud flow: Physical mud properties and parameterization of vertical transport processes SILTMAN ; set-up of a POINT-MUD MODEL. WL|Delft Hydraulics, report Z2005

Winterwerp, J.C. (1999) On the dynamics of high-concentrated mud suspensions. PhD Thesis, Delft University of Technology.

Zyserman, J.A. and Fredsoe, J. (1994). Data analysis of bed concentration of suspended sediment. J. Hydr. Eng. ASCE, vol. 120, no.9, pp. 1021-1042.

A Organisation of appendices

The appendices included with this report are listed below, including a short description of their contents:

- Appendix A: Overview and short description of appendices (this page)

- Appendix B: Conceptual and mathematical description of the Lagrangian 1DV model

In this Appendix, the Lagrangian 1DV model is conceptually described. Furthermore, the equations that are solved in the model are given.

- Appendix C: Model development

In this Appendix, we elaborate on the model development and present detailed descriptions of the work packages discussed in Chapter 3 of the main report.

- Appendix D: User guide

In this Appendix, we present a user guide for the Lagrangian 1DV model, providing guidelines on how to set up and run the model.

B Conceptual and mathematical description of the Lagrangian 1DV model

B.1 Conceptual description

In this section, we conceptually describe the Lagrangian 1DV model and the assumptions underlying the model. We start by describing the 1DV point model, and then explain how the governing equations of the 1DV point model can be transformed to arrive at the Lagrangian 1DV model.

B.1.1 1DV point model – Eulerian reference frame

The 1DV point model is based upon the Delft3D-Flow model, by stripping all the horizontal gradients, except for the horizontal pressure gradient. This model was originally developed to study the implementation of the k-ε turbulence model by Uittenbogaard et al. (1992) and van Kester (1994) (Winterwerp, 1999). The computational domain is bordered by the water surface and a reference plane (bed).

The 1DV point model basically redistributes velocity and sediment over the vertical computational domain (”the water column”). Sediment may be added or lost by erosion from and deposition to a sediment stock below the reference plane. Because the 1DV model is essentially a single water and bed column of Delft3D, all processes implemented and tested in 1DV are also included or can eventually be included in Delft3D.

The 1DV point model is forced with a depth-mean flow velocity U(t), which may vary over time, a time varying water level h(t), constant wave forcing (H_s and T_p), and an initial vertical sediment concentration distribution $c_0(z)$.

The computational domain of the 1DV point model is drawn in Figure B.1. This is an Eulerian reference frame as it is fixed in space.

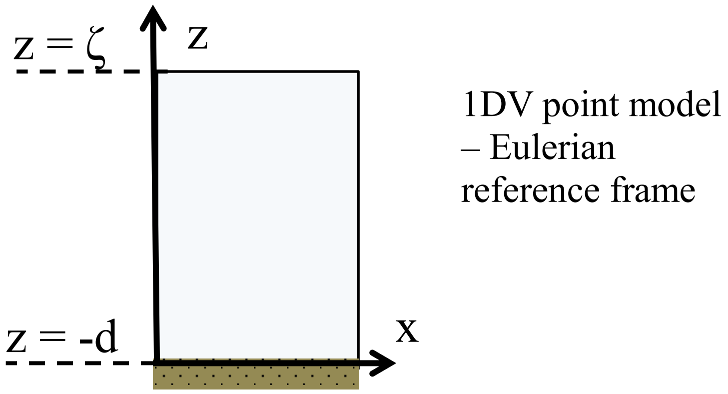

Figure B.1 1DV point model in the Eulerian reference frame. The water surface is located at z=ζ and the reference plane (bed) is located at z=-d

The main assumptions underlying this Eulerian 1DV approach can be summarized in the formulaic description in Equation (2.1).

$$
\begin{aligned}
&u_i(x,y,z,t) = u_i(z,t) \\
&v \equiv 0 \\
&\frac{\partial}{\partial x} \equiv 0\,;\frac{\partial}{\partial y} \equiv 0
\end{aligned}
\tag{2.1}
$$

These assumptions mean that the velocity in x-direction (u) is only a function of the vertical position z and of time. The velocity in y-direction (v) is zero by definition. Apart from the horizontal pressure gradient, all other horizontal gradients are zero.

These are the main assumptions for 1DV modelling in a Eulerian reference frame, i.e. when only changes in time and over the vertical are considered. The following section discusses the adaptations needed to go from an Eulerian to Lagrangian frame of reference.

B.1.2 Lagrangian 1DV reference frame

Indeed, if we want to follow a fluidized layer, spreading in space, we need to adopt an approach different from the Eulerian reference frame. Instead of time stepping at a fixed location (Eulerian) we now follow the fluidized layer through space (Lagrangian) under the assumption that the fluidized layer flow is stationary.

We define the coordinate frame with x and y as the horizontal coordinates, z as the vertical coordinate and the time coordinate as t. The reference frame can be drawn as shown in Figure 4.2. x=0 is set as the location where the initial conditions apply. z=ζ at the water surface and z=-d at the bed.

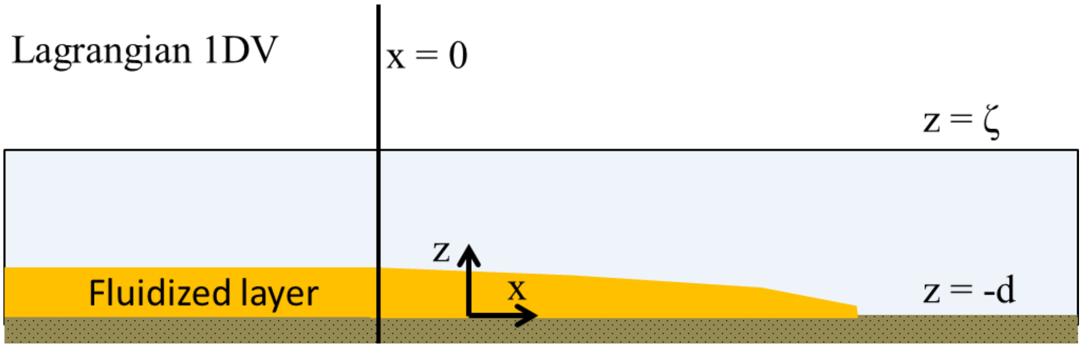

Figure B.2 Conceptual sketch of a fluidized sediment layer, moving over a flat bed. Fluidized sediment is generated at the left hand side of this figure. The fluidized layer is driven by an initial velocity and is sustained by the density difference between the layer and its environment.

In formulaic description, the main assumptions underlying the Lagrangian 1DV approach are:

$$
\begin{aligned}
&u_i(x,y,z,t) = u_i(x,z) \\
&v \equiv 0 \\
&\frac{\partial}{\partial t} \equiv 0\,;\frac{\partial}{\partial y} \equiv 0
\end{aligned}
\tag{2.2}
$$

Hence, observed changes when moving with the flow (Lagrangian reference frame) are only space-dependent and the velocity in y-direction (v) is, by definition, equal to zero. Given these assumptions and approximations, the equations to be solved are given in the next section. For the full derivation, see Appendix B.2.

B.1.3 Governing equations

B.1.3.1 Continuity

Under the assumption that there are no variations in y-direction, the continuity equation simplifies to:

$$\frac{\partial u}{\partial x}+\frac{\partial w}{\partial z}=0 \tag{2.3}$$

B.1.3.2 Momentum equations

To arrive at a 1DV momentum equation set, the Reynolds-Averaged Navier Stokes (RANS) equations need to be reduced, based on the assumptions outlined in Equation (2.2) and the shallow water approximation. The full RANS equations are given in Appendix B.2, Equation (2.19). Here, the reduced equations in x-direction and z-direction are presented:

$$\begin{aligned} u\frac{\partial u}{dx}&=-\frac{1}{\rho}\frac{\partial p}{\partial x}+\frac{\partial}{\partial z}\left\{(\nu+\nu_T)\frac{\partial u}{\partial z}\right\} \\ \frac{\partial p}{\partial z}&=-\rho g \end{aligned} \tag{2.4}$$

From Equation (2.4), the applicable Lagrangian 1DV equation set is derived. The two key aspects in this derivation are listed below, and are treated in more detail in Appendix B.2.

The first step involves linearizing the left-hand side (LHS) of the momentum equation (Equation (2.4)) in x-direction, by rewriting the velocity *u* as dx/dτ. Here, τ is the time that is needed for the fluidized layer to travel along a distance L_x in x-direction. A conceptual sketch is given in Figure B.3 for the case when the depth-averaged velocity $\bar{U}$ is equal to zero. This first step leads to the following momentum equation in x-direction:

$$\frac{\partial u}{\partial \tau}=-\frac{1}{\rho}\frac{\partial p}{\partial x}+\frac{\partial}{\partial z}\left\{(\nu+\nu_T)\frac{\partial u}{\partial z}\right\} \tag{2.5}$$

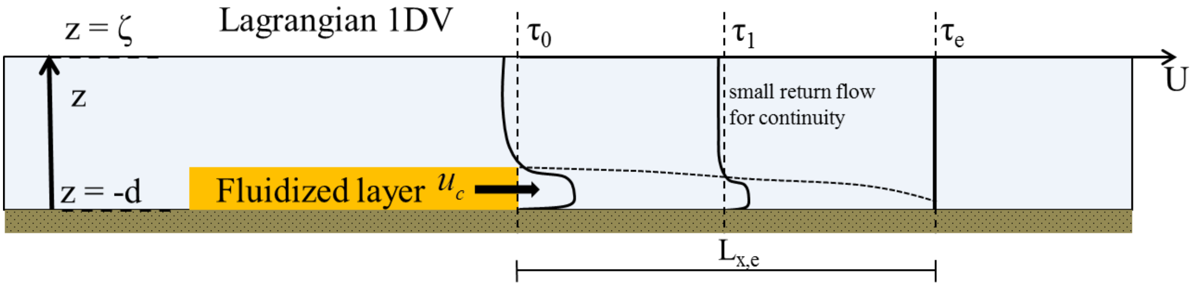

Figure B.3 Vertical velocity profiles along the fluidized layer trajectory. The distance travelled by the fluidized layer is denoted by L_x and its velocity is denoted by u_c. If the depth-averaged velocity $\overline{U}$ is equal to zero, a small return velocity must develop to satisfy the continuity equation.

The second step involves formulating an expression for the horizontal pressure gradient. The horizontal pressure gradient dp/dx drives the flow and consists of both a barotropic and baroclinic contribution. The barotropic pressure gradient only depends on the water level slope, whereas the baroclinic pressure gradient depends (in this case) on sediment-induced density differences over the vertical.

The horizontal pressure gradient (i.e. the driving force) is derived in Appendix B.2.3, and is given by:

$$\frac{\partial p}{\partial x} = \rho(x,\zeta) g \frac{\partial \zeta}{\partial x} - g\left(1 - \frac{\rho_w}{\rho_s}\right) c(\mathrm{x},\mathrm{z}) \tan \beta(x) \tag{2.6}$$

The first term on the RHS of Equation (2.6) is the barotropic contribution, the contribution to the pressure gradient that is independent of density differences over the vertical. The second term on the RHS is the baroclinic contribution to the pressure gradient. This contribution depends on the sediment concentration and the bed slope. The definition sketch for fluidized layer flow down a slope is given in Figure B.4.

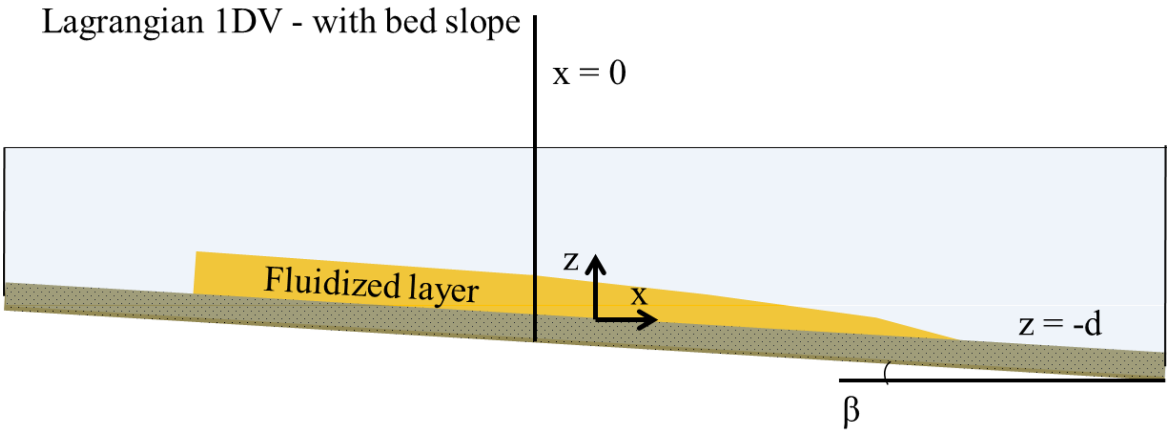

Figure B.4 Conceptual sketch of fluidized layer flow along a slope, with an indication of the bed slope β and the reference frame.

B.1.3.3 *Along-slope distance travelled by the fluidized layer*

The along-slope distance L_x indicated in Figure B.3 is one of the main points of interest when modelling fluidized layer flow. It is computed through the following procedure:

The distance L_x travelled by the fluidized layer along the slope is approximated by integrating the fluidized layer velocity u_c over time, see Equation (2.7).

$$L_x = \int_0^{\tau} u_c \, d\tau \tag{2.7}$$

The fluidized layer velocity u_c is, in turn, approximated by computing the concentration-weighted velocity over the entire vertical (Equation (2.8)).-d and ζ are defined in Figure B.2, and correspond with the lower and upper boundary of the water column, respectively.

$$u_c = \frac{\int_{-d}^{\zeta} Uc \, dz}{\int_{-d}^{\zeta} c \, dz} \tag{2.8}$$

Through these two steps, we can compute the distance travelled by the fluidized layer in the Lagrangian 1DV sense.

B.1.3.4 *Sediment transport, erosion and deposition*

Apart from a correct description of the flow along the slope, the main point of interest of this model is the amount of sediment that is either transported with the fluidized layer or mixed into the water column. To describe this, a sediment transport equation needs to be formulated. The derivation can be found in Section A.4. The sediment transport equation is given by:

$$\frac{\partial c}{\partial \tau} + w\frac{\partial c}{\partial z} = \frac{\partial J_c}{\partial z} + E - D \tag{2.9}$$

Here, E is erosion and D is deposition. Since erosion and deposition are processes taking place at the lower boundary of the computational domain, they are specified in Section B.1.4.

The vertical sediment flux J_c is given by the sum of settling and the diffusive (turbulent) flux. The settling velocity is denoted by w_s and eddy diffusivity is denoted by Γ_T.

B.1.3.5 *Turbulence closure model*

For turbulence closure, the k-ε model is used. This is well-established turbulence closure model, and therefore, the reader is referred to Winterwerp and Uittenbogaard (1997) for the governing equations and the accompanying boundary conditions.

B.1.4 Boundary conditions

Apart from the differential equations, boundary conditions are also needed to actually solve the differential equations in a numerical model. The applied boundary conditions are listed here and are grouped per differential equation. The surface is specified at level ζ and the bed is specified at level –d.

Momentum:
For the momentum equation, the shear stresses at the surface and at the bed need to be specified. If we assume a wind-shear stress is exerted at the surface, these two boundary conditions are:

$$\begin{aligned} \tau(\zeta) &= \tau_s = \rho_{air} C_d \, |\mathrm{U}_{10}| \, \mathrm{U}_{10} \\ \tau(-d) &= \tau_b = \rho \, |u_*| \, u_* \end{aligned} \tag{2.10}$$

Where:
ρ_{air} is the density of air [kg/m^3]
C_d is a friction factor [-]
U_{10} is the wind speed 10 meters above the water surface [m/s]
ρ is the water density [kg/m^3]
u_* is the friction velocity [m/s]

Sediment transport: the sediment fluxes due to settling and turbulent mixingat both the surface (i.e. it cannot rain sediment) are set to zero.

$$w_s c\big|_{z=\zeta} = 0 \, ; \, \Gamma_T \frac{\partial c}{\partial z}\bigg|_{z=\zeta} = 0 \tag{2.11}$$

Where:
w_s is the settling velocity [m/s]
c is the sediment concentration [kg/m^3]
Γ_T is the eddy diffusivity [m^2/s]

At the bed, the boundary condition is specified as:

$$w_s c + \Gamma_T \frac{\partial c}{\partial z} = E - D \tag{2.12}$$

E and D are erosion and deposition, respectively. When the turbulent flux at the bed is zero, the LHS of Equation (2.12) can be split into two parts and is equal to the terms shown in Equation (2.11).

For erosion and deposition, different options are available in the model. For sand, one can either choose between a no-erosion criterion or a reference concentration as formulated by Zyserman and Fredsoe (1994). For the no-erosion criterion, erosion and deposition are specified as follows:

$$\begin{aligned} D &= w_s c_b \\ E &= 0 \end{aligned} \tag{2.13}$$

Where:
w_s is the settling velocity [m/s]
c_b is the near-bed sediment concentration [kg/m^3]

For the reference concentration case, there are no fluxes described on the lower boundary of the computational domain. A reference concentration is described for the lowest grid cell of the domain, and is defined as:

$$c_b = \frac{A(\theta^{'} - 0.045)^n}{1 + \frac{A}{c_m}(\theta^{'} - 0.045)^n} \tag{2.14}$$

Where:
θ' is the Shields parameter related to skin friction [-]
c_b is the near-bed concentration [kg/m^3]
A is a fitting parameter with value: 0.331
N is a fitting parameter with value 1.75
c_m is a fitting parameter with value: 0.46

For mud, one can either choose between a no-erosion criterion or a the Partheniades-Krone formulation. The no-erosion is the same as the one implemented for sand, see Equation (2.13) . The Partheniades-Krone formulation is given by:

$$\begin{aligned} E &= M\, S(\tau_b, \tau_{cr,e}) \\ D &= w_s\, c_b\, S(\tau_b, \tau_{cr,d}) \end{aligned} \tag{2.15}$$

Where:
M is the erosion parameter [kg/m^{2}s]
w_s is the near-bed settling velocity [m/s]
c_b is the near-bed sediment concentration [kg/m^3]

S denotes a step function, and is defined as follows for the erosion formulation:

$$S(\tau_b, \tau_{cr,e}) = \begin{cases} \left(\frac{\tau_b}{\tau_{cr,e}} - 1\right), \text{ when } \tau_b > \tau_{cr,e} \\ 0 \qquad\quad , \text{ when } \tau_b < \tau_{cr,e} \end{cases} \tag{2.16}$$

Where τ_b is the bed shear stress, and $\tau_{cr,e}$ is the critical erosion bed shear stress.
For the deposition formulation, S is defined as follows:

$$S(\tau_b, \tau_{cr,d}) = \begin{cases} \left(1 - \frac{\tau_b}{\tau_{cr,d}}\right), \text{ when } \tau_b < \tau_{cr,d} \\ 0 \qquad\quad , \text{ when } \tau_b > \tau_{cr,d} \end{cases} \tag{2.17}$$

Where τ_b is the bed shear stress, and $\tau_{cr,d}$ is the critical deposition bed shear stress. These step functions express the two following concepts: below a critical bed shear stress, no erosion takes place and above a critical bed shear stress, no deposition takes place.

B.1.5 Initial conditions

The initial conditions passed to the Lagrangian 1DV model consist of three vertical profiles:

- Velocity profile
- Density (or concentration) profile
- Turbulence profile

Apart from the initial profile, another initial condition is the bathymetry over which the fluidized layer will flow.

B.1.6 Staggered grid

The computational domain of the model is divided in a number of layers in the vertical direction denoted by k. At each layer the unknown scalar quantities are defined. Since the 1DV model is based on Delft3D, it also uses a staggered grid. The velocity and concentration are defined in the cell centre (position k) whereas the settling velocity, viscosity, turbulence and fluxes are defined at the cell interface (position k±1/2) (Hanssen, 2016). Figure B.5 visualizes the position of the variables on the vertical grid. For further reference, the reader is referred to the Delft3D-FLOW manual (Deltares, 2016).

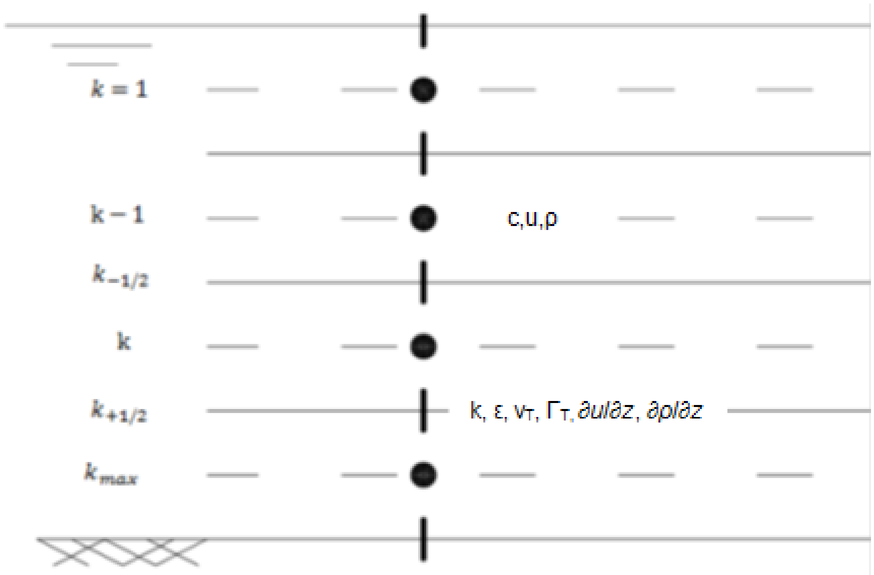

Figure B.5 1DV model staggered grid, modified from Winterwerp (1999) and Hanssen (2016).

B.2 Mathematical description

The equations that are solved in the Lagrangian 1DV model are presented in this section.

B.2.1 Continuity equation

The continuity equation for flow in an incompressible fluid reads:

$$\frac{\partial u}{\partial x}+\frac{\partial v}{\partial y}+\frac{\partial w}{\partial z}=0 \qquad (2.18)$$

B.2.2 Momentum equation

The equations describing the conservation of momentum in a fluid flow are the Navier Stokes equations. For matters of simplicity, we start with the Reynolds-Averaged Navier Stokes (RANS) equations for our derivation of the relevant 1DV model formulations.

In x, y, and z-direction these equations read (respectively):

$$\begin{aligned}
&\frac{\partial u}{\partial t}+u\frac{\partial u}{dx}+v\frac{\partial u}{dy}+w\frac{\partial u}{\partial z}=-\frac{1}{\rho}\frac{\partial p}{\partial x}+\frac{\partial}{\partial z}\left\{(\nu+\nu_T)\frac{\partial u}{\partial z}\right\}\\
&\frac{\partial v}{\partial t}+u\frac{\partial v}{dx}+v\frac{\partial v}{dy}+w\frac{\partial v}{\partial z}=-\frac{1}{\rho}\frac{\partial p}{\partial y}+\frac{\partial}{\partial z}\left\{(\nu+\nu_T)\frac{\partial v}{\partial z}\right\}\\
&\frac{\partial w}{\partial t}+u\frac{\partial w}{dx}+v\frac{\partial w}{dy}+w\frac{\partial w}{\partial z}=-\frac{1}{\rho}\frac{\partial p}{\partial z}+\frac{\partial}{\partial z}\left\{(\nu+\nu_T)\frac{\partial v}{\partial z}\right\}-g
\end{aligned} \tag{2.19}$$

Instead of time stepping at a fixed location (Eulerian) we follow the (fluidized layer) flow through space (Lagrangian) under the assumption that the fluidized layer flow is stationary. This means that observed changes when moving with the flow (i.e. the Lagrangian reference frame) are only space-dependent. This assumption is the key element of the approach adopted in this study.

Furthermore, we assume there are no variations in y-direction and velocity in y-direction (v) is equal to zero. The shallow water approximation is also used, which implies that horizontal scales (wave length l) are much larger than vertical scales (undisturbed water height h). From Equation (2.18) it then follows that $W \approx U\frac{h}{l}$ where h/l <<1.

Using the three assumptions discussed above, we can simplify the RANS equations to:

$$\begin{aligned}
&u\frac{\partial u}{dx}+w\frac{\partial u}{\partial z}=-\frac{1}{\rho}\frac{\partial p}{\partial x}+\frac{\partial}{\partial z}\left\{(\nu+\nu_T)\frac{\partial u}{\partial z}\right\}\\
&\frac{\partial p}{\partial z}=-\rho g
\end{aligned} \tag{2.20}$$

The LHS of the x-direction momentum equation is simplified in two steps: first, W is neglected (applicable if sigma-transformation is applied). The second assumption is the following:

$$u\frac{\partial u}{\partial x}\approx\frac{\partial x}{\partial \tau}\frac{\partial u}{\partial x} \tag{2.21}$$

In this equation, dx/dτ is defined as the concentration-weighted velocity u_c:

$$\begin{aligned}
&\frac{\partial x}{\partial \tau}=u_c\\
&L_x=\int_0^\tau u_c\ d\tau
\end{aligned} \tag{2.22}$$

Herein, u_c is defined as the concentration-weighted velocity:

$$u_c = \frac{\int_{-d}^{\zeta} Uc\,dz}{\int_{-d}^{\zeta} c\,dz} \tag{2.23}$$

This means that the distance L_x travelled along the slope is determined by the bulk of the sediment in the fluidized layer, and not by the ambient velocity. Rewriting Equation (2.21) gives:

$$u\frac{\partial u}{\partial x} \approx u_c\frac{\partial u}{\partial x} = \frac{\partial u}{\partial \tau} \tag{2.24}$$

If this approach is taken, the following two equations remain. The momentum equation in x-direction is the governing equation for this 1DV approach.

$$\begin{aligned} \frac{\partial u}{\partial \tau} &= -\frac{1}{\rho}\frac{\partial p}{\partial x} + \frac{\partial}{\partial z}\left\{(\nu+\nu_T)\frac{\partial u}{\partial z}\right\} \\ \frac{\partial p}{\partial z} &= -\rho g \end{aligned} \tag{2.25}$$

In the upper equation, the term on the RHS can also be written as:

$$\frac{\partial}{\partial z}\left\{(\nu+\nu_T)\frac{\partial u}{\partial z}\right\} = \frac{1}{\rho_w}\frac{\partial \tau_{xz}}{\partial z} \tag{2.26}$$

B.2.3 Pressure gradient

The pressure gradient is the driving force of the 1DV equation. Integrating the momentum equation in z-direction over depth yields:

$$p(\mathrm{x},\mathrm{z}') = \mathrm{p}_{atm} + g\int_{z}^{\zeta} \rho(x,z')dz' \tag{2.27}$$

For a constant density, the equation can be written as:

$$p(\mathrm{x}) = \mathrm{p}_{atm} + \rho g(\zeta - \mathrm{z}) \tag{2.28}$$

Differentiating this equation with respect to x yields:

$$\left(\frac{\partial p}{\partial x}\right)^{BT} = \rho(x)g\frac{\partial \zeta}{\partial x} \tag{2.29}$$

This is the barotropic pressure gradient, which is sketched in Figure B.6. It is independent of depth.

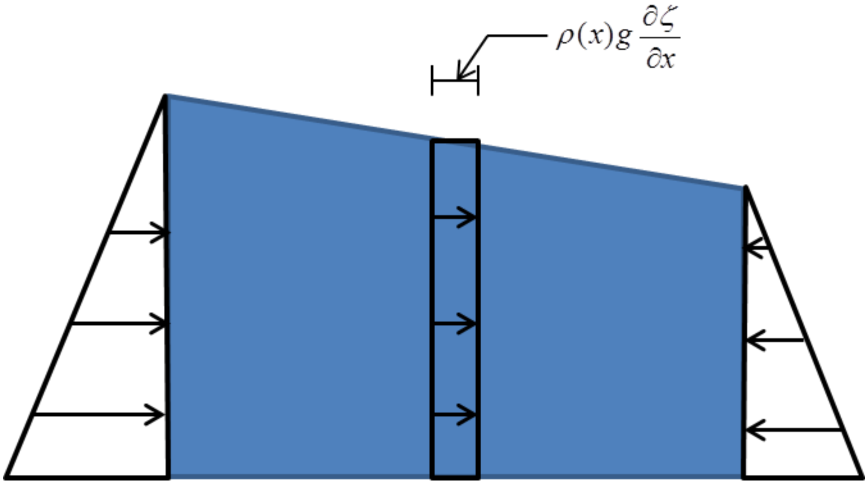

Figure B.6 Sketch of barotropic pressure gradient. As can be seen from the sketch, it is independent of depth.

If density is not constant, differentiating Equation (2.27) with respect to x yields:

$$\frac{\partial p}{\partial x}=\rho(x)g\frac{\partial\zeta}{\partial x}+g\int_z^{\zeta}\frac{\partial\rho(x,z')}{\partial x}dz' \tag{2.30}$$

In this case, the total horizontal pressure gradient consists of a barotropic and a baroclinic contribution. The first term on the RHS of Equation (2.30) is the barotropic contribution and the second term is the baroclinic contribution. To solve the baroclinic term in this equation, an expression is needed for the variation of density along the x-axis. It is assumed that this density difference is induced by sediment concentration gradients only. The density can be expressed as:

$$\rho=\rho_w(1-\phi)+\rho_s\phi \tag{2.31}$$

Where:

$$\phi=\frac{c}{\rho_s} \tag{2.32}$$

Hence:

$$\begin{aligned}\rho&=\rho_w(1-\frac{c}{\rho_s})+\rho_s\frac{c}{\rho_s}\\ \rho&=\rho_w+(1-\frac{\rho_w}{\rho_s})\text{c}\end{aligned} \tag{2.33}$$

If ρ_w and ρ_s are regarded constant, the x-derivative of Equation (2.33) is:

$$\frac{\partial\rho}{\partial x}=(1-\frac{\rho_w}{\rho_s})\frac{\partial c}{\partial x} \tag{2.34}$$

To solve this equation, we need an expression for the variation in sediment concentration along the x-direction. To obtain this, the sediment transport equation is utilized:

$$\frac{\partial c}{\partial t}+u\frac{\partial c}{\partial x}+v\frac{\partial c}{\partial y}+w\frac{\partial c}{\partial z}=\frac{\partial J_c}{\partial z} \tag{2.35}$$

Where J_c is given by:

$$J_c=w_s c+\Gamma_T\frac{\partial c}{\partial z} \tag{2.36}$$

Where the first term on the RHS denotes settling, and the second term on the RHS denotes turbulent vertical mixing of sediment. Note: in Equation (2.36), ws is defined such that it is positive when pointing downwards.

We can simplify Equation (2.35) by assuming stationarity and $v\equiv 0$, which was already assumed during the derivation of the 1DV momentum equations. We then obtain:

$$u\frac{\partial c}{\partial x}+w\frac{\partial c}{\partial z}=\frac{\partial J_c}{\partial z} \tag{2.37}$$

Rewriting this gives:

$$\frac{\partial c}{\partial x}=-\frac{w}{u_c}\frac{\partial c}{\partial z}+\frac{1}{u_c}\frac{\partial J_c}{\partial z} \tag{2.38}$$

As we can see from the sketch in Figure B.7, the tangent of the bottom slope is equal to $-w/u_c$.

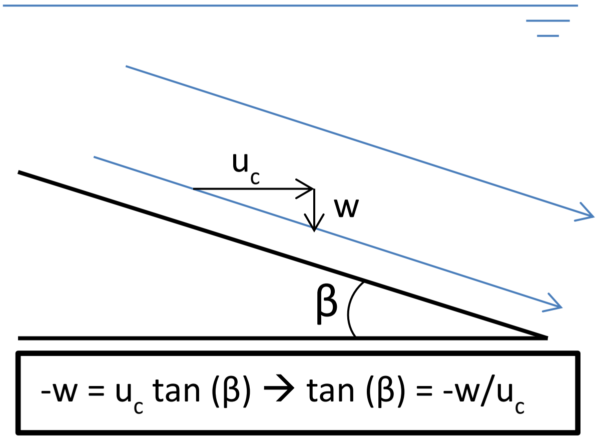

Figure B.7 Sketch of relation between slope angle β, vertical velocity w, and concentration-averaged velocity u_c

$$\frac{\partial c}{\partial x}=\tan\beta(x)\frac{\partial c}{\partial z}+\frac{1}{u_c}\frac{\partial J_c}{\partial z} \tag{2.39}$$

Integrating Equation (2.39) over depth gives:

$$\int_z^{\zeta}\frac{\partial c}{\partial x}=\tan\beta(x)\left[c(\zeta)-c(z)\right]+\frac{1}{u_c}\left[J_c(\zeta)-J_c(z)\right] \tag{2.40}$$

Since there are no fluxes through the water surface, and the concentration at the surface c(ζ)=0, this equation simplifies to:

$$\int_{z}^{\zeta}\frac{\partial c}{\partial x} = -\tan\beta(x)\,c(z) - \frac{1}{u_c}\left(w_s c(z) + \Gamma_T \left.\frac{\partial c}{\partial z}\right|_z\right) \tag{2.41}$$

Combining Equation (2.41) with Equations (2.30) and (2.34) can be achieved if we realize that:

$$\left(1-\frac{\rho_w}{\rho_s}\right)\int_{z}^{\zeta}\frac{\partial c}{\partial x}dz' = \int_{z}^{\zeta}\frac{\partial \rho}{\partial x}dz' \tag{2.42}$$

Thereby, the baroclinic pressure term can be rewritten as:

$$\left(\frac{\partial p}{\partial x}\right)^{BC} = g\left(1-\frac{\rho_w}{\rho_s}\right)\left(-\frac{1}{u_c}J_c(\mathrm{z}) - c(\mathrm{z})\tan\beta(x)\right) \tag{2.43}$$

Substituting the baroclinic contribution in Equation (2.30) with the formulation from Equation (2.43), we arrive at an expression for the total horizontal pressure gradient:

$$\frac{\partial p}{\partial x} = \rho(x,\zeta)g\frac{\partial \zeta}{\partial x} - g\left(1-\frac{\rho_w}{\rho_s}\right)\left(-\frac{1}{u_c}J_c(\mathrm{z}) - c(\mathrm{z})\tan\beta(x)\right) \tag{2.44}$$

The water level gradient (dζ/dx) can be solved through the following procedure. First, the momentum equation is integrated over depth:

$$\int_{-d}^{\zeta}\frac{\partial u}{\partial \tau}dz = -\frac{1}{\rho_w}\int_{-d}^{\zeta}\frac{\partial p}{\partial x}dz + \frac{1}{\rho_w}\int_{-d}^{\zeta}\frac{\partial \tau_{xz}}{\partial z}dz \tag{2.45}$$

The above equation can also be written as:

$$\frac{1}{H}\int_{-d}^{\zeta}\frac{\partial u}{\partial \tau}dz = -\frac{1}{\rho_w}\frac{1}{H}\int_{-d}^{\zeta}\frac{\partial p}{\partial x}dz + \frac{1}{H}\int_{-d}^{\zeta}\frac{\partial \tau_{xz}}{\partial z}dz \tag{2.46}$$

If we now introduce:

$$\overline{U} = \frac{1}{H}\int_{-d}^{\zeta}u\,dz \tag{2.47}$$

Where H=ζ+d, we can write Equation (2.46) as:

$$\frac{\partial \overline{U}}{\partial \tau} = -\frac{1}{\rho_w}\frac{\partial p}{\partial x} + \frac{\tau_{xz}(\zeta) - \tau_{xz}(-d)}{\rho_w H} \tag{2.48}$$

The evolution of the depth-averaged velocity is now controlled by adjusting the total pressure gradient. This is done by adjusting the total pressure gradient so that it follows a user-defined depth-averaged velocity. This is achieved by rewriting Equation (2.48) such, that it becomes:

$$\frac{1}{\rho_w}\frac{\partial p}{\partial x}=\frac{\tau_{xz}(\zeta)-\tau_{xz}(-d)}{\rho_w H}-\frac{\overline{U}_{ref}-\overline{U}}{T_{rlx}} \tag{2.49}$$

If the computed depth-averaged velocity deviates from the reference velocity, the horizontal pressure gradient is adjusted. Using this adjusted pressure gradient, the water level slope can be solved through Equation (2.44). Since the barotropic pressure gradient is depth-independent, the vertical distribution of the horizontal pressure gradient then only depends on the baroclinic term on the RHS of Equation (2.44). With this vertical distribution of the driving force, the horizontal momentum equation (Equation (2.25)) is solved, yielding a new vertical velocity profile.

Combining Equations (2.49) and (2.43) yields an expression for the total pressure gradient:

$$\frac{\partial p}{\partial x}=\rho_w\frac{\overline{U}-\overline{U}_{ref}}{T_{rlx}}+\frac{\tau_{xz}(\zeta)-\tau_{xz}(-d)}{H}-g\left(1-\frac{\rho_w}{\rho_s}\right)\left(-\frac{1}{u_c}J_c(\mathrm{z})-c(\mathrm{z})\tan\beta(x)\right) \tag{2.50}$$

B.2.4 Sediment transport equation

The suspended sediment transport equation reads as follows:

$$\frac{\partial c}{\partial t}+u\frac{\partial c}{\partial x}+v\frac{\partial c}{\partial y}+w\frac{\partial c}{\partial z}=\frac{\partial J_c}{\partial z}+E-D \tag{2.51}$$

Where P_c and ε_c are source and sink terms, respectively. Furthermore, J_c is defined as:

$$J_c=w_s c+\Gamma_T\frac{\partial c}{\partial z} \tag{2.52}$$

Using the assumption described in Equation (2.24), as well as the assumptions of stationarity, zero gradients in y-direction and neglecting the vertical velocity w, this equation can be rewritten to:

$$\frac{\partial c}{\partial \tau}=\frac{\partial J_c}{\partial z}+E-D \tag{2.53}$$

B.3 Flow chart 1DV model

This section is analogous to Section A.9 in Winterwerp & Uittenbogaard (1997). It describes the steps that are subsequently completed in the 1DV model code. Note: this flow chart is only valid for the Lagrangian 1DV model and not for other versions of the 1DV model.

	Description	**Subroutine name**	**Comment**
	<u>start program dpm</u>		
1	initialise arrays	iniarr	
2	create output files	sesam	out1dv, dayzti and daycti files created
3	read input	input	
4	initialise output	iniout	
5	initialise turbulence coefficients	turcof	
6	initialise bed friction	taubot	
7	intialise u, k and ε	init	
8	copy old to new values	f1isf0	
9	initialise density	dens	at t=0, only reference density
10	eddy viscosity and diffusivity	turclo	
11	copy old to new values	f1isf0	
12	construct initial profiles	profil	
13	copy old to new values	f1isf0	
14	write input and t=0 to file	output	
15	wind- and surface-wave properties	updwin	not used in Lagrangian 1DV
16	convert wind speed and direction to friction	windxy	not used in Lagrangian 1DV
17	friction velocity	ustar	
18	initialise online visualisation	online	
	<u>start of time loop, timestep Δt</u>		
19	copy new to old values	f0isf1	
20	alongslope position and slope	updts	
21	bed shear stress	taubot	
22	harmonic series depth-averaged velocity	updfou	not used in Lagrangian 1DV
23	wind- and surface-wave properties	updwin	not used in Lagrangian 1DV
24	convert wind speed and direction to friction	windxy	not used in Lagrangian 1DV
25	eddy viscosity and diffusivity	turclo	
26	friction velocity	ustar	
27	pressure gradient	gradep	barotropic and baroclinic (sediment-induced) pressure gradient calculation
28	solve momentum equation	ucmom	
29	copy new to old values	f0isf1	
30	directional angle of velocity	compas	not used in Lagrangian 1DV
31	friction velocity	ustar	

32	solve k-ε equations	tratur	
33	transport salt and heat	difu	not used in Lagrangian 1DV
34	settling velocity	fallve	with Richardson-Zaki hindered settling
35	reference concentration for SAND	refcon	Zyserman-Fredsoe (1994) formulation
36	transport sediment	difsed	
37	density	dens	reference density and sediment-induced density
38	write results at ref. heights to separate output files	tserie	reference heights specified through zrefs.dat
39	write output to file	output	
40	update online visualisation	online	
	end of time loop		
41	write scratch file to output	outmap	
42	close all open files	shutup	
	end of program dpm		

C Model development

In this Appendix, we elaborate on the model development and present detailed descriptions of the project tasks discussed in Chapter 3 of the main report. The main tasks of this project are:

- Validation of the Lagrangian 1DV approach
- Specify initial conditions for 1DV model
- Test the sensitivity of model outcome on initial conditions
- Implement mud dynamics formulations

C.1 Validation of Lagrangian 1DV approach

In this section, we present the results of the 1DV model validation. This validation consists of three different steps:

1. 1DV model computations are compared with laboratory experiments on turbidity currents

In the past decades, turbidity currents have been extensively studied by means of laboratory experiments and numerical model studies. As we want to validate the 1DV model, we focus on two experimental studies, carried out by Parker et al (1987) and Sequeiros et al (2009), respectively. In these studies, the dynamics of self-accelerating turbidity currents were investigated, using non-cohesive sediment.

2. 1DV model computations are compared with data from Scripps Canyon

After validating the 1DV model against laboratory data, we also performed a brief validation using data from Scripps Canyon, USA. This is one of the few well-documented sites where non-cohesive turbidity currents occur. These have been reported by, for instance, Inman et al. (1976) and by Marshall (1978).

3. 1DV model is tested with upsloping and downsloping bathymetry

The third step is to validate if the 1DV model can be used for both downsloping and upsloping beds.

C.1.1 Experiments of Parker et al. (1987)

C.1.1.1 Description of experiments

From Parker et al. (1987):
“Experiments were conducted to determine the behaviour of turbidity currents laden with non-cohesive silt (silica flour) moving down a slope the bed of which is covered with similar silt. Each current was sustained with constant inlet conditions for six to eight minutes. The motion of the head was not studied; measurements were concentrated on the continuous part of the current that was essentially constant in time but developing in space. Only supercritical currents were studied. The currents were free to erode sediment from, and deposit sediment on, the

bed. Measurements of vertical profiles of downstream velocity and sediment concentration allowed for the development of approximate similarity relations.”

C.1.1.2 Experimental setup

Experiments were carried out at the St. Anthony Falls Laboratory of the University of Minnesota. The flume used in this experiment is drawn in Figure C.1. The water depths at the upstream and downstream end are 0.7 and 1.7m, respectively. The length of the flume is between 23 and 17.5m, dependent on the bed slope of the sloping false bottom. The flume has a constant width (b) of 0.7m.

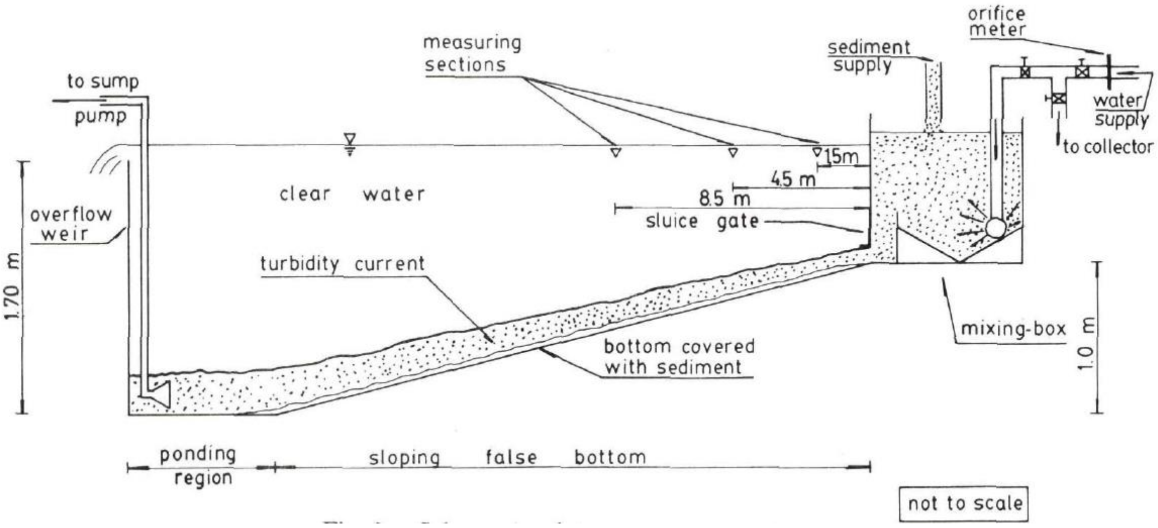

Figure C.1 Overview of experimental setup as reported by Parker et al. (1987)

C.1.1.3 Collected measurements

In total, 24 experimental runs were executed in this experimental setup. After a steady, continuous turbidity current had developed, measurements commenced. Velocity and concentration measurements were taken along the vertical at three stations located along the channel centerline. These stations were located 1.5 m, 4.5 m and 8.5 m downstream from the inlet from the mixing box, respectively.

C.1.1.4 Experimental run 13: settings and measured profiles

The experimental run that is described most extensively by Parker et al. (1987) is Run 13. The settings of this run, as given by Parker et al. are summarized in Table C.1. The run is characterized as an accelerating and depositing turbidity current. The turbidity current-averaged velocity increases, whereas the total sediment transport rate decreases between the first and third measurement station.

Table C.1 Parameter settings in Experiment 13 of Parker et al. (1987)

Parameter	Value
d_{50} sediment	30 µ
Slope	0.05
Depth-averaged inlet velocity (U_0)	0.27 m/s
Inlet height (h_0)	0.08 m
Water discharge through inlet (Q_{w0})	15 l/s
Sediment discharge through inlet (Q_{s0})	164.6 g/s
Volumetric sediment concentration at inlet (C_0)	$4.1*10^{-3}$
Sediment density	2650 kg/m^3
Sediment concentration in g/l at inlet	10.9 g/l

A depth-mean velocity was not given by Parker et al. but this was calculated. From continuity, it follows that, $Q_{w0}=Q_{out}$. Under the assumption that there is no ambient flow through the flume, $\overline{U}$ can be calculated by dividing the discharge by the flow area. Since the measurements were taken along the upper part of the slope, we use the average water depth between the inlet and the third measurement section (at 8.5m) which was calculated to be 0.9m. If we then use the expression $\overline{U} = Q_{w,0}/(h*b)$ we arrive at an approximate value of $\overline{U}$=0.025 m/s.

The measurements taken during this experimental run are shown in Figure C.2. These measurements have been digitized and will be compared with model runs in the following subsection.

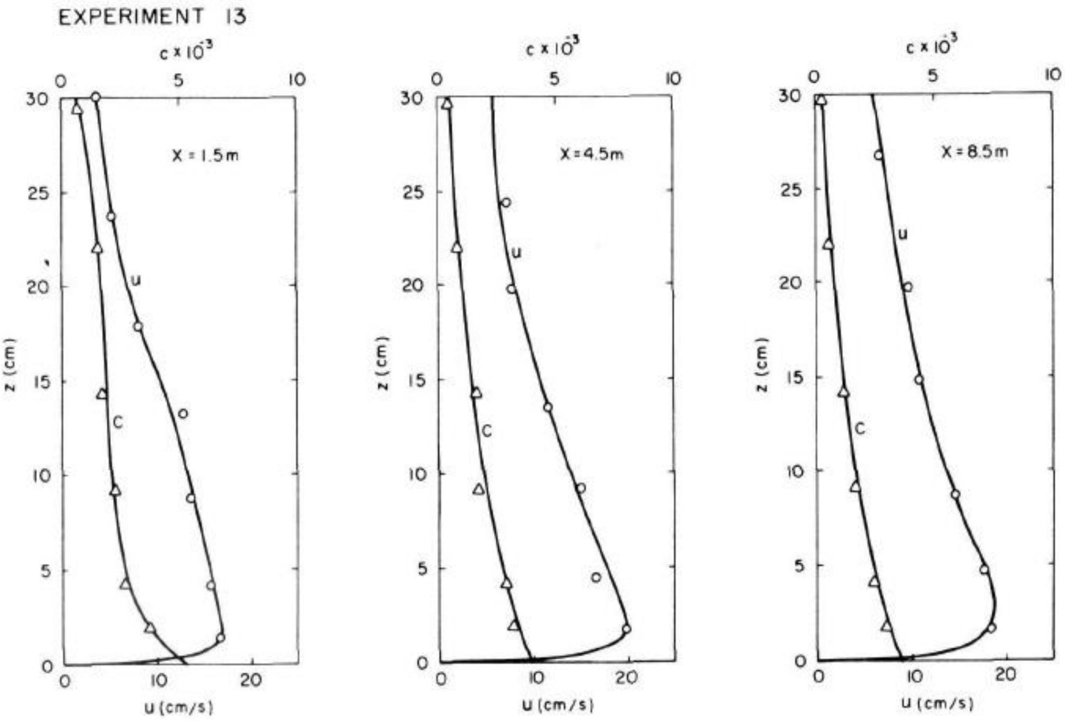

Figure C.2 Velocity and concentration profiles measured at 1.5, 4.5 and 8.5m from the inlet, during experiment 13. After Parker et al. (1987).

“The behaviour of continuous silt-laden turbidity currents moving over a bed of similar sediment was studied in the laboratory. Experimental data were used to establish approximate similarity laws for the velocity and concentration distribution. Most of the runs displayed neither strong deposition nor strong erosion.” Self-acceleration of the turbidity current could not be directly verified, which is attributed to the shortness of the sloping bed (maximum 20m long). During the experimental runs, small bedforms developed on the sediment bed, with typical heights of several millimetres and typical lengths of several centimeters. Furthermore, downstream fining of the substrate was observed during the runs.

C.1.2 Lagrangian 1DV model vs. experiments of Parker et al. (1987)

This section describes the model runs performed with the Lagrangian 1DV model. The goal of these runs is to verify that the Lagrangian 1DV model produces results that are similar to the experiments performed by Parker et al (1987). We do not aim to obtain perfect fits, but much rather a qualitative agreement based on the experimental settings given by the authors.

To reproduce the experimental setup by Parker et al. (1987) for Experiment 13, computations were set up with a time step of 0.01 seconds, a total duration of 120 seconds and 300 grid cells over the vertical. The parameters listed in Table C.2 are kept constant throughout the model runs.

Table C.2 Parameter settings for model runs based on experimental setup Parker et al (1987)

Parameter	Value
d_{50} sediment	30 µ
Slope	0.05
Inlet velocity (U_0)	0.27 m/s
Inlet height (h_0)	0.08 m
Sediment concentration in g/l (c_0)	10.9 g/l
Velocity profile at inlet	double logarithmic function
sediment profile at inlet	step function
d_{90} sediment (for bed roughness)	50 µ
z_0	$5*10^{-6}$ m

The initial velocity profile is comparable with turbulent pipe flow velocity profiles.
The bed roughness is calculated using the expression by van Rijn (1984) for the Nikuradse roughness height:

$$k_s = 3 * d_{90}$$

The roughness coefficient is then calculated as:

$$z_0 = \frac{k_s}{30} \Rightarrow z_0 = \frac{d_{90}}{10}$$

C.1.2.1 Model results and discussion – run t25a

Model run t25a can be seen as a base case, and was performed with a depth-averaged flow velocity ($\overline{U}$) of 0.025 m/s. Vertical profiles are obtained for the three measurement stations (at 1.5, 4.5 and 8.5m downstream of the inlet).

Vertical profiles of velocity and concentration are shown in Figure C.3 and Figure C.4, respectively.

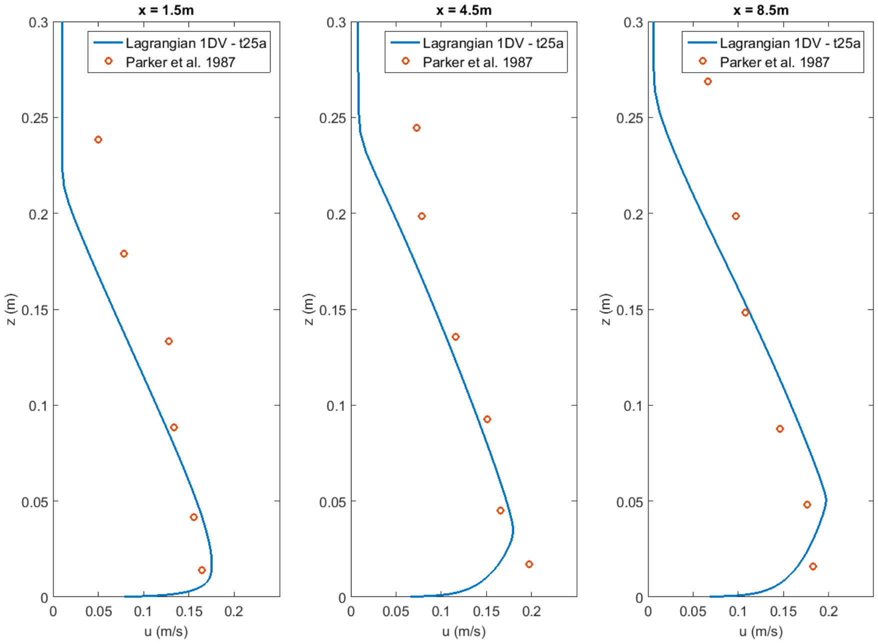

Figure C.3 Results of model run t25a. Velocity profiles computed using the Lagrangian 1DV model compared to the measurements of Parker et al. (1987)

Qualitatively, the model results agree quite well with the measurements. Acceleration is observed between x=1.5 and x=8.5. Furthermore, the sediment transport rate decreases as the turbidity current moves downstream.

The computations are mainly sensitive to the following two settings:

- Depth-averaged velocity ($\bar{U}$)
- Formulation of deposition and erosion

Although Parker et al did not report any flow velocities outside the turbidity current itself, the measured velocity profiles suggest an ambient velocity did occur during the experiments. This is also visible in Figure C.2. The velocities computed with the Lagrangian 1DV model approach zero for z-coordinates larger than the turbidity current height, but the measurements show a persistent offset of 0.05 m/s. This may be due to water being dragged along by the turbidity current, which may also affect the overall flow velocity in the experimental facility.

In the Lagrangian 1DV model, erosion and deposition are modelled using the Zyserman and Fredsoe (1994) reference concentration. This reference concentration is equal to zero when the computed Shields parameter θ is smaller than the critical Shields parameter θ_{cr}. If $\theta < \theta_{cr}$, the concentration in the lowest grid cell is calculated as the sum of the advective and diffusive fluxes to and from this grid cell. In this case, the shield parameter is often close to θ_{cr}, which may yield unrealistically low sediment concentrations. A flux formulation specifying an erosion flux into the lowest grid cell (a ‘pickup’ function) may be more appropriate in this case.

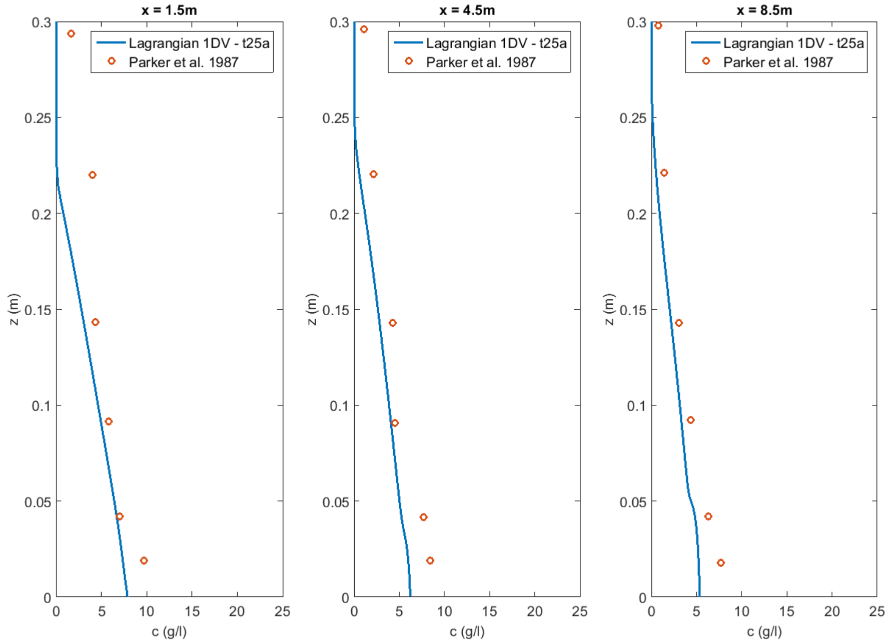

Figure C.4 Results of model run t25a. Concentration profiles computed using the Lagrangian 1DV model compared to the measurements of Parker et al. (1987)

C.1.3 Experiments of Sequeiros et al. (2009)

C.1.3.1 Description of experiments

Summary taken from Sequeiros et al. (2009):

“This study presents the results of laboratory experiments where self-acceleration of the head of a turbidity current has been achieved for certain combinations of velocity, concentration and characteristics of the sediment. These characteristics include grain size distribution, sediment cohesiveness or lack thereof, and density. All the above parameters play an important role in the development of the turbidity current; only under appropriate conditions will the entrainment of sediment from the bottom overcome deposition, so creating a necessary condition for self-acceleration.”

C.1.3.2 Experimental setup

Experiments were carried out at the Ven Te Chow Hydrosystems Laboratory of the University of Illinois. The flume used in this experiment is drawn in Figure C.5. The water depths at the upstream and downstream end are 0.47 and 1.19m, respectively. The length of the flume is 14.6m, dependent on the bed slope of the sloping false bottom. The flume has a constant width of 0.45m.

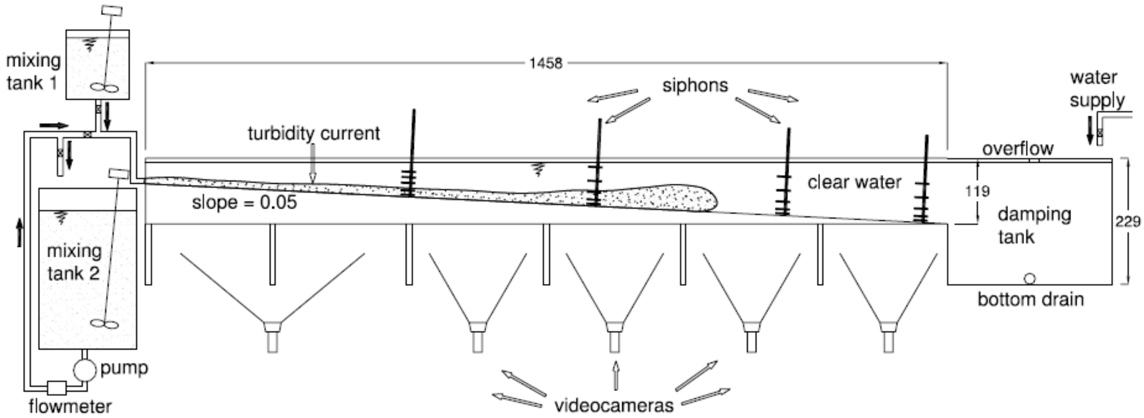

Figure C.5 Sketch of turbidity current flume and location of siphons that are used for measuring suspended sediment concentration. Length units are in centimeters. After Sequeiros et al. (2009)

C.1.3.3 Collected measurements

“Four sets of experiments were run, corresponding to four different sediment mixtures (A, B, C, and D) and two sediment types (I and II). A total of 27 tests were performed.
Four rakes of siphons located 4.8, 8.0, 11.6 and 14.3 meters from the inlet were used to obtain suspended sediment samples at distances of 0.9, 3.1, 7.7, 12.2, and 20.3 cm from the bed as the turbidity current head passed through them (see also Figure C.5). The sampling procedure was controlled manually for each siphon in all sets. All siphons were triggered before the passing of the current, and were kept flowing continuously. As the head of the current arrived at a given rake, the samples were collected in beakers, one for each siphon.”

C.1.3.4 Experimental run 11: settings and measured profiles

The experimental run that is examined further is Experiment 11. The turbidity current generated in this experiment is classified as an accelerating/bypassing turbidity current. This means that the turbidity current is self-accelerating and may achieve autosuspension along its path. Parameter settings for this run are listed in Table C.3.

Table C.3 Parameter settings in Experiment 11 of Sequeiros et al (2009)

Parameter	Value
d_{50} sediment	71 µm
Slope	0.05
Depth-averaged inlet velocity (U_0)	0.256 m/s
Inlet height (h_0)	0.05 m (diffuser)
Water discharge through inlet (Q_0)	5.77 l/s (at t=0)
Volumetric sediment concentration at inlet (C_0)	0.2331
Sediment density	1300 kg/m^3
Sediment concentration in g/l	300 g/l

U_0 is calculated by dividing the water discharge through the inlet by the flume width and the inlet height ($U_0=Q_0/(h_0*b)$).

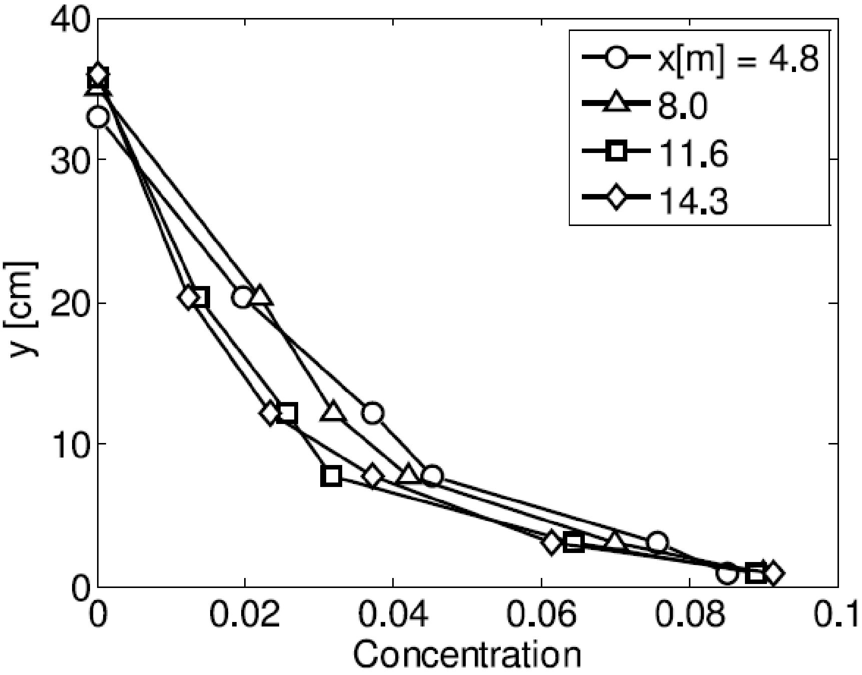

Figure C.6 Concentration profiles within the head of the turbidity current at different locations downstream from the inlet, during experiment 11. After Sequeiros et al. (2009).

C.1.3.5 *Conclusions*

A total of 27 experiments, using both pulsed and continuous flow conditions, are reported in the paper by Sequeiros et al (2009): “In all the experiments, a dense bottom flow driven by a suspension of lightweight plastic particles flowed out over a bed of similar particles emplaced by an antecedent flow. Self-acceleration of the head was identified in three of these experiments. The criterion used to identify self-acceleration was the existence of a significant reach over which both the velocity of the head and the suspended sediment carried within it increased in tandem in the downstream direction. All of the flows that were observed to undergo self-acceleration were created by introducing the sediment as a surface plume into the flume. After a short distance, this surface plume plunged.
Evidently, the loss of sediment from the surface plume by settling, and in particular the loss of the coarser sizes, created advantageous conditions for self-acceleration downstream of the plunging point.”

C.1.4 Lagrangian 1DV model vs. experiments of Sequeiros et al. (2009)

This section describes the model runs performed with the Lagrangian 1DV model. The goal of these runs is to verify that the Lagrangian 1DV model produces results that are similar to the experiments performed by Sequeiros et al (2009). It is important to realize measurements were made while the head of the turbidity current passed the measurement stations. The head of the turbidity current is non-stationary, which violates the primary assumption of the Lagrangian 1DV model. Therefore, the measurements may differ substantially from the Lagrangian 1DV model results.

C.1.4.1 Model setup

To reproduce the experimental setup by Sequeiros et al. (2009) for Experiment 11, computations were set up with a time step of 0.01 seconds, a total duration of 120 seconds and 300 grid cells over the vertical. The parameters listed in Table C.4 are kept constant throughout the model runs.

Table C.4 Parameter settings for model runs based on experimental setup Sequeiros et al (2009)

Parameter	Value
d_{50} sediment	71 µm
Slope	0.05
Inlet velocity (U_0)	0.256 m/s
Inlet height (h_0)	0.05 m
Sediment concentration in g/l (c_0)	300 g/l
Velocity profile at inlet	double logarithmic function
sediment profile at inlet	step function
d_{90} sediment (for bed roughness)	90 µm
z_0	$9*10^{-6}$ m

C.1.4.2 Model results and discussion

Model run t30a is the base case and was performed with a depth-averaged flow velocity ($\bar{U}$) of 0.015 m/s. Vertical profiles are obtained for the four measurement stations (at 4.6, 8.0, 11.6 and 14.3 m downstream of the inlet).

Vertical concentration profiles are shown in Figure C.7.

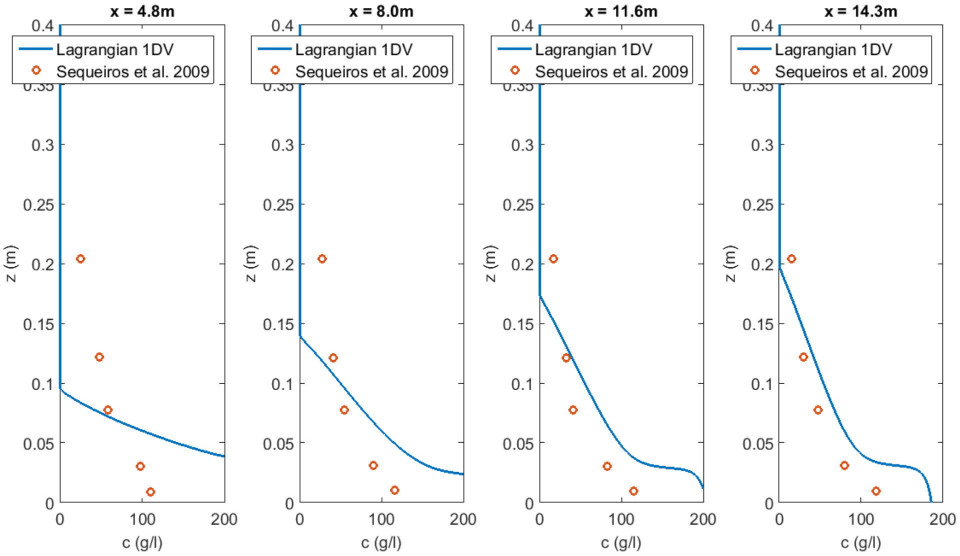

Figure C.7 Results of model run t30a. Concentration profiles computed using the Lagrangian 1DV model compared to the measurements of Sequeiros et al. (2009)

In spite of the non-stationary nature of the turbidity current head, the model results show a satisfactory agreement for the two most downstream measurement stations.

For the first measurement station, modelled near-bed concentrations are very high, due to the high flow velocities. These flow velocities directly translate to high concentrations through the Zyserman & Fredsoe (1994) reference concentration. In this case, a pickup function as formulated by van Rijn (1984) or Mastbergen and van den Berg (2003) is more appropriate. As velocities decrease along the slope, the near-bed concentrations approach the measured concentrations.

C.1.5 Scripps canyon tests

After validating the Lagrangian 1DV approach with lab data, we also validate the model with field data. For this, we use Scripps Canyon as the field site of interest. Turbidity currents that occur in Scripps Canyon have been documented by several authors. We base the description of the study site on the work by Mastbergen and van den Berg (2003). We will also use the results from their study as input for the 1DV model setup.

C.1.5.1 Scripps canyon

After Mastbergen and van den Berg (2003):”Scripps Canyon is one of the nine major submarine canyons that intersect the continental shelf off southern California. It consists of a number of branches, eroded in sedimentary bedrock. A map showing the hydrography is shown in Figure C.8. The tributaties and the head of the branches are filled with sand most of the time, which may reach a thickness of 5m. The sediment that is temporarily stored at the head of the canyon has a median grain size ranging between 95 and 125 µm.

By comparing successive hydrographic surveys, Chamberlain (1964) demonstrated large sand losses, in the order of 1-2 × 10^5 m^3, occurred nine times in a period of 11 years. Such losses were often restricted to one branch, and the sand was transported down the valley by sediment gravity flows.

As Scripps Submarine Canyon is a more or less linear feature, a one-dimensional model should be able to represent satisfactorily the main characteristics of a turbidity current flowing through it. In their paper, Mastbergen and van Berg present the results of a modelling study where they use a non-uniform, quasi-steady, two-layer, depth-averaged model.

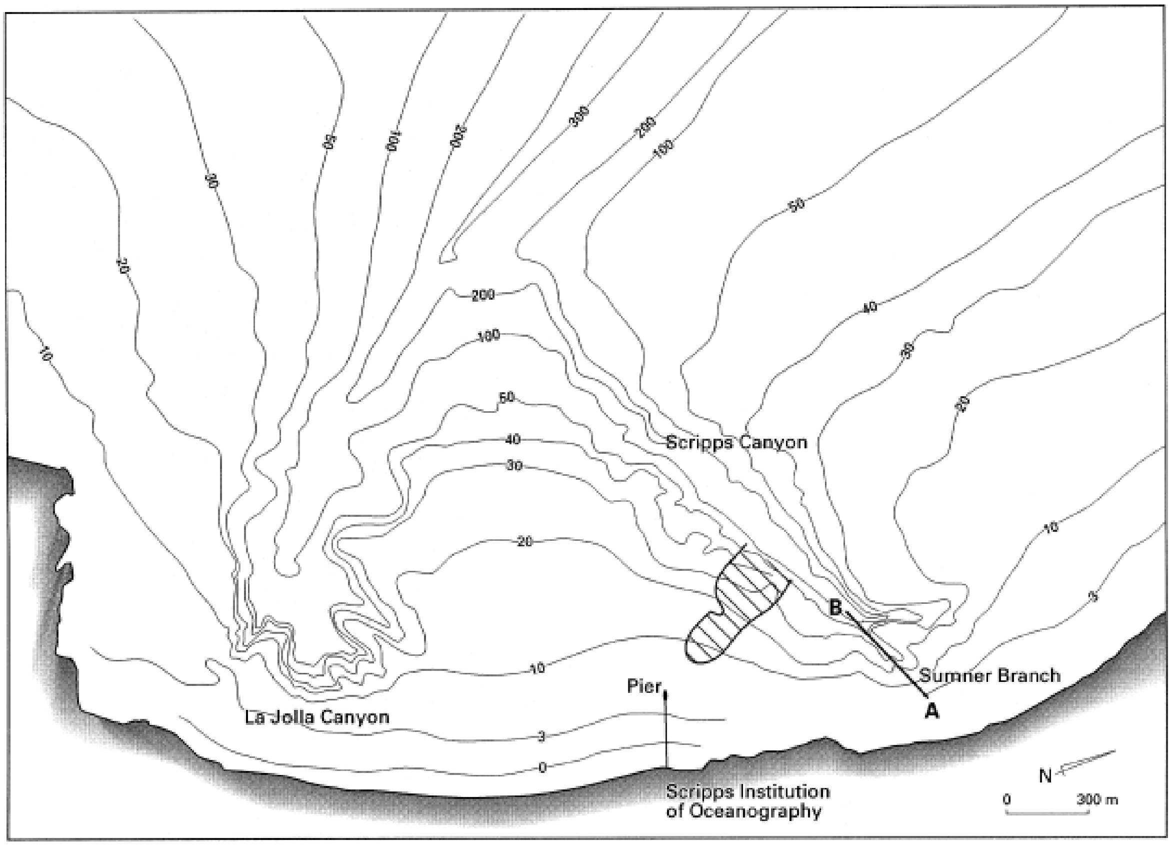

Figure C.8 Hydrography of La Jolla and Scripps submarine canyons. A-B denotes the thalweg of Sumner Branch (shown in Figure C.9). Cross-hatched area marks the location of 1975 'flushing' event (Marshall, 1978). Contours in meters below mean low water at spring tide (after Mastbergen and van den Berg, 2003).

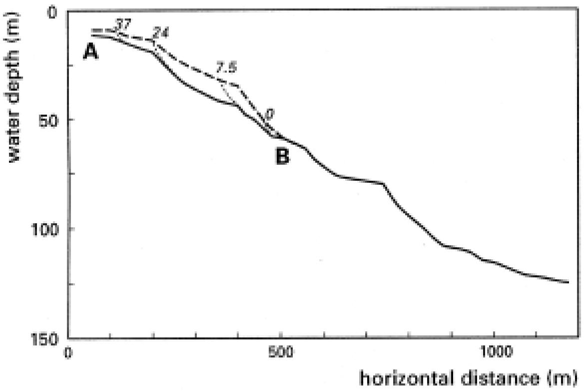

Figure C.9 Thalweg profile of Sumner Branch (see Figure C.8 for location). Solid line is sedimentary bedrock, dashed line is top of sand fill. Indicated numbers are the hours after breach was initiated (after Mastbergen and van den Berg, 2003).

C.1.5.2 Model setup

The 1DV model is initialized using the results from the modelling efforts by Mastbergen and van den Berg (2003). We base the initial sediment flux for the 1DV model on the sand transport rate values in Figure C.10. Two separate test cases are formulated: the first test case corresponds to the ‘37’ case, whereas the second case corresponds to the ‘24’ case. The starting point for the 1DV along the slope corresponds to the x-coordinate for which the maximum sand transport rate is reached in the two cases. For the ‘37’ case, this is after 150m along the slope. For the ‘24’ case, this is after 300m along the slope.

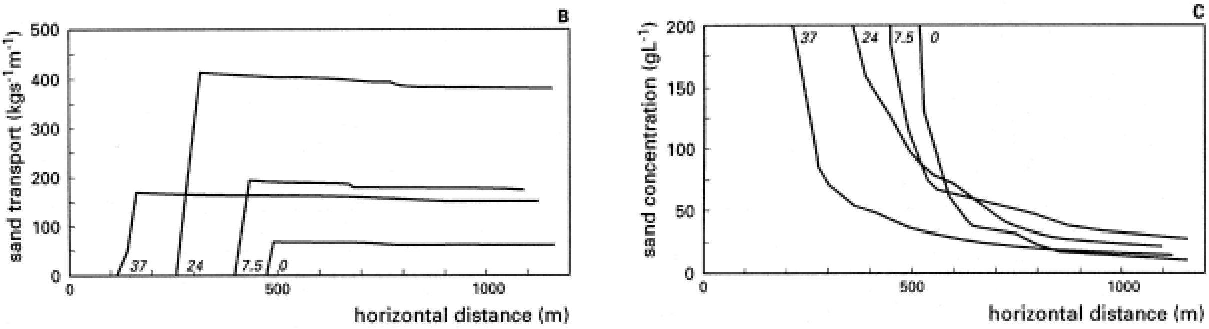

Figure C.10 Sand transport rate (panel B - left) and sediment concentration (panel C - right) along the slope, as calculated by Mastbergen and van den Berg (2003).

The settings that are equal for the two test cases are listed in Table C.5. We assume that the turbidity current does not erode sedimentary bedrock along its path, and thus specify that erosion should be zero.

Table C.5 Parameter settings in the 1DV model that are equal for both test cases

Parameter	**Value for both case 1 & 2**
water depth [m]	30
depth-averaged flow velocity [m/s]	0
roughness height (z_0) [m]	$1.5*10^{-5}$
background eddy viscosity [m^2/s]	$1.0*10^{-4}$
water density [kg/m^3]	1020
Number of sediment fractions	1 – SAND
Median grain size [m]	$1.1*10^{-4}$
Erosion formulation	No erosion
Initial turbidity current velocity [m/s]	1.0
Initial turbidity current concentration [kg/m^3]	200

We assume that the initial average concentration ($\bar{c}$) in the turbidity current does not exceed 200 g/l (see right panel Figure C.10), and the initial average velocity is equal to 1 m/s. We apply the initial concentration as a step function, and the initial velocity as a profile consisting of a logarithmic velocity profile combined with a hyperbolic tangent profile (mixing layer form).
Based on these assumptions, we can calculate the height of the turbidity current which will be set as the initial condition for the 1DV model. These settings are listed in Table C.6.

Table C.6 Parameter settings in the 1DV model that differ for both test cases

Parameter	Case 1: “37”	Case 1: “24”
Initial sediment transport rate [kg/m*s]	160	400
initial turbidity current height [m]	0.8	2.0

C.1.5.3 Model results

First, we compare the model results with a velocity measurement taken in Scripps Canyon at the end of 1968. At 44m water depth, 2 meters above the bed, a current meter recorded a flow velocity of 1.9 m/s for almost two hours. Afterwards, the current meter was lost due to the sheer force of the turbidity current. When we compare the modelled velocities with this measurement (Figure C.11), we see that the model computes velocities that have the correct order of magnitude.

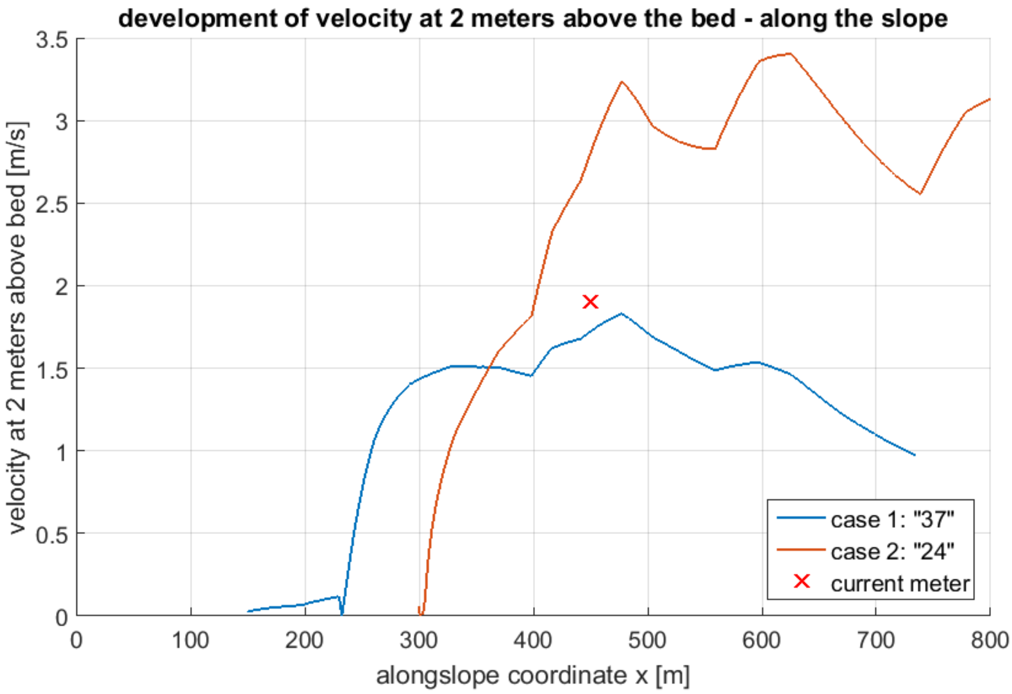

Figure C.11 Velocities computed by the 1DV model, compared to the flow velocity measurement at 2 meters above the bed.

We also compare the results of the 1DV model with the model results of Mastbergen and van den Berg (2003). We compare two output parameters:

- The turbidity current velocity (in 1DV model: concentration-averaged velocity)
- The sediment transport rate

The results of this comparison can be seen in Figure C.12 and Figure C.13. The turbidity current velocities show similar developments, of which the agreement is satisfying given the large uncertainties in model input and further settings.

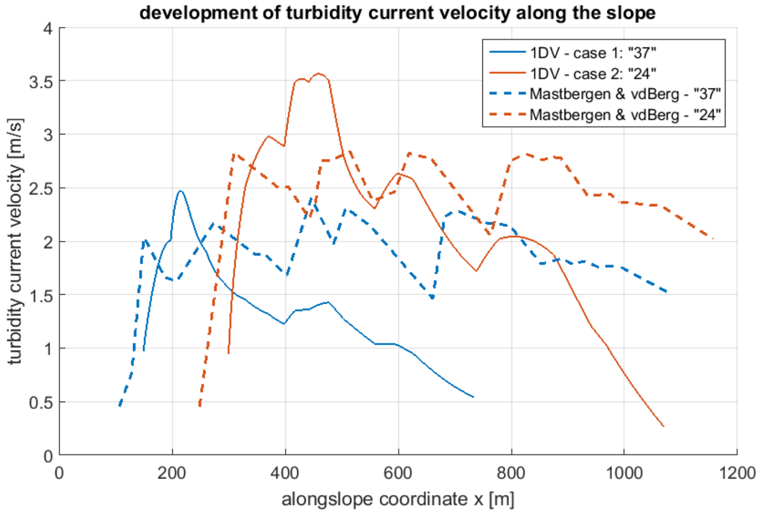

Figure C.12 Comparison of 1DV model output with results of Mastbergen and van den Berg (2003) - turbidity current velocity.

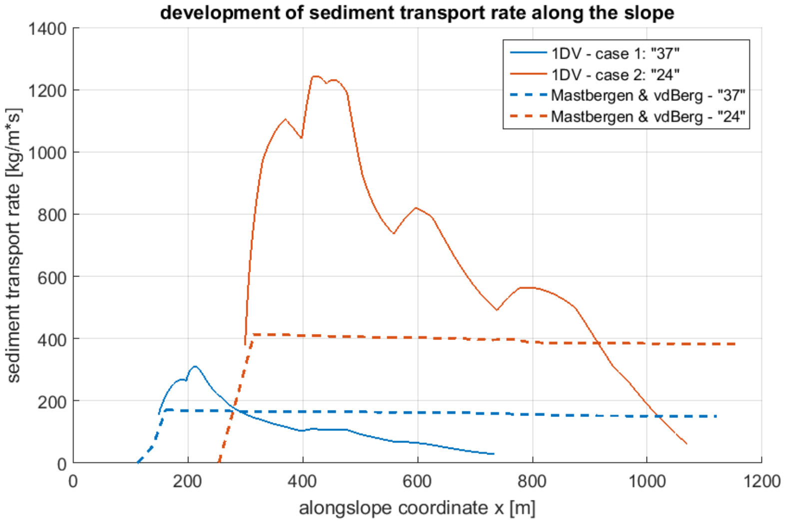

Figure C.13 Comparison of 1DV model output with results of Mastbergen and van den Berg (2003) – sediment transport rate.

The sediment transport rates computed with the Lagrangian 1DV model are initially higher than the model results of Mastbergen and van den Berg (2003) (Figure C.13). To understand where these deviations originate from, we also plot the concentration-weighted velocity (u_c) and the suspended sediment mass (c_{total}) in 1DV (Figure C.14).

The lower panel of Figure C.14, we see that the total suspended sediment mass decreases along the slope. This is expected, as there deposition takes place along the entire slope and there is no erosion. The upper panel shows that the concentration-weighted velocity strongly increases for the first hundreds of meters along the slope. As the sediment transport rate is the product of these two terms, this also increases. However, this large increase is not realistic, as it implies a source of sediment in the domain that is not present.

The increase in sediment transport rate is caused by the baroclinic contribution to the pressure gradient. Due to the steep slope and large sediment mass, there is a strong acceleration in the turbidity current and thus in concentration-weighted velocity (u_c). When a gravity current strongly accelerates or decelerates along its trajectory, the streamlines of the gravity current may converge or diverge strongly. In these cases, we may no longer neglect the advective contributions to the alongslope pressure gradient and sediment transport, as we have done in deriving Equation (2.39), (2.50) and (2.53). Hence, the Lagrangian 1DV approach may no longer be valid. This appears to be the case for the computed test case of the Scripps canyon.

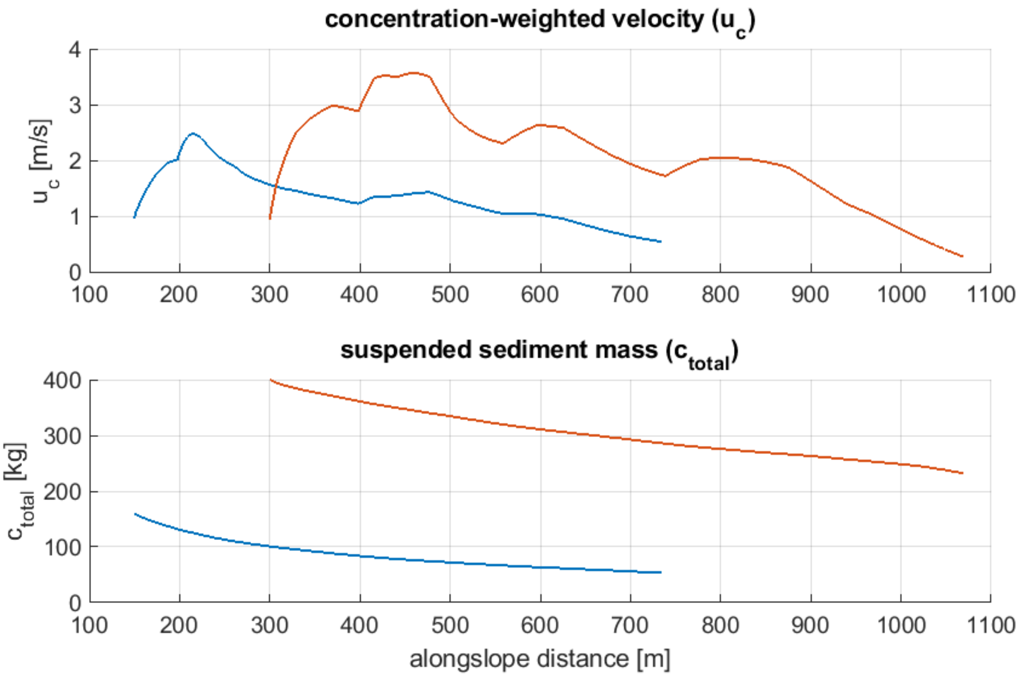

Figure C.14 concentration-weighted velocity and total suspended sediment mass for the Scripps canyon test case

The Lagrangian 1DV approach is most accurate when the initial conditions lie close to stationary conditions, i.e. the driving force due to gravity is almost in equilibrium with the friction term. Additionally, if the gravity current does not decelerate nor accelerate suddenly along its trajectory, the streamlines of the gravity current run parallel to the slope. If this is the case, the development of the alongslope pressure gradient driving the gravity current can accurately be approximated by Equation (2.50) (Appendix B.2.3), assuming Equation (2.39) is valid, and sediment transport can be approximated by Equation (2.53). This is the case for mild slopes (1:100 or less) and when initial conditions do not deviate strongly from stationary conditions. The approach may still work for steeper slopes, when initial conditions are in close agreement with stationary conditions.

C.1.5.4 Conclusions

- Lagrangian 1DV model validated against turbidity current observations and previous modelling work
- 1DV model computes velocities that have the same order of magnitude as observed velocities in Scripps Canyon
- Modelled sediment transport rates increase strongly along the slope. Such an increase is not realistic,

- Lagrangian 1DV approach is probably not valid for the Scripps canyon test case, using the current set of initial conditions. The gravity current strongly accelerates after initiation, hence advective terms become important. These are neglected in the setup of Lagrangian 1DV.
- Lagrangian 1DV approach is most accurate when a gravity current does not decelerate nor accelerate suddenly along its trajectory. This is the case for mild slopes (1:100 or less) and when initial conditions do not deviate strongly from stationary conditions.

C.1.6 Upsloping and downsloping bathymetries

The third step is to validate if the 1DV model can be used for both downsloping and upsloping beds. The lab experiments and field data were collected for turbidity currents. These generally occur on steep, downsloping bathymetries. For fluidized layer flow, the slopes are expected to be much milder, and may switch between up- and downsloping. Therefore, it is necessary to test how the model performs when fluidized layer flow over an upsloping bed is computed. To this end, three computations are performed and their results compared:

- Fluidized layer flow over a <u>flat</u> bed
- Fluidized layer bed over a <u>downsloping</u> bed
- Fluidized layer flow over an <u>upsloping</u> bed

All three bathymetric profiles start with a flat section of 30m long. Afterwards, the downsloping bed goes down with a slope of 0.05 for 200m. The upsloping bed has the same slope but goes up for 200m. It is important to note that these profiles do not influence the computational domain, i.e. the height of the water column. This remains constant throughout all runs. Furthermore, erosion is not enabled in these model runs.

C.1.6.1 Model settings & initial profile

The model is run with the same set of parameters for all three runs, apart from the imposed bathymetric profiles. The fluidized layer is modelled by imposing a logatrithmic velocity profile at x = 0m over the fluidized layer height (h_0), and by imposing sediment as a step function over the same height h_0. The initial profiles are drawn in Figure C.15.

The model is run for 300s, with a time step of 0.01 seconds. The computational domain consists of 300 grid cells. Physical parameters are listed in Table C.7.

Table C.7 Parameter settings for model runs to test sloping bed

Parameter	Value
Water depth	10 m
d_{50} sediment	100 µm
Depth-averaged velocity ($\bar{U}$)	0.1 m/s
Fluidized layer velocity (U_0)	1.0 m/s
Fluidized layer height (h_0)	1.0 m
Fluidized layer concentration in g/l (c_0)	100 g/l
Velocity profile fluidized layer	logarithmic function
sediment profile fluidized layer	step function
z_0	$1.5*10^{-5}$ m

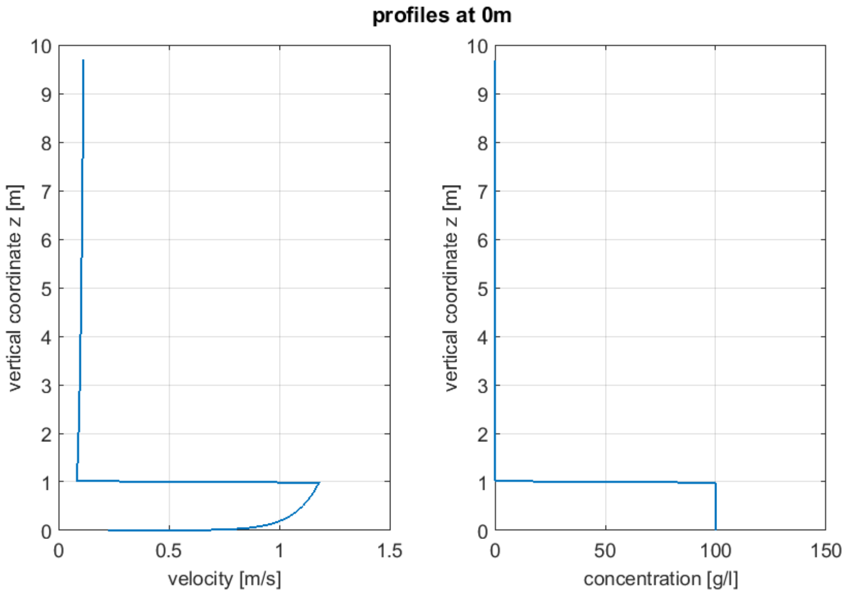

Figure C.15 Initial profiles for testing upsloping and downsloping bathymetries

C.1.6.2 *Model results for initial phase*

For the first 30m of the model domain, the model settings are identical and thus, the model results are identical. In this section, we show how the velocity and concentration profile develop over the first 30m, by plotting vertical profiles of the pressure gradient, velocity and concentration for the lower 3m of the water column. Profiles for x = 15m and x = 30m are shown in Figure C.16 and Figure C.17, respectively.

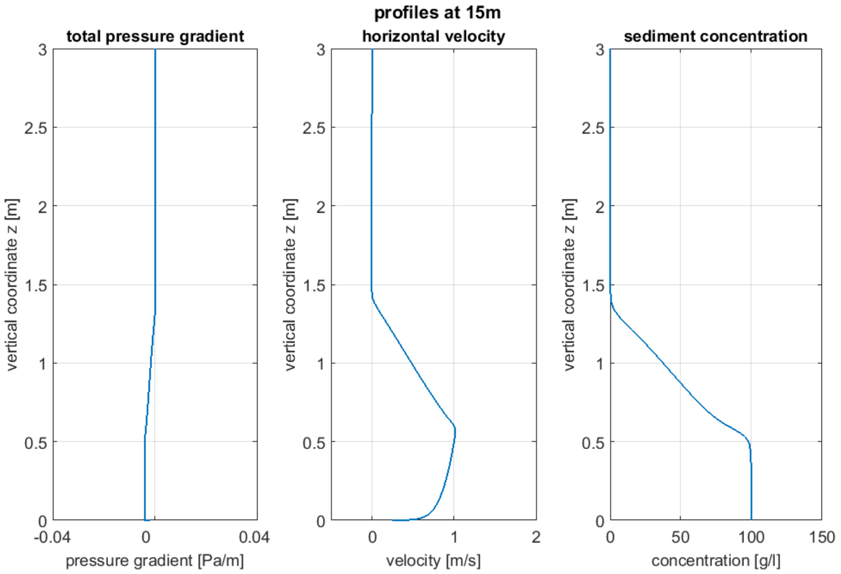

Figure C.16 Pressure gradient, velocity and concentration profile for x = 15m.

For x = 15m, we see that the initial logarithmic velocity profile has been diffused over the vertical, and this also applies to the concentration profile. The baroclinic contribution to the pressure gradient is clearly visible over the lower 1.5m of the vertical profile. This negative pressure gradient leads to an increase in velocity, since $\frac{\partial u}{\partial t} \propto -\frac{\partial p}{\partial x}$.

The results for x=30m are similar to x=15m. The maximum velocity has increased slightly, whereas the total sediment mass decreased. For both x = 15m and x = 30m, the transition from the maximum velocity to the ambient velocity bears resemblance to a hyperbolic tangent. This is sensible, as a mixing layer is likely to develop at the interface between the fluidized layer and the ambient velocity. This mixing layer also affects the concentration profile.

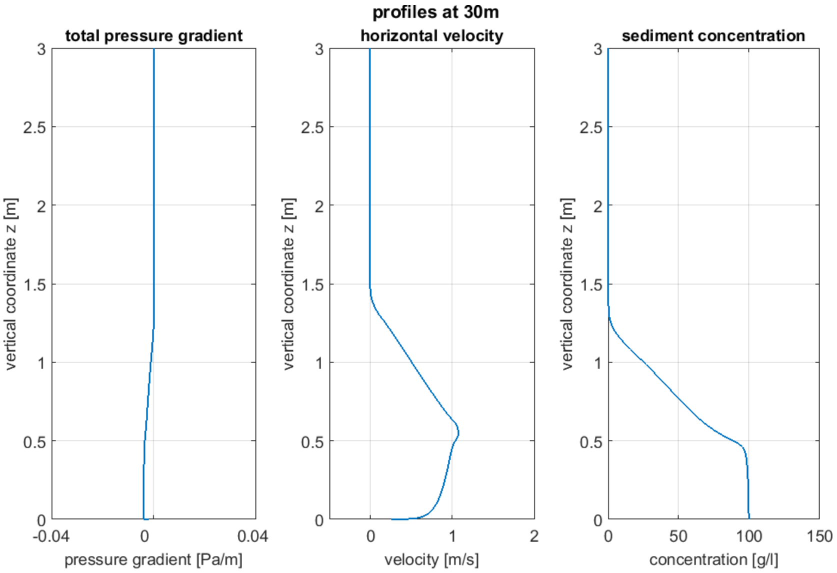

Figure C.17 Pressure gradient, velocity and concentration profile for x = 30m.

C.1.6.3 Alongslope development of velocity and concentration

After x=30m, the slopes for the three defined cases differ. In the following, we define the three cases as ‘flat’, ‘downslope’ and ‘upslope’. Again, vertical profiles of the pressure gradient, velocity and sediment concentration are plotted, now at locations x = 35m (Figure C.18) and x = 55m (Figure C.19).

x = 35m lies shortly after the onset of the sloping bathymetry, and clearly shows the enhanced barotropic contributions to the pressure gradient. For the downsloping case, the baroclinic contribution shows a sharp increase. The upsloping case shows an opposing pressure gradient, slowing down the flow. This is already visible in the velocity profiles for this location, but not yet in the concentration profile.

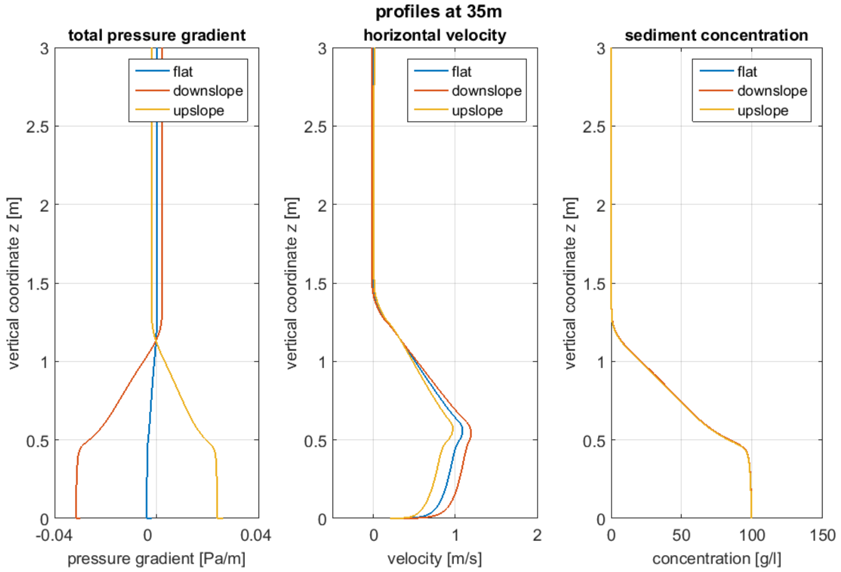

Figure C.18 Pressure gradient, velocity and concentration profile for x = 35m. Three cases: flat bed, downsloping bed and upsloping bed.

At x = 50m, we see that the developments on the slope have continued. The velocity on the upsloping bed has decreased further, and the velocity on the downsloping bed has increased. Since no erosion is possible, the total sediment mass decreases for all three cases, and thus all three barotropic contributions to the pressure gradient have decreased in magnitude. The direction of these contributions has not changed, though. Near the bed, the horizontal velocity for the upsloping bed is slightly negative. Although the model is able to handle this negative velocity, this may give physically unrealistic results, since the total sediment mass is moved along the slope with the concentration-averaged velocity (u_c). In such a case, the model overestimates the total sediment mass transported along the slope.

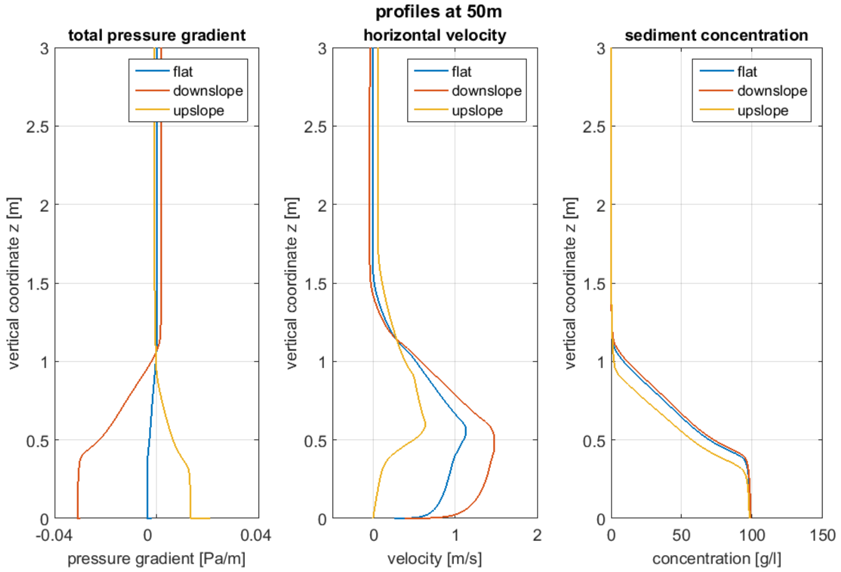

Figure C.19 Pressure gradient, velocity and concentration profile for x = 50m. Three cases: flat bed, downsloping bed and upsloping bed.

C.1.6.4 Alongslope variations of sediment transport rate

As a final model performance evaluation, sediment transport rate (q_s) along the slope is discussed. Variation of this parameter along the slope is shown in Figure C.20. q_s is defined as:

$$q_s = \int_{-d}^{\zeta} Uc \, dz$$

The sediment transport rate q_s shows expected behaviour. q_s decreases gradually for the flat and upsloping bathymetry case, with the upsloping bathymetry showing the fastest decrease. For the downsloping case, sediment transport rate increases for the first part of the slope, caused by the increase in velocity along this stretch. After x = 50m, sediment settling out of suspension leads to a decrease in q_s.

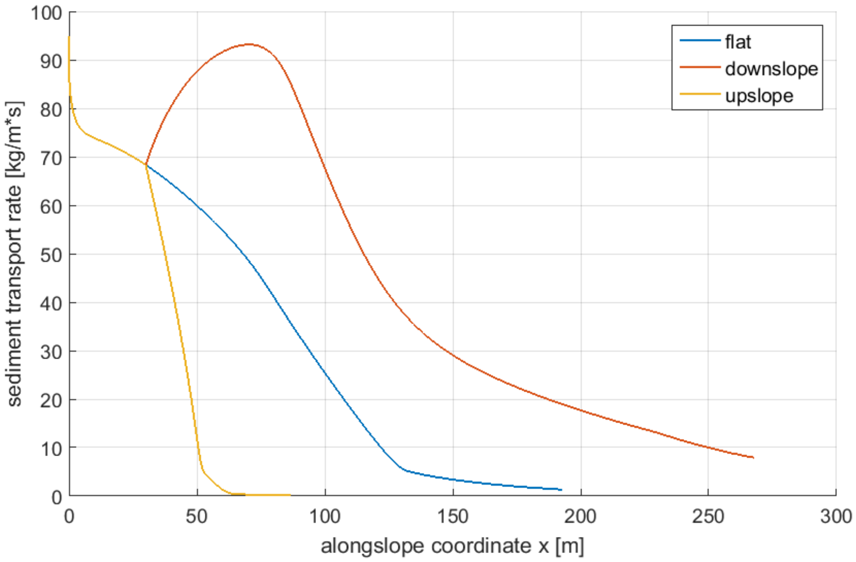

Figure C.20 Alongslope variation of sediment transport rate for flat bed, downsloping bed and upsloping bed.

C.1.6.5 Conclusions

Based on the test cases using the three different bathymetries, the following conclusions are drawn:

- The 1DV model code correctly handles up- and downsloping bathymetry, judging from the alongslope development of the total pressure gradient (being the sum of the barotropic and baroclinic contributions)
- When modelling an upsloping bathymetry, one should be wary for encountering negative velocities. This may lead to physically unrealistic model results.

C.2 Initial conditions for the Lagrangian 1DV model

In this section, the initial conditions for the 1DV model are discussed as well as the implementation in the code.

C.2.1 Properties to be conserved

The initial conditions for the fluidized layer flow can be characterised by three main parameters:

- Fluidized layer height (h_{fl})
- Average fluidized layer velocity (u_{fl})
- Average fluidized layer concentration (c_{fl})

These parameters can be specified through the model input. Using these parameters, initial profiles for the fluidized layer can be constructed. However, before constructing these profiles, we need to specify which properties of the fluidized layer need to be conserved. Theoretically, 4 properties of the fluidized layer can be conserved:

- Velocity
- Sediment mass
- Momentum
- Sediment mass flux

We can write the balances for velocity and sediment mass as given in Equation (3.1):

$$\begin{aligned} h_{fl} u_{fl} &= \int_0^{h_{fl}} u \, \mathrm{dz} \\ h_{fl} \, \mathrm{c}_{fl} &= \int_0^{h_{fl}} c \, \mathrm{dz} \end{aligned} \tag{3.1}$$

u_{fl}, h_{fl} and c_{fl} are the input parameters whereas the variables on the right-hand side of the equation are depth-dependent variables in the 1DV model. Here, we assume that the bed is located at depth z=0, and that the top of the fluidized layer is located at h_{fl}. All sediment that is initially available in the 1DV model computation is located within the fluidized layer, i.e., between 0 and h_{fl}.

The amount of momentum in the fluidized layer can be written as:

$$\rho_{fl} u_{fl} h_{fl} = \int_0^{h_{fl}} \rho(\mathrm{z}) \, u(\mathrm{z}) \, dz \tag{3.2}$$

Similar to Equation (3.1), u_{fl}, h_{fl} and ρ_{fl} are the parameters specified in the input. The variables on the right-hand side of the equation are depth-dependent variables in the 1DV model. Analogous to Equations (3.1) and (3.2), we can write the mass flux as:

$$u_{fl} c_{fl} h_{fl} = \int_0^{h_{fl}} u(\mathrm{z}) \, c(\mathrm{z}) \, dz \tag{3.3}$$

What we can see from Equations (3.2) and (3.3), is that the sediment mass flux and momentum are directly influenced by changes in the velocity profile and concentration profile, since ρ(z) is directly dependent on c(z). Furthermore, the sediment mass flux and momentum and are defined by the product of density/concentration and velocity. This coupling makes it complicated to conserve both the sediment mass flux and momentum. As is explained in Section C.2.2, we cannot conserve both sediment mass and velocity if we want to conserve the sediment mass flux.

After discussing with experts from Boskalis and Deltares, we have opted to conserve the following two quantities:

- Sediment mass
- Sediment mass flux

It is essential to conserve sediment mass when making the transition between the two models, as the baroclinic pressure gradient (the main forcing of the turbidity current on a slope) depends on the available sediment mass and the bed slope. This will also influence the sedimentation footprint, and the distance travelled by the fluidized layer. In practice, this means that the sediment mass specified in the 1DV input file, through the concentration and fluidized layer height, is exactly matched by the 1DV code.

The sediment mass flux is preferably conserved, rather than the amount of momentum, as the goal of the numerical tool is to calculate a sedimentation footprint. This is more likely to be influenced by the sediment mass flux than the momentum.

C.2.2 Relation between sediment mass flux conservation and average fluidized layer velocity

The sediment mass flux described in Equation (3.3) can also be written as:

$$u_{fl} c_{fl} h_{fl} = \overline{u(\mathrm{z})\, c(\mathrm{z})}\, h_{fl} \tag{3.4}$$

From this equation, we can eliminate h_{fl}, and if we then decompose u(z) and c(z) in a depth-averaged part and a depth-varying part. The overbar is used for the depth-averaged part and Δ for the depth-varying part:

$$u_{fl} c_{fl} = \overline{\left(\bar{u} + \Delta u\right)\left(\bar{c} + \Delta c\right)} \tag{3.5}$$

When we elaborate on the RHS of the equation, we see that it simplifies to:

$$u_{fl} c_{fl} = \bar{u}\bar{c} + \overline{\Delta u \Delta c} \tag{3.6}$$

Since we also specified that sediment mass must be conserved between the models, this means that $c_{fl}=\bar{c}$. We then arrive at an expression for $\bar{u}$:

$$\bar{u} = \frac{u_{fl} c_{fl} + \overline{\Delta u \Delta c}}{c_{fl}} \tag{3.7}$$

This implies that if the product of variations of u and c (around the mean) over depth is unequal to zero, this will directly affect the depth-averaged velocity. This is an important implication and should be kept in mind when setting up the model.

C.2.3 Initialisation of profiles in subroutine PROFIL

The initialisation of the velocity profile and the concentration profile is described in this section. To this end, the subroutine PROFIL was created. We mainly focus on the structure of the subroutine PROFIL and in which order the steps in the process are passed through. The structure of the subroutine is schematically depicted below:

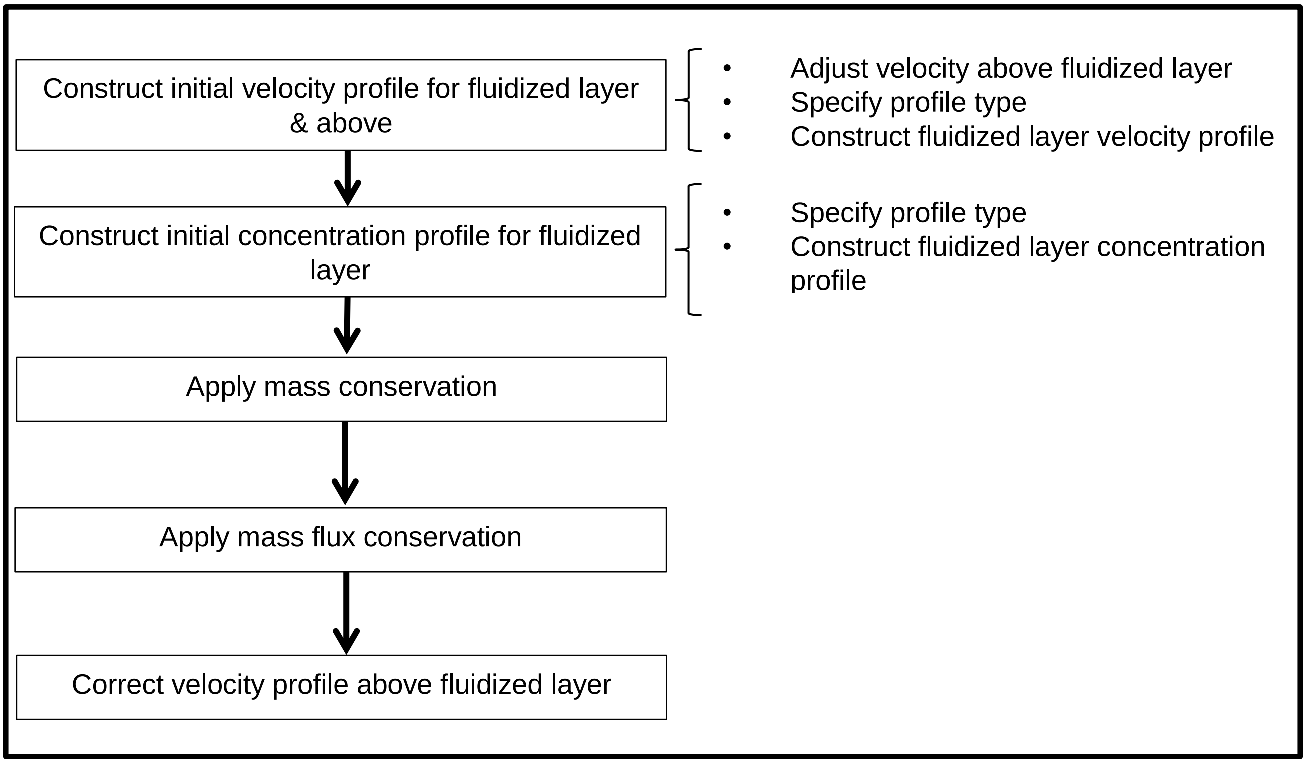

Figure C.21 Schematic overview of the PROFIL subroutine

Before the PROFIL subroutine is called, a logarithmic velocity profile is already constructed over the vertical, based on the user-specified velocity $\bar{U}$. In the PROFIL subroutine, a new velocity profile is assigned to the part of the water column that is lower than h_{fl}. However, this leads to a velocity surplus for the entire vertical compared to the user-specified velocity $\bar{U}$. To correct for this, the velocity profile is adjusted based on the user-specified settings for the fluidized layer velocity and fluidized layer height.

Afterwards, the initial velocity and concentration profiles are constructed based on the settings provided in the input file. After constructing these profiles, mass conservation and mass flux conservation are applied. As we have seen in the previous paragraph, the latter leads to a change in average fluidized layer velocity. This will also influence the depth-averaged velocity. Hence, we make one final adjustment to the vertical velocity profile before continuing to the next subroutine.

C.2.4 Comparison between old and new subroutine: DIFFUS vs PROFIL

The DIFFUS subroutine was previously used to construct the initial profile. However, there are two main differences with the PROFIL subroutine. In the DIFFUS subroutine, sediment mass and velocity were conserved for the fluidized layer, and not the sediment mass flux. Furthermore, the velocity profile above the fluidized layer is not corrected for the additional velocity that is supplied by the fluidized layer, i.e., there is a velocity surplus over the vertical.

To show the differences between the two subroutines, we have plotted three figures in this section. These profiles are based on an input of the 1DV model where the overall water depth is 10m, h_{fl} is 1m, u_{fl} is 1 m/s and c_{fl} is 100 kg/m^3 and the depth-averaged velocity $\bar{U}$ is 0.2 m/s.

Figure C.22 shows the vertical profiles of horizontal velocity and concentration at x=0m, where the initial profiles constructed by the DIFFUS subroutine are plotted in blue, and the initial profiles constructed by PROFIL are plotted in red. Here, we clearly see the difference between the velocity profile constructed by the two subroutines. As mass is conserved in both subroutines, the concentration profile is identical.

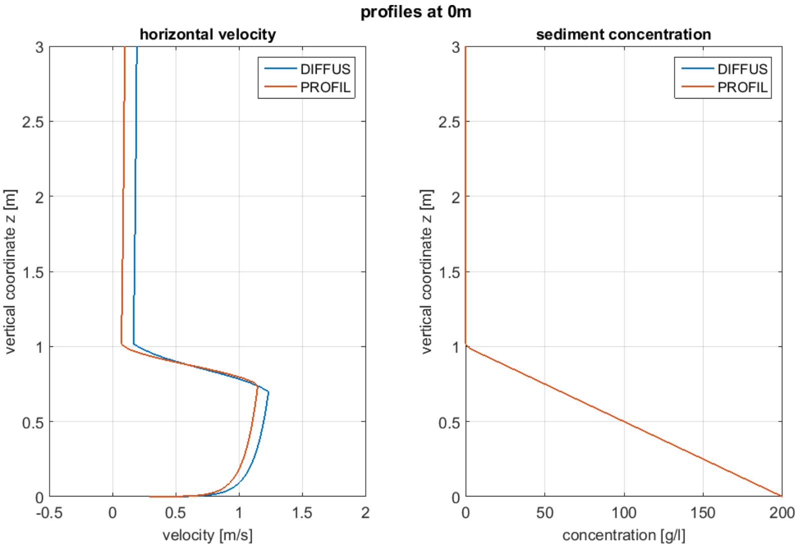

Figure C.22 Velocity and concentration profiles for x=0m

When we move a small distance along the slope, we see that the 1DV model has corrected for the velocity surplus and has adjusted the vertical profile so the total depth-averaged velocity matches the user-specified velocity $\bar{U}$ (Figure C.23). We see a very small deviation in the fluidized layer velocity profile between the two subroutines, probably caused by a larger shear between the fluidized layer velocity and the velocity of the ambient water.

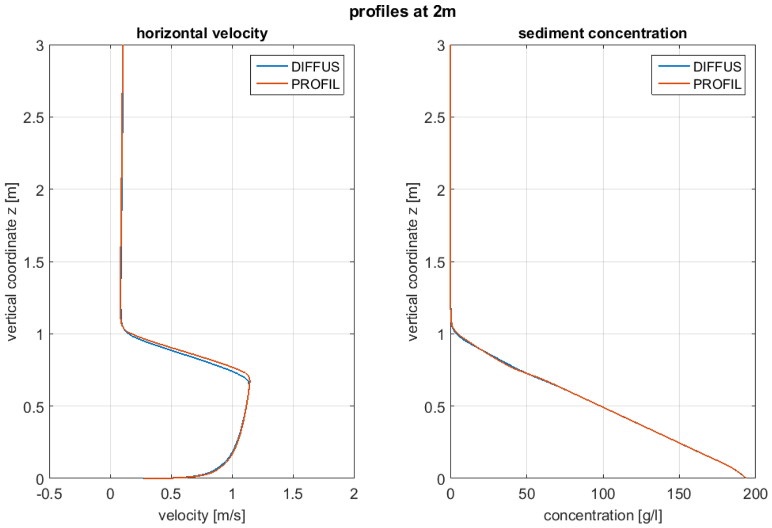

Figure C.23 Velocity and concentration profiles for x=2m

Figure C.24 shows the mass flux as a function of alongslope distance. We see that in the PROFIL subroutine, the mass flux is exactly set to 100 kg/m^{2}s as specified in the input. The DIFFUS subroutine overshoots the initial mass flux, and mass flux drops considerably after the first time step. However, we see that further along the slope, the mass fluxes converge.

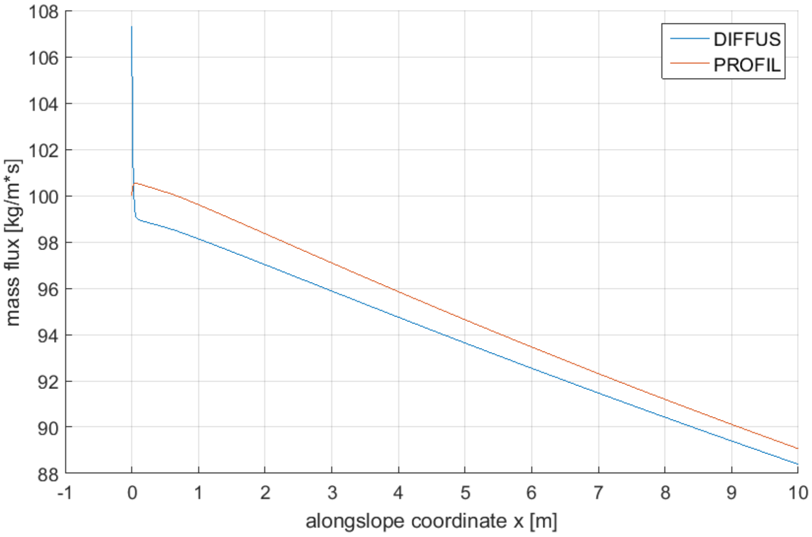

Figure C.24 Mass flux as a function of alongslope coordinate for both the DIFFUS and PROFIL subroutine

C.2.5 Conclusions

- A new subroutine, called PROFIL, was developed for constructing the initial profiles. This subroutine replaces the DIFFUS subroutine.
- In the PROFIL subroutine, both the fluidized layer sediment mass and mass flux are conserved.
- Using Equation (3.7) we can calculate how conservation of mass and mass flux influence the average fluidized layer velocity.
- The PROFIL subroutine also adjusts the velocity profile above the fluidized layer, so the initial depth-averaged velocity (for the entire water column) is equal to the user-specified velocity $\overline{U}$.

C.3 Testing sensitivity of model outcome to initial profile

For its current application, the 1DV model is set up using the output from a dedicated near-field model. A set of constant values is converted to a set of profiles that serve as the initial conditions for the 1DV computations. Before working on this conversion, we want to test the sensitivity of model outcome on the applied initial conditions. This gives us a handle for conversion and model setup, as we know on which aspects we need to focus

First, a base case is defined based on typical fluidized layer flow conditions. Afterwards, the sensitivity of the model outcome to the following parameters is tested:

- velocity profile
- concentration profile

C.3.1 Base case definition

C.3.1.1 Definition

To make a proper sensitivity analysis, we must define a base case first. Afterwards, variations on the parameter set can be made systematically. A definition sketch of the relevant parameters is presented in Figure C.25. The arrow indicates the direction of the fluidized layer flow. Three parameters characterize the fluidized layer flow at x=0:

- Fluidized layer height (h_{fl})
- Average fluidized layer velocity (u_{fl})
- Average fluidized layer concentration (c_{fl})

Flow conditions are characterized by the water depth (d) and the depth-averaged flow velocity ($\bar{U}$).

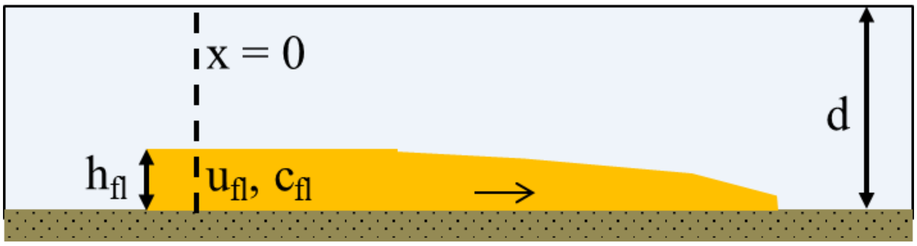

Figure C.25 Definition sketch of fluidized layer and characterizing parameters. Arrow indicates direction of fluidized layer flow. Three parameters characterize the fluidized layer flow at x=0. x=0 is indicated with the dashed line.

C.3.1.2 Base case parameters

Based on discussion with counterparts at Boskalis, the parameters characterizing the fluidized layer and flow conditions are chosen as listed in Table C.8. Apart from the parameters that were specified in the previous section, the d_{50} is also set to a constant value for all model runs.

Table C.8 Base case parameters for initial profile sensitivity testing

Parameter	value
h_{fl}	1 m
u_{fl}	1 m/s
c_{fl}	100 g/l
d	10 m
$\bar{U}$	0.2 m/s
d_{50}	100 µm

C.3.2 Initial velocity profile sensitivity

The sensitivity of model outcome to the shape of the initial velocity profile is verified first. To test this sensitivity, the following conditions need to be met when constructing initial profiles:

- Velocity needs to be conserved for the fluidized layer, i.e. $h_{fl} * u_{fl} = \int_0^{h_{fl}} u(z)\,dz$, where h_{fl} and u_{fl} are constant values for the fluidized layer height and average fluidized layer velocity, respectively.

- Momentum needs to be conserved for the fluidized layer. Given the previous condition, this means that we should opt for a constant concentration profile for the fluidized layer.

If these conditions are not met, differences in model outcome may be the result of the difference in momentum or velocity. Since we want to test the sensitivity of model outcome to the shape of the initial velocity profile, we should be cautious about whether the above conditions are met.

C.3.2.1 Definition of initial velocity profile

For the sensitivity analysis, three initial fluidized layer velocity profiles are defined. These are described below:

- Logarithmic velocity profile, standard velocity profile for turbulent boundary layer flow
- Double logarithmic profile, which develops for turbulent pipe flow
- Combined logarithmic-hyperbolic tangent profile, which is a combination of the logarithmic velocity profile and a mixing layer. Flow velocity in mixing layers is typically described by hyperbolic tangent functions. This profile is called the hybrid profile hereafter.

The three initial velocity profiles are sketched in Figure C.26. The fluidized layer height h_{fl} and the height of the mixing layer h_{mix} (only applicable to the hybrid profile) are also indicated in this figure. Above the fluidized layer, the velocity is given by the depth-averaged input velocity. The logarithmic velocity profiles are constructed using the bottom roughness and average fluidized layer velocity (u_{fl}) as input parameters.

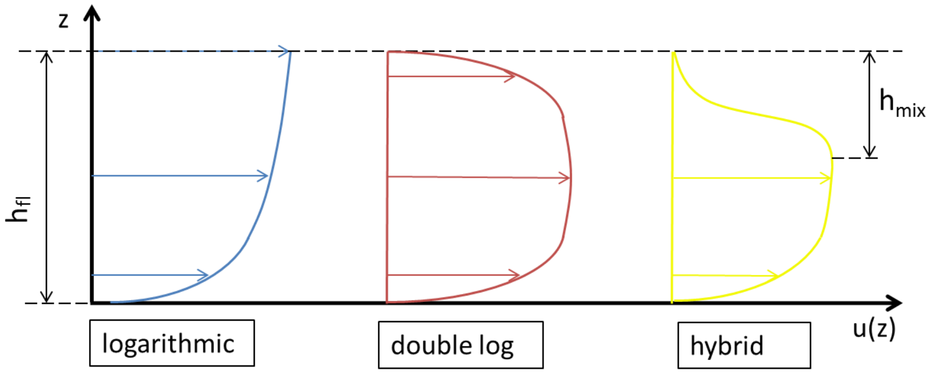

Figure C.26 Definition sketch of the three velocity profiles.

C.3.2.2 Model runs

To test the sensitivity of model outcome to the initial velocity profile, we set up three cases. Parameters are taken from the defined base case, and three different initial profiles (Figure C.26) are applied. We compare the three different cases by examining the alongslope development of the following profiles:

- Horizontal velocity
- Concentration
- Eddy viscosity

These profiles characterise the fluidized layer flow and the interaction of the fluidized layer with the ambient water. The horizontal velocity profile is used to evaluate the propagation velocity of the fluidized layer, and the amount of momentum carried by the fluidized layer flow. The concentration profile gives us an indication of the amount of sand in the fluidized layer and the ambient water, and about how far the bulk of the fluidized layer is transported. The eddy viscosity is a measure for the amount of turbulent mixing taking place over the vertical. Turbulent mixing leads to suspension of more material from the fluidized layer into the overlying water. The eddy viscosity profile also gives us information about how stratified the fluidized layer-ambient water interface is.

C.3.2.3 Model results

The initial profiles for the three quantities mentioned in the previous section are plotted in Figure C.27. Although the water depth is 10 m, the lower meters of the water column are most relevant. Therefore, only the lower 3 m of the vertical profiles are plotted.

In the left panel, we see the three different initial velocity profiles and the transition from the fluidized layer velocity to the ambient velocity at z = 1 m. Whereas the double log and the hybrid profiles show a gradual transition to the ambient velocity, the logarithmic profile shows a rather steep gradient at the transition from the fluidized layer to ambient velocity. In the middle panel, we see the concentration profile, which is the same for all three model runs. The same holds for the initial eddy viscosity profile: at x = 0m, the contribution of the fluidized layer velocity to the eddy viscosity profile are not yet included (although k and ε are already computed for turbulence closure). This contribution is included at the first time step.

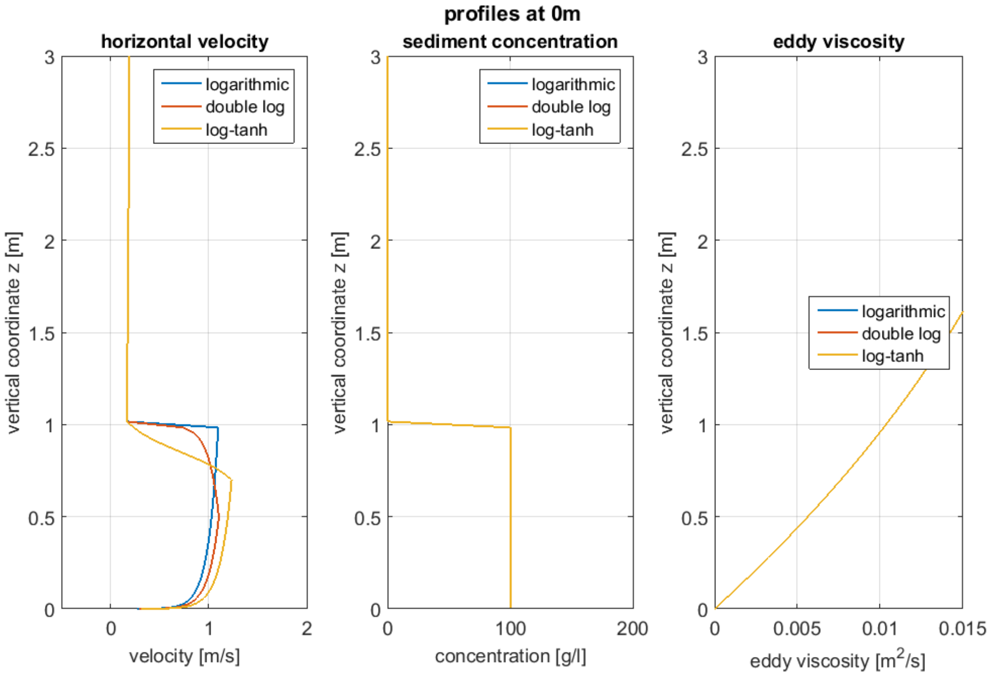

Figure C.27 Velocity, concentration and eddy viscosity profile at x = 0m for the velocity sensitivity runs. Please note that the hybrid profile results are labelled 'log-tanh' in the subplot legend

At x = 20m (Figure C.28), we see that the shape of the three velocity profiles has become remarkably similar (left panel). The logarithmic velocity profile has mixed the sediment highest up into the water column, because of the large shear at the interface between fluidized layer and ambient velocity. We also see that the eddy viscosity is close to zero over the concentration gradient, showing that turbulent mixing is largely suppressed.

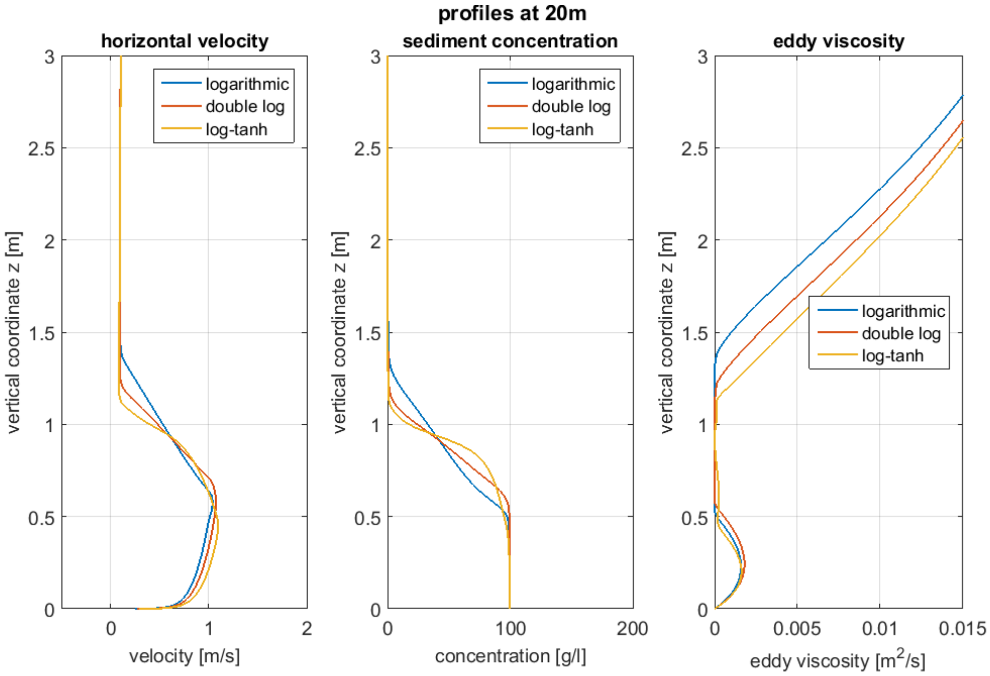

Figure C.28 Velocity, concentration and eddy viscosity profile at x = 20m for the velocity sensitivity runs. Please note that the hybrid profile results are labelled 'log-tanh' in the subplot legend

When we follow the development of the fluidized layer along the slope, we see that the stratification on the water-fluidized layer interface slowly decreases. This is an effect of deposition of sediment along the slope, and the associated decrease of sediment in the fluidized layer. Hereby, the density gradient also decreases and thus, the suppression of turbulence production decreases.

At x = 100m (Figure C.29), we see that the fluidized layer height has decreased and is roughly 1/3 of its initial height (middle panel). At the same height, we see eddy viscosities that are close to zero. This can be attributed to the large density gradient and the small velocity gradients. Both the velocity and concentration profiles coincide largely for the three test cases. This suggests that model outcome is not particularly sensitive to the shape of the initial velocity profile.

C.3.2.4 *Stratification – Richardson Number calculations*

We estimate whether stratification plays an important role by calculating the gradient Richardson number. This dimensionless parameter gives a ratio between buoyancy destruction and turbulence production. It is defined as:

$$Ri = -\frac{g}{\rho_0} \frac{\frac{\partial \rho}{\partial z}}{\left(\frac{\partial u}{\partial z}\right)^2} \tag{3.8}$$

Where:
ρ_0 = reference density [kg/m^3]
g = gravitational acceleration [kg/m^3]
ρ = density of fluid water mixture [kg/m^3]
u = horizontal velocity [m/s]

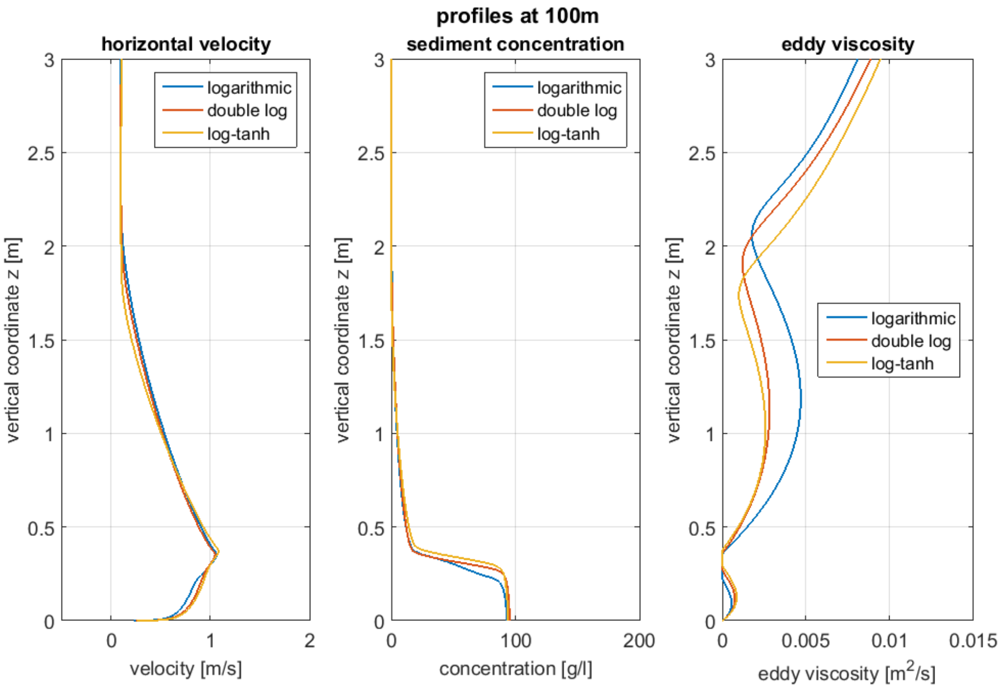

Figure C.29 Velocity, concentration and eddy viscosity profile at x = 100m for the velocity sensitivity runs. Please note that the hybrid profile results are labelled 'log-tanh' in the subplot legend

If we now approximate the Richardson number for the water-fluidized layer gradient of the profile at x=20m (Figure C.28), estimating that the velocity increases from 0 to 1 m/s in 0.5 m, and the concentration increases from 0 to 100 g/l in 0.5 m:

$$Ri = -\frac{9.81}{1*10^3}\frac{-200}{4} = 0.5$$

Stratification is stable when *Ri* > 0.25 (Galperin et al. 2007). Hence, this first approximation already shows that the interface is likely to remain stratified. Even more so: local velocity gradients may be much smaller than we calculated here. For instance: at the velocity maximum, the velocity is gradient is 0, making the Richardson number infinitely large.

Given the typical concentrations and velocities for the foreseen application, stratification is to be expected.

C.3.2.5 Results of initial velocity profile sensitivity test

Model outcome appears not to be very sensitive to the form of the initial velocity profile, if momentum is preserved. However, we do observe strong stratification over the vertical in all three test cases. By estimating the Richardson number for this case, we confirm that stratification is to be expected for these conditions. Stratification leads to suppression of turbulent mixing. If we want to introduce turbulent mixing in the model, we can choose to impose a background eddy diffusivity through the 1DV model input.

C.3.3 Initial concentration profile sensitivity

After testing the sensitivity of model outcome to initial velocity profile, we continue with testing the sensitivity of model outcome to the initial concentration profile. To test this sensitivity, the following conditions need to be met when constructing initial profiles:

- Sediment mass is conserved for the fluidized layer: $h_{fl}c_{fl} = \int_0^{h_{fl}} c(z)\,dz$, where h_{fl} and c_{fl} are constant values for the fluidized layer height and average fluidized layer concentration, respectively.
- The centre of gravity of the fluidized layer should remain constant. The importance of this condition is illustrated in Section C.3.3.1.

As was discussed in Section C.2, sediment mass flux is also conserved by the 1DV code. This is an additional condition that is met during the sensitivity test.

C.3.3.1 Conservation of sediment mass

We start the sensitivity analysis by imposing a set of initial concentration profiles that are only mass-conservative. To construct this set, we describe the initial concentration profile in the fluidized layer by means of a hyperbolic tangent function. In these runs, the fluidized layer height is equal to 1m, and the total sediment mass is 100 kg/m^2. The resulting initial concentration profiles are shown in Figure C.30. In total, six different profiles are tested. These vary from a stepwise profile (blue) to a hyperbolic tangent function where the maximum fluidized layer concentration is twice the average concentration (light blue).

If we follow the development of these fluidized layers over a flat bed, we note large differences between the six different profiles. After 50 m, we see that the total sediment mass in the fluidized layer differs between 66.5 kg/m^2 and 47.4 kg/m^2. This is illustrated in Figure C.31.

The differences in sediment mass and vertical profile affect the model outcome in two different ways. First, the sediment mass in the fluidized layer drives the baroclinic pressure gradient, and thus, the development of the fluidized layer velocity along its path. If this changes in magnitude, this influences both the propagation speed of the fluidized layer along its path and the amount of vertical mixing (since du/dz changes). Second, one of the relevant model outcomes is the distance travelled by the bulk of the fluidized layer. We see in Figure C.32 that the sediment transport rate along the slope differs significantly for the different fluidized layers. If we define the distance travelled by the bulk of the fluidized layer as the moment where the sediment transport rate falls below 10 kg/m^{2}s, we see that this varies between 75m and 120m. This is a significant difference, and shows that the model outcome is very sensitive to the initial concentration profile, if only a mass-conserving condition is applied.

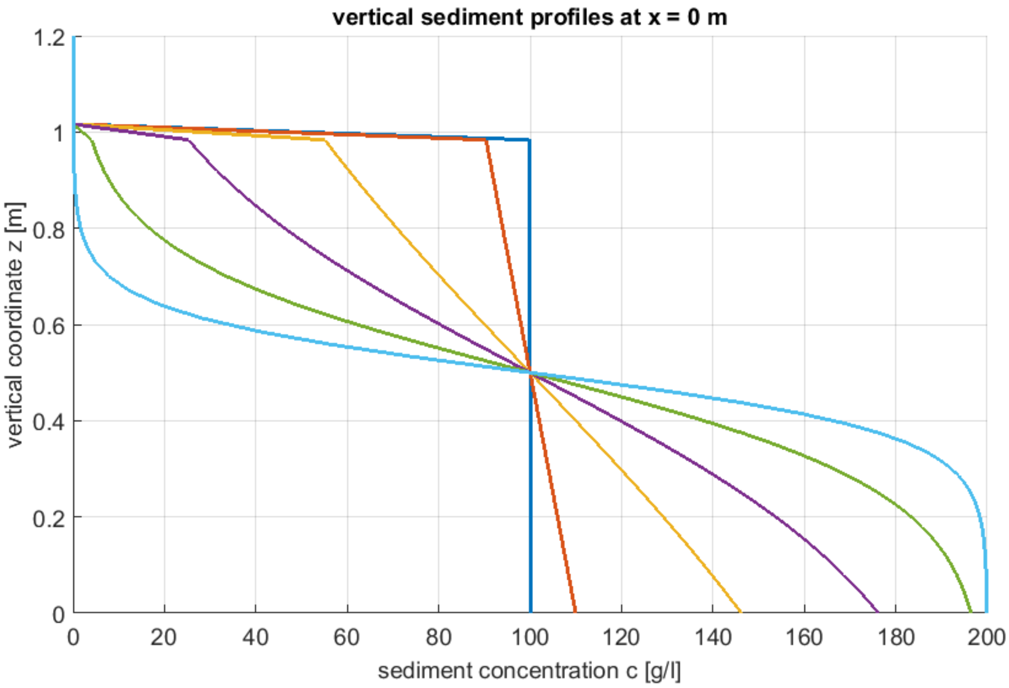

Figure C.30 Initial concentration profiles described by hyperbolic tangent functions. All imposed fluidized layers have a sediment mass of 100 kg/m^2.

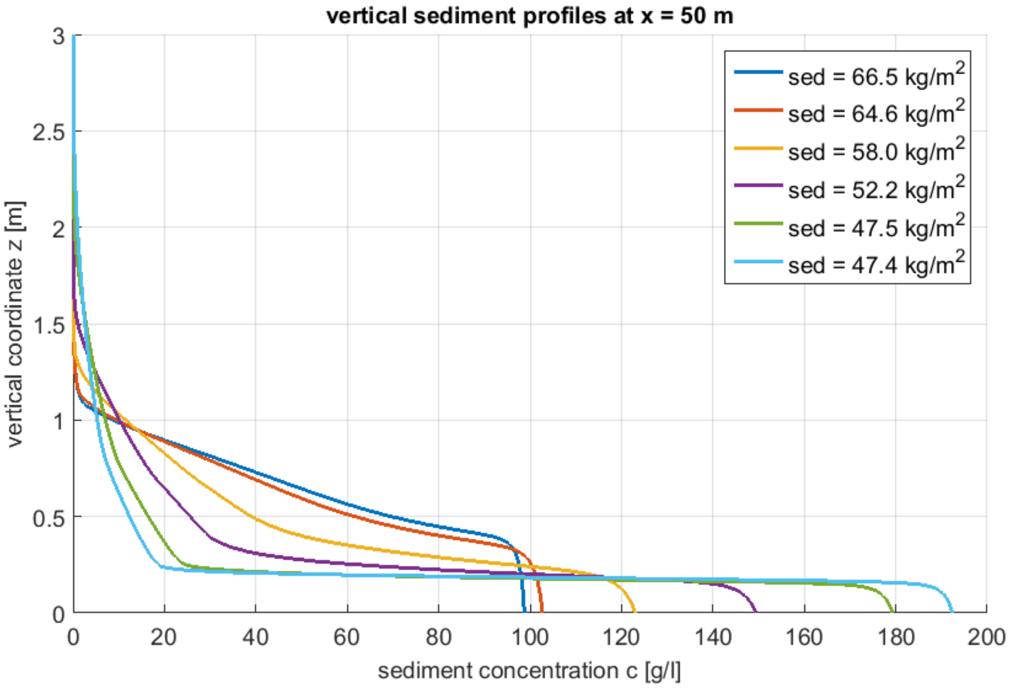

Figure C.31 Vertical concentration profiles at x=50m for the concentration sensitivity runs.

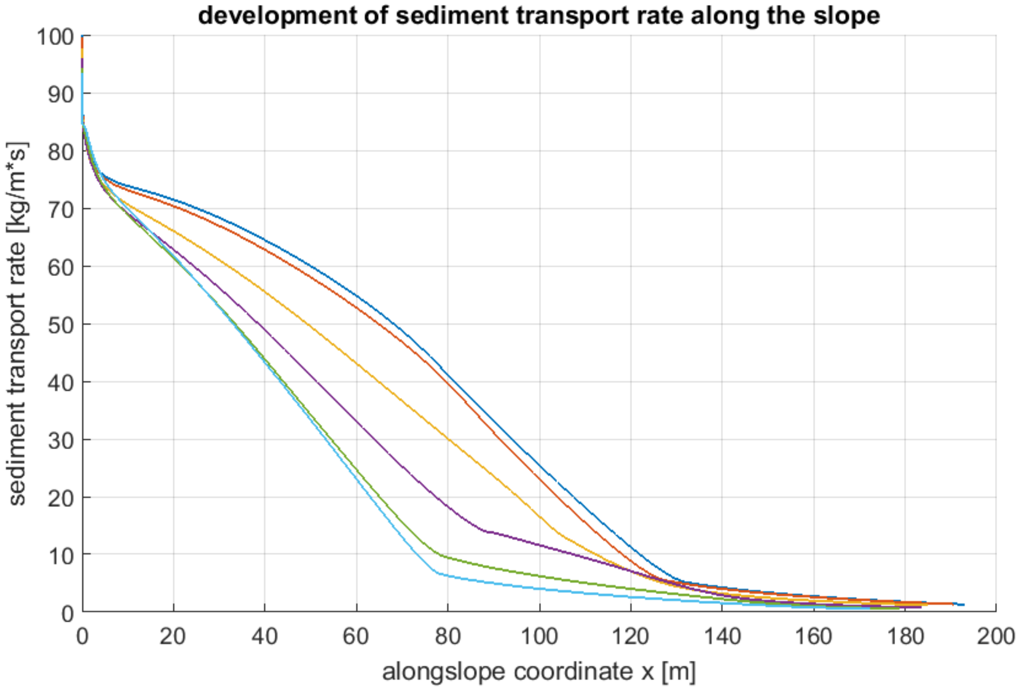

Figure C.32 Development of sediment transport rate along the slop for set of hyperbolic tangent concentration profiles.

C.3.3.2 Centre of gravity of fluidized layer

Apart from making mass-conservative profiles, we now include the condition that the centre of gravity of the fluidized layer must be conserved as well. To do so, we construct the three profiles as sketched in Figure C.33. The height of the centre of gravity of these three profiles is denoted with $h_{gravity}$ and should be equal for the different profiles. If we want to keep the centre of gravity equal, as well as the total sediment mass, the height of the sediment profiles will differ. However, this is inevitable if we want to meet the conditions as outlined in the beginning of this section. The height to which the velocity profile of the fluidized layer is set, remains equal to h_{fl}.

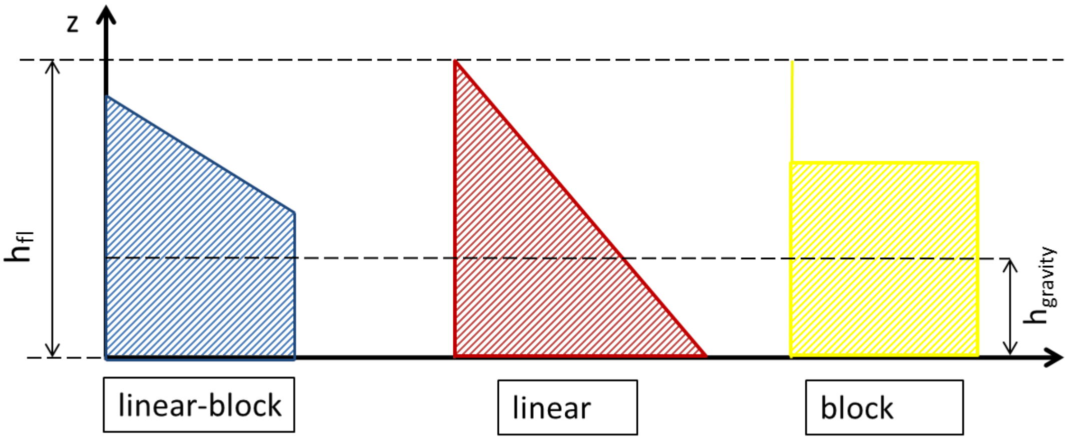

Figure C.33 Definition sketch of the three concentration profiles.

C.3.3.3 Model runs

We test the sensitivity of the model outcome to the shape of the initial concentration profile in a similar way as we did for the initial velocity profile. This means that we compare three test cases, for which the concentration profiles were defined in the previous paragraph, other parameters are taken from the defined base case (Section C.3.1). We compare the three different cases by examining the alongslope development of the following profiles:

- Horizontal velocity
- Concentration
- Eddy viscosity

C.3.3.4 Model results

The initial profiles for the three quantities mentioned in the previous section are plotted in Figure C.34. Although the water depth is 10 m, the lower meters of the water column are most relevant. Therefore, only the lower 3 m of the vertical profiles are plotted.

In the left panel, we see the initial fluidized layer velocity profile (hybrid type), and the transition from the fluidized layer velocity to the ambient velocity at z = 1 m. In the middle panel, we see the three concentration profiles. As mentioned in Section C.3.3.1, these profiles have an equal sediment mass and centre of gravity at the same height above the bed. The initial eddy viscosity profile, displayed in the right panel, is the same for all three runs.

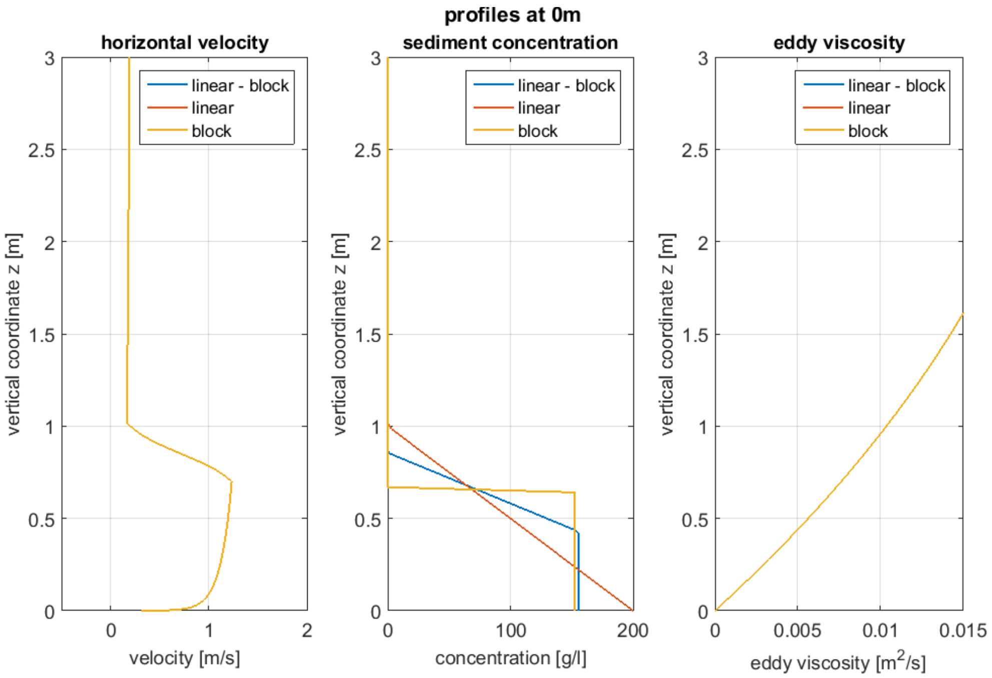

Figure C.34 Velocity, concentration and eddy viscosity profile at x = 0m for the concentration sensitivity runs.

If we now follow the evolution of these vertical profiles along the slope, we see that at x=20m (Figure C.35), the linear-block profile and the block profile show very similar results. The linear sediment profile has more sediment in the lower 0.3m of the profile, and with a more gradual transition. Hence, turbulence production is also suppressed over a large area, which can be seen in the eddy viscosity profile plot (red line).

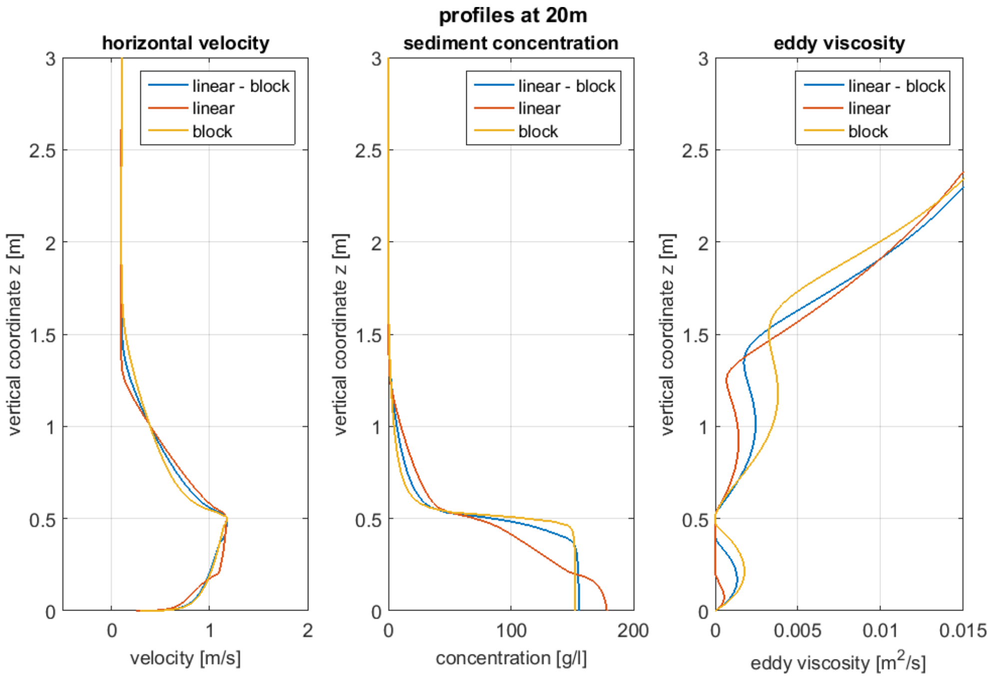

Figure C.35 Velocity, concentration and eddy viscosity profile at x = 20m for the concentration sensitivity runs.

At x=50m (Figure C.36), the three velocity profiles are almost identical, apart from the small increase in velocity at z=0.3 for the linear concentration test case. This could be related to the more gradual concentration decrease for the linear test case, which was also observed at x=20m. Apart from these two deviations from the other test cases, results look very similar.

As a final check, we also examine the sediment transport rate along the slope. This is plotted in Figure C.37. We see that for these three cases, the sediment transport rates along the slope are very similar. Again, we define the distance travelled by the bulk of the fluidized layer as the moment where the sediment transport rate falls below 10 kg/m^{2}s. We see that this only varies between 95 and 100 meters, so within a rather narrow window. This indicates that if the initial concentration profile meets the two conditions we mentioned earlier, i.e. mass-conservative and centre of gravity at an equal height, the outcome of the model is not very sensitive to the initial conditions.

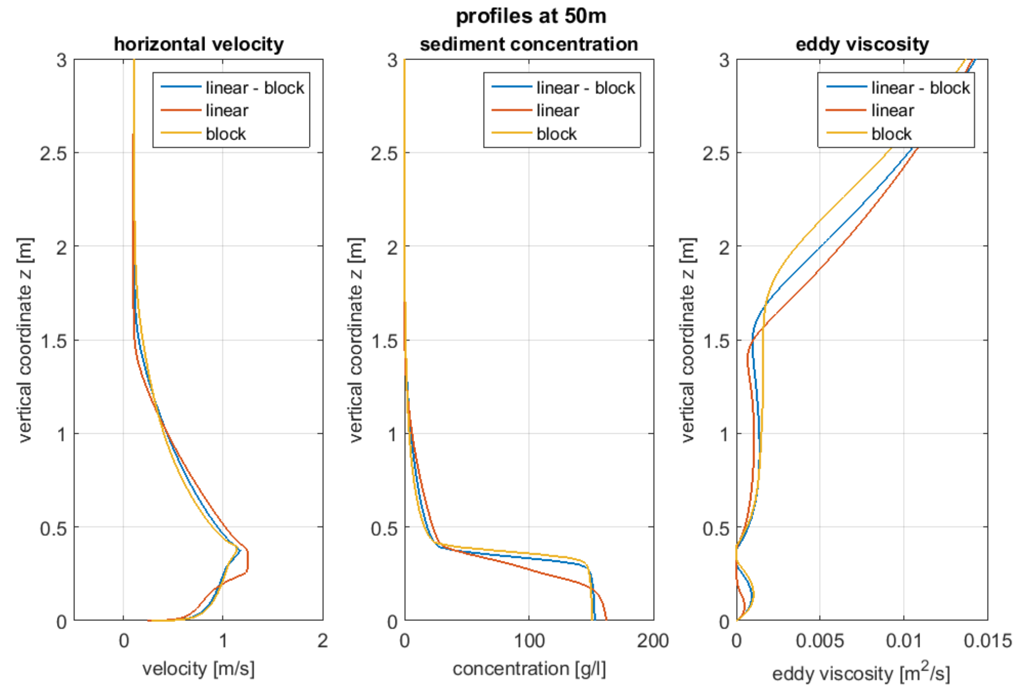

Figure C.36 Velocity, concentration and eddy viscosity profile at x = 50m for the concentration sensitivity runs.

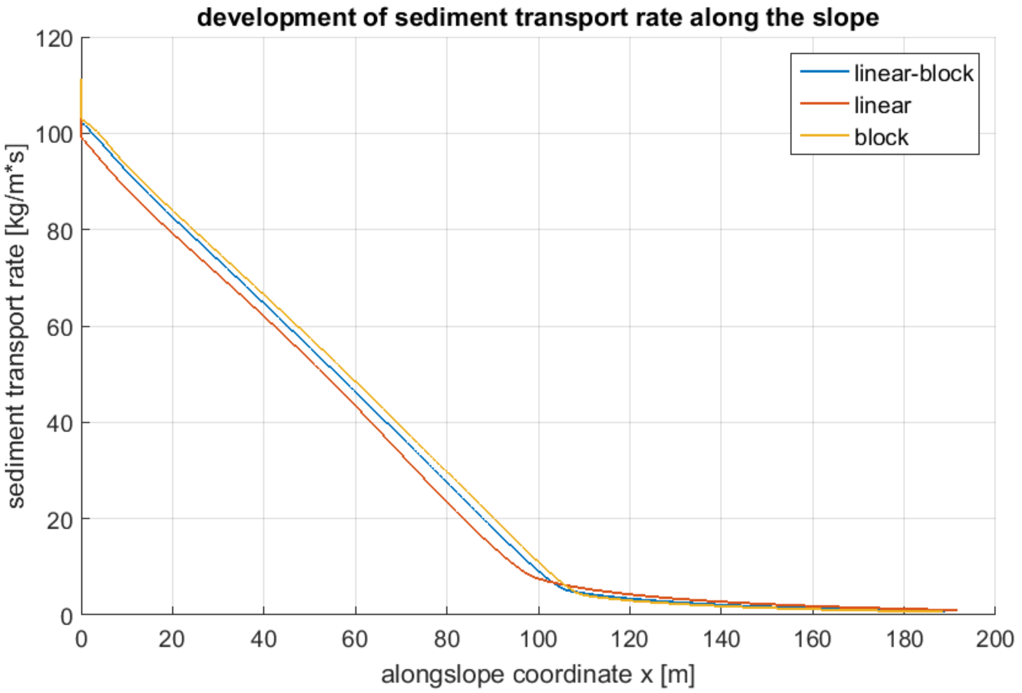

Figure C.37 Development of sediment transport rate along the slope for concentration sensitivity runs.

C.3.3.5 Results of initial concentration profile sensitivity test

From the test runs, we conclude that the initial concentration profile may have a large effect on model outcome. If only the sediment mass is conserved when constructing an initial concentration profile, large differences in model outcome may arise. This is mainly due to the contribution of the sediment mass to the total pressure gradient, by driving the baroclinic pressure gradient. In turn, the pressure gradient affects the fluidized layer velocity and has a direct influence on the development of the fluidized layer flow along the slope.

If the centre of gravity is included as an additional condition for the constructed profiles, we see that three differently-shaped concentration profiles yield practically the same results. On the other hand, estimating the centre of gravity of a fluidized layer flow is not straightforward. However, if we want to make a reliable prediction with the 1DV model, we should give it proper attention when setting up the model.

C.3.4 Conclusions

- Model outcome not very sensitive to shape of initial velocity profile, if the following two conditions apply:
  - Conservation of momentum
  - Conservation of velocity
- Three different velocity profiles were tested. The combination of the logarithmic and hyperbolic tangent velocity profile appears to be most realistic.
- Model outcome is very sensitive to the initial concentration profile, when only conservation of mass is set as a condition. When the centre of gravity of the fluidized layer is also set as a condition, the shape of the initial concentration profile does not have a large effect.
- When setting up the 1DV model, it is advised to give most attention to the setup of the initial concentration profile.

C.4 Implementing mud dynamics

To make sure the 1DV model can also be used for sediment flows that consist of mud (i.e. cohesive sediment), two types of processes need to be included in the 1DV code. These processes are:

- Hindered settling
- Erosion and deposition

In the following paragraphs, these processes are shortly discussed and the used formulations are presented. Afterwards, the used base case is discussed and the results of model verification runs are presented.

C.4.1 Processes and formulations

C.4.1.1 Hindered settling

In high concentration mixtures, the settling velocity of a single particle is reduced due to the presence of other particles. This effect is called hindered settling. The formulation used to account for hindered settling is the Richardson-Zaki formulation, which in its most general form reads:

$$w_s = w_{s,0}(1-\phi_s)^n \tag{3.9}$$

The settling velocity of a single particle is given by $w_{s,0}$. The exponent n depends on the particle Reynolds number and default values are: 5.0 for sand, and 4.0 for mud. The volume concentration ϕ_s is given by:

$$\phi_s = \frac{c}{\rho_{gel}} \tag{3.10}$$

Here, please note that ρ_s denotes the structural dry density of a sediment mixture (also referred to as the gelling concentration). Generally, this is much lower for mud (order 50-250 kg/m^3) than for sand (1600-1700 kg/m^3).

C.4.1.2 Erosion and deposition

For mud, the sources and sinks of sediment in the water column are calculated with the well-known Partheniades-Krone formulations. Erosion is included in the sediment transport equation as a source, and deposition is included as a sink. As there is no morphological update in the model, erosion and deposition do not influence the morphology or bathymetry of the model area. The Partheniades-Krone formulations read as follows:

$$\begin{aligned} E &= M\, S(\tau_b, \tau_{cr,e}) \\ D &= w_s\, c_b\, S(\tau_b, \tau_{cr,d}) \end{aligned} \tag{3.11}$$

Where M is the erosion parameter in kg/m^{2}s, w_s is the near-bed settling velocity in m/s and c_b is the near-bed concentration in kg/m^3. These near-bed values are specified in the lowest grid cell in the water column. S denotes a step function, and is defined as follows for the erosion formulation:

$$S(\tau_b, \tau_{cr,e}) = \begin{cases} \left(\dfrac{\tau_b}{\tau_{cr,e}} - 1\right), & \text{when } \tau_b > \tau_{cr,e} \\ 0 & \text{, when } \tau_b < \tau_{cr,e} \end{cases} \tag{3.12}$$

Where τ_b is the bed shear stress, and $\tau_{cr,e}$ is the critical erosion bed shear stress.
For the deposition formulation, S is defined as follows:

$$S(\tau_b, \tau_{cr,d}) = \begin{cases} \left(1 - \dfrac{\tau_b}{\tau_{cr,d}}\right), & \text{when } \tau_b < \tau_{cr,d} \\ 0 & \text{, when } \tau_b > \tau_{cr,d} \end{cases} \tag{3.13}$$

Where τ_b is the bed shear stress, and $\tau_{cr,d}$ is the critical deposition bed shear stress. These step functions express the two following concepts: below a critical bed shear stress, no erosion takes place and above a critical bed shear stress, no deposition takes place.

C.4.2 Base case definition

To verify whether these formulations have been implemented correctly, several test runs have been performed. The base case for these test runs is defined in this section and is analogous to previous test runs (for initial profile sensitivity).

After defining the base case, we systematically vary the newly specified parameters to test the correct implementation of the added formulations.

C.4.2.1 Definition

A definition sketch of the relevant parameters is presented in Figure C.38. The arrow indicates the direction of the fluidized layer. Three parameters characterize the fluidized layer flow at x=0:

- Fluidized layer height (h_{fl})
- Average fluidized layer velocity (u_{fl})
- Average fluidized layer concentration (c_{fl})

Flow conditions are characterized by the water depth (d) and the depth-averaged flow velocity ($\overline{U}$). The specified bathymetry is a flat bed.

Initial concentration profile in the fluidized layer is specified as a linear profile, increasing from 0 kg/m^3 at the top of the fluidized layer to twice the average concentration at the bed.
Initial velocity profile in the fluidized layer is specified as a combination of a logarithmic velocity profile and a hyperbolic tangent (mixing layer).

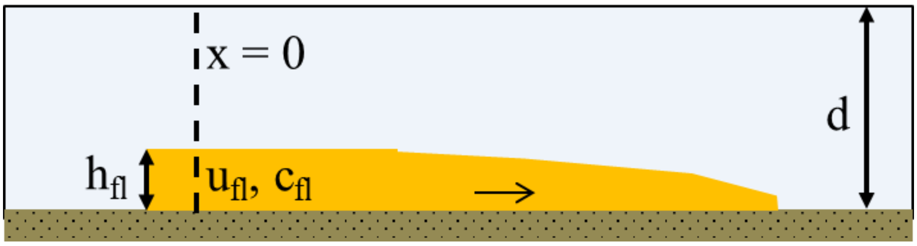

Figure C.38 Definition sketch of fluidized layer and characterizing parameters. Arrow indicates direction of fluidized layer flow. Three parameters characterize the fluidized layer flow at x=0. x=0 is indicated with the dashed line.

C.4.2.2 Base case parameters

Based on discussion with counterparts at Boskalis, the parameters characterizing the fluidized layer and flow conditions are chosen as listed in

Table C.9. These values are based on typically encountered conditions. Apart from the parameters that were specified in the previous section, we also need to specify default values for $w_{s,0}$, ρ_s and n. These three parameters are used in the Richardson-Zaki hindered settling formulation (Equation (3.9)).

Table C.9 Base case parameters for mud dynamics verification

Parameter	value
h_{fl}	1 m
u_{fl}	1 m/s
c_{fl}	100 g/l
d	10 m
$\bar{U}$	0.2 m/s
$w_{s,0}$	1.0e-3 m/s
ρ_{gel}	600 kg/m^3
n	4.0

C.4.3 Hindered settling model runs

To test the implementation of the hindered settling formulation, we perform two sets of test runs. In the first set, the settling velocity of a single particle ($w_{s,0}$) is varied, whereas in the second set, we vary the structural dry density (ρ_{gel}). For both runs, erosion is disabled, since adding an additional source of sediment may affect the outcome of the model runs.

C.4.3.1 Single particle settling velocity

Three values for the single particle settling velocity $w_{s,0}$, were used in the first set of test runs. These are: $w_{s,0}$ = 1.0e-5, $w_{s,0}$ =1.0e-4 and $w_{s,0}$ =1.0e-3. All units are in m/s.

To illustrate the effect of the differences in settling velocity, we plotted profiles of velocity, sediment concentration and settling velocity after 600 m along the trajectory (Figure C.40). The behaviour is as expected. Because of the decrease in $w_{s,0}$, the sharp concentration gradient lies higher for the blue and red lines, but the gradient itself is less steep than for the yellow line. This also affects the hindered settling effect, as we see in the settling velocity plot. Please note that the settling velocities are plotted on a logarithmic x-scale.

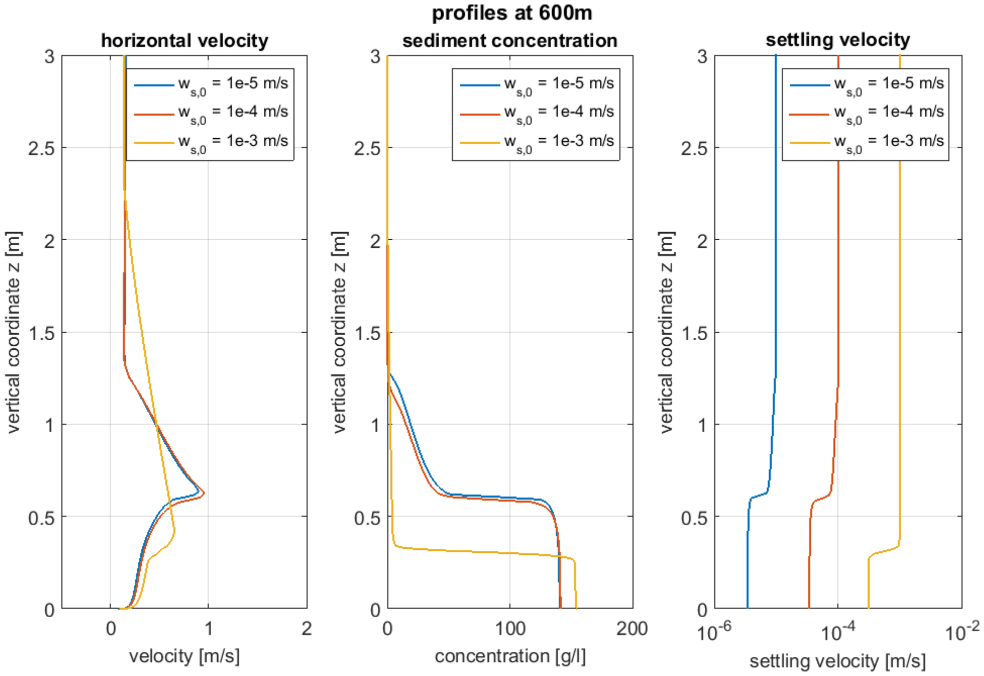

Figure C.39 Velocity, concentration and settling velocity profile at x = 600 m for the hindered settling test runs set 1.

The effective settling velocity also influences the deposition rate, see Equation (3.11). This may be an important factor in determining the sedimentation footprint of the fluidized layer and can also be observed from Figure C.39. We see that for the smaller single particle settling velocities, most of the sediment is still suspended after 600m.

C.4.3.2 *Structural dry density*

Three values for the structural dry density ρ_{gel} were used in the second test run set. These are: ρ_{gel}= 300, ρ_{gel} = 600 and ρ_{gel}= 1000. All units are in kg/m^3.

To illustrate the effect of the differences in structural dry density, we plotted profiles of velocity, sediment concentration and settling velocity after 300m along the trajectory (Figure C.40). We see that the differences in ρ_{gel} lead to large differences in settling velocity for the lower 0.5 meter of the profile, up to one order of magnitude.

In turn, these differences in settling velocity cause pronounced differences in the velocity profile and the suspended sediment mass at this point. Since the deposition rate depends linearly on $w_{s,b}$, this decreases with decreasing ρ_{gel}. Hence, the total amount of suspended matter increases. We observe that the strong concentration gradient moves upward with decreasing ρ_s, and since the sediment mass influences the baroclinic pressure gradient, it also affects the resulting velocity profile. The influence of the ρ_{gel} parameter on model results is significant. This is mainly due to the strongly nonlinear exponent (n=4) for the volume concentration in the Richardson-Zaki formulation.

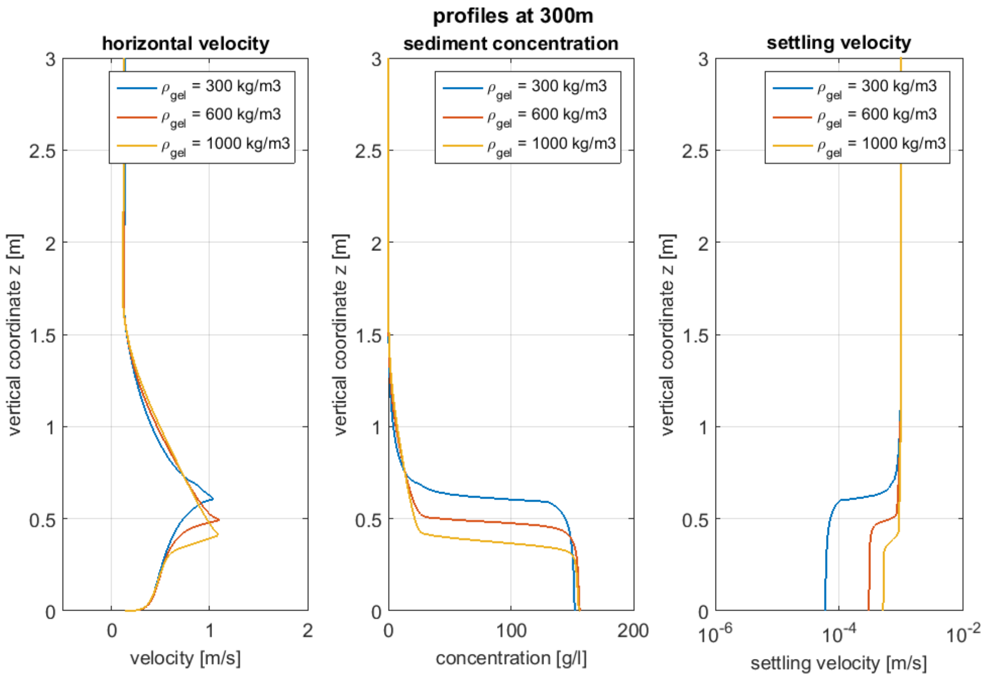

Figure C.40 Velocity, concentration and settling velocity profile at x = 300 m for the hindered settling test runs set 2.

The structural dry densities that were used in these test runs are rather high for muddy suspensions. Normally, ρ_{gel} is in the order of magnitude of 100-200 kg/m^3. However, there is one main reason why we opt for higher values for ρ_{gel}. Calculating the amount of deposition along the trajectory is one of the key outputs of the model. If the concentration c exceeds ρ_{gel}, the settling velocity will become 0, and deposition goes to 0 as well. In reality, other physical processes may result in deposition or slowing down of the fluidized layer, such as increasing viscosity (linked to non-newtonian rheology) and the first stages of consolidation. Hence, we use the ρ_{gel} parameter as a 'dustbin' parameter to account for several of these physical processes that are not included in the model at this moment.

C.4.4 Erosion and deposition

To test the implementation of the Partheniades-Krone formulations, we perform two sets of test runs. In the first set, the critical shear stress for deposition ($\tau_{cr,d}$) is varied, whereas in the second set, we vary the critical shear stress for erosion ($\tau_{cr,e}$). The erosion parameter M is set to 1*10^{-3} and is kept constant throughout all runs. Hindered settling values are set to the base case values as specified in Table C9.

Table C.9

C.4.4.1 Deposition

Three values for the critical shear stress for deposition ($\tau_{cr,d}$) were used in the first set of test runs. These are: $\tau_{cr,d}$= 0.1, $\tau_{cr,d}$=10 and $w_{s,0}$ =1000. All units are in Pa. The critical erosion shear stress $\tau_{cr,e}$ is set to 10 Pa. The deposition formulation is repeated here for convenience:

$$
\begin{aligned}
&D = w_s \, c_b \, S(\tau_b, \tau_{cr,d}) \\
&\text{where:} \\
&S(\tau_b, \tau_{cr,d}) = \begin{cases} \left(1 - \dfrac{\tau_b}{\tau_{cr,d}}\right), & \text{when } \tau_b < \tau_{cr,d} \\ 0 & \text{, when } \tau_b > \tau_{cr,d} \end{cases}
\end{aligned} \tag{3.14}
$$

To illustrate the differences between the three runs, we plot the deposition rate as a function of alongslope distance in the upper panel of Figure C.41. In the lower panel of Figure C.41, we plot the computed bed shear stress as a function of alongslope distance. We see that for the imposed velocity and sediment load, resulting bed shear stresses are in the order of 1 Pa. This means that for a $\tau_{cr,d}$ of either 10 Pa or 1000 Pa, deposition will always occur. The only difference between the deposition flux for these threshold values is caused by the $\tau_b/\tau_{cr,d}$ term in step function S, as this term is negligible for a $\tau_{cr,d}$ of 1000 Pa.

We see that for a $\tau_{cr,d}$ of 0.1 Pa, deposition is not possible for the majority of the trajectory along the slope. Only after 170 m along the slope, the bed shear stress decreases below the threshold so deposition can occur. Before 170m, sediment cannot deposit. Hence, it accumulates in the lower grid cells of the computational domain. This has two consequences. First, the velocity profile is influenced through a change in the baroclinic pressure gradient, as the latter depends on the sediment-induced density gradient. Second, the accumulation of fines in the lowest grid cell leads to a temporary increase in the velocity profile is influenced. This leads to a decrease in bottom shear stress.

Since sediment has been accumulating in the lowest grid cell of the water column, the resulting deposition rate will increase when τ_b becomes smaller than $\tau_{cr,d}$, since c_b is larger. However, this is a direct result of the chosen settings and not necessarily of a physical process.

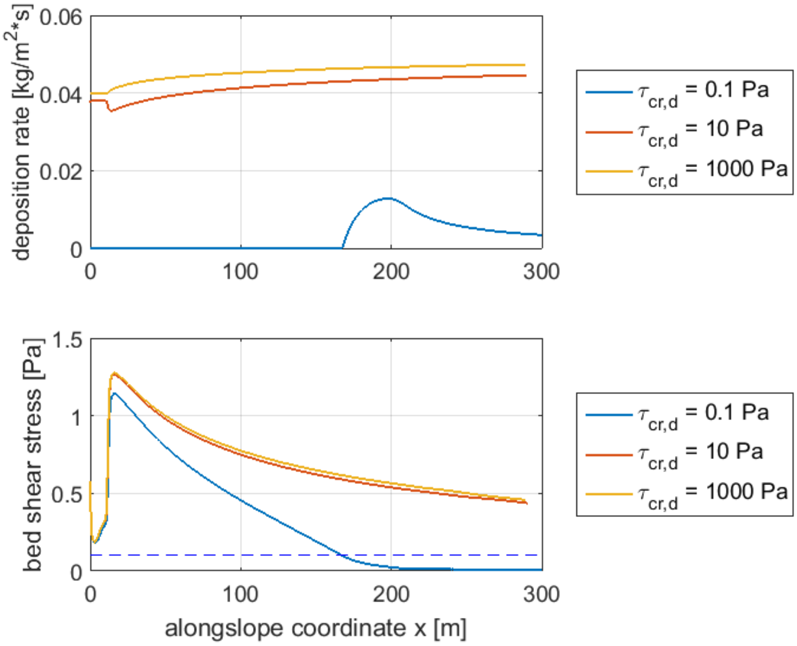

Figure C.41 Deposition rate and bed shear stress as a function of alongslope distance for three different values of $\tau_{cr,d}$. The critical shear stress of 0.1 Pa is indicated with a dashed blue line.

C.4.5 Erosion

Three values for the critical shear stress for erosion ($\tau_{cr,e}$) were used in the first set of test runs. These are: $\tau_{cr,e}$= 0.1, $\tau_{cr,e}$=1.0 and $\tau_{cr,e}$ =10. All units are in Pa. The critical deposition shear stress $\tau_{cr,d}$ is set to 10 Pa, meaning that deposition will occur throughout the domain.
The erosion formulation is repeated here for convenience.

$$E = M\,S(\tau_b, \tau_{cr,e})$$

where: (3.15)

$$S(\tau_b, \tau_{cr,e}) = \begin{cases} \left(\dfrac{\tau_b}{\tau_{cr,e}} - 1\right), & \text{when } \tau_b > \tau_{cr,e} \\ 0 & , \text{when } \tau_b < \tau_{cr,e} \end{cases}$$

The erosion rate is plotted as a function of alongslope distance in the upper panel of Figure C.42. In the lower panel of Figure C.42, we plot the computed bed shear stress as a function of alongslope distance. We see that for the imposed velocity and sediment load, resulting bed shear stresses are in the order of 1 Pa. This means that for a $\tau_{cr,e}$ of 10 Pa there is no erosion in a realistic range of far field flow velocities.

The only critical erosion threshold that yields any erosion is 0.1 Pa, which is very low. Even in that case, erosion rates are an order of magnitude smaller than deposition rates.

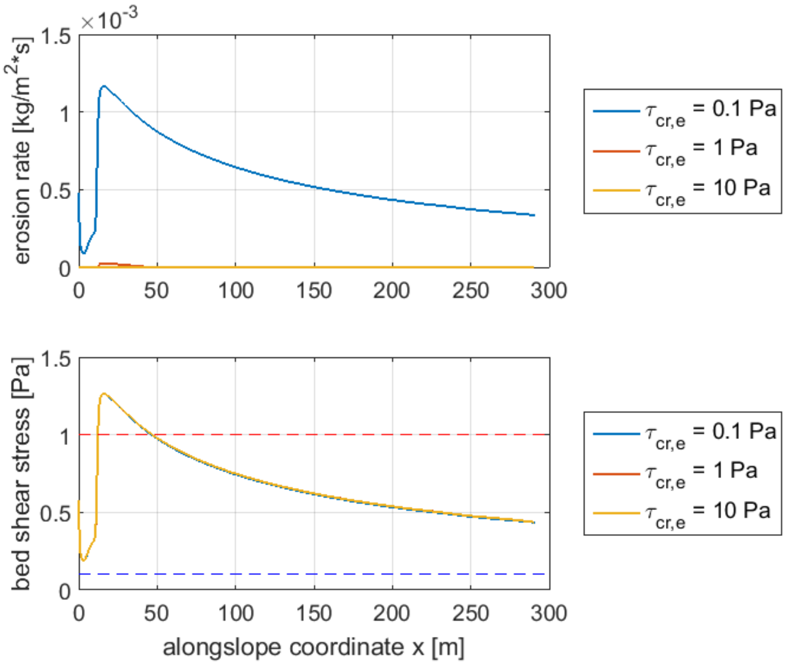

Figure C.42 Deposition rate and bed shear stress as a function of alongslope distance for three different values of $\tau_{cr,e}$. The critical shear stresses of 0.1 and 1.0 Pa are indicated with a dashed blue line and dashed red line, respectively.

C.4.6 Conclusions

- Richardson-Zaki hindered settling formulation was implemented and tested for mud. It gives the expected results.
- Both the single particle settling velocity $w_{s,0}$ and the structural dry density ρ_{gel} have a clear influence on the model results
- The effect of the single particle settling velocity $w_{s,0}$ mainly becomes apparent over longer distances, since the smaller settling velocity directly influences the deposition flux. Hence, more sediment will remain in the system, allowing the fluidized layer to travel further.
- Due to the strongly nonlinear exponent in the Richardson-Zaki formulation for the volume concentration, the values for ρ_{gel} influence model results for the entire computational domain.
- For erosion and deposition of mud, the Partheniades-Krone formulation has been implemented and tested.
- Deposition is clearly dominant over erosion for the specified test cases.
- It is advised to set the critical shear stress for deposition $\tau_{cr,d}$ to a large value, so deposition will always occur.

D User guide

The User Guide is provided upon request as a separate document.